C.P. No. 1351

C.P. No. 1351

PROCUREMENT EXECUTIVE, MINISTRY OF DEFENCE

AERONAUTICAL RESEARCH COUNCIL

CURRENT PAPERS

Wind-tunnel Simulation of the Effects of Flight on Radiated Sound

by

J. Jacques

Engineering Department, University of Cambridge

LONDON: HER MAJESTY'S STATIONERY OFFICE

1976

£2.30 net

WIND-TUNNEL SIMULATION OF THE EFFECTS OF FLIGHT ON RADIATED SOUND

- by -
J. Jacques
Engineering Department, University of Cambridge

SUMMARY

The validity of wind-tunnel simulation of the noise radiated by a moving source is studied. Theoretical corrections are derived that allow acoustic measurements in a wind tunnel with microphones outside of the flow to be transposed to a real flight situation. Some corrected coaxial jet data are then compared with real flight data.

CONTENTS

---

* Replaces A.R.C.36 641

calculation initially carried out to study the effect of flight on nozzle-based sources turns out to include flight and wind-tunnel cases. Particularised to these situations, Howe's result gives the overall correction factors to be applied to wind-tunnel datum so as to make it relevant to flight when the shear layer thickness is small compared with the wavelength of the acoustic signal and when the observer is far from the interface. The other approach isolates and quantifies the effect of the various physical phenomena such as convection, sound transmission, curvature and multiple reflection effects. Both approaches give the same result. However, the second approach permits the removal of the far field condition on the observer by providing an astigmatism correction.

Sound levels measured outside the flow do depend on the flow geometry because of curvature effects which turn out to be particularly large in the forward arc. Unlike curvature effects, multiple reflections are shown to be negligible over a very wide range of incidence angles provided the successive reflected waves be uncorrelated. This is very likely to be the practical case especially at the higher frequencies because of the continuous and random variation of the position of the interface. However, if reflected waves are assumed to be correlated, then phase effects due to phase shifts between successive reflected waves make sound levels frequency-dependent and rapidly oscillating at high frequencies. The amplitude of these oscillations gets specially large in the neighbourhood of the limiting angle for total reflection. Several remarks are in order concerning the "wind tunnel to flight" correction factors. Whatever the geometry, upstream of the flow, ie in the forward arc of the corresponding flight case, intensity levels as measured in a wind tunnel are smaller than those measured in flight. Conversely, they are bigger in the rear arc. There is no effect of interface crossing at 90°. However, these corrections are less for a circular interface than for a slab due to curvature effect. This difference is particularly significant in the forward arc at angles approaching the limiting angle for total reflection. This angle actually limits the angular range in which the simulation is valid. Waves which propagate inside the flow at incidence angles bigger than this limiting angle get trapped inside the flow. At a flow Mach number of 0.4, this limiting angle measured from the direction of fluid motion is about 135°. Therefore a rather wide part of the forward arc radiation is not accessible to measurements made outside of the flow. This is a serious disadvantage because of the special interest we take in forward arc effects of flight.

Multiple reflection effects make the correction factors frequency-dependent and rapidly oscillating at high frequencies. As mentioned before, if we postulate that transmitted waves are uncorrelated, then correction factors no longer display frequency-dependent properties and are not significantly different from those obtained by considering that all reflected waves are completely damped during their propagation inside the jet. Only the first transmitted wave needs be assumed to contribute to the far sound field. However, whichever case is considered, the analytical expressions for the correction factors are involved and the corrections sufficiently large to make their practical application rather dubious.

The practical application of these correction factors requires wind-tunnel data to be expressed in terms of the angle characterising wave-fronts inside the flow. A set of curves connecting this angle to the geometrical angle of observation of the source in a fly-over situation, is given in Figs. 20 to 24. These curves actually describe the angular distortion of the sound field due to interface crossing and show that this distortion is particularly strong at small and large observation angles. Another set of curves given in Figs. 25 to 34 allow an astigmatism correction to be performed. This is a distance correction taking into account the fact that the apparent distance of

the source from the interface varies with the observation angle. The combination of these various corrections allow one to perform relatively easily the operation by which wind-tunnel data is made relevant to flight.

The next step was to apply these corrections to some experimental wind-tunnel data and compare the so-corrected wind-tunnel results to corresponding experimental flight data. It was not possible to carry out any experiments in an anechoic wind tunnel, none being available yet. We had to choose between a wind tunnel with a necessarily bad acoustical environment and an anechoic chamber designed for coaxial jet noise studies. The availability of existing facilities and the risk of irremediable contamination of noise data by reflection effects dueto a bad anechoicity led us to choose the second possibility. A coaxial jet configuration with a secondary flow of small diameter has been preferred although it enhances the main disadvantages of a "microphone outside the flow" technique already mentioned. However, it has been judged as desirable to conduct some measurements with such a configuration, establish the main features of the noise data and determine whether the theoretical corrections for the interface crossing are still sensible in spite of the highly criticisable experimental conditions. Some noise measurements with a coaxial jet configuration characterised by a secondary to primary flow diameter of approximately 5 have then been performed in the anechoic chamber of the Centre d'Essais de Propulseurs (Saclay, France). It turns out that coaxial flow data with a subsonic jet exhausting from a convergent nozzle is characterised by a most remarkable feature. When the secondary flow is switched on, overall sound levels are reduced by about the same amount at all angles. This reduction affects all frequencies but is less at low frequencies where the noise from the secondary flow is of the same order of magnitude as that of the primary jet. Therefore, the relative velocity effect which is missing in the forward arc in a real flight situation is actually present at all angles in this wind-tunnel situation! However, the overall theoretical corrections tend to increase the forward arc noise levels as measured in the coaxial jet situation and to decrease the rear arc levels. Consequently, once corrected, wind-tunnel data look a bit more like flight data. Wind-tunnel data before and after correction had been compared with available in-flight data. The agreement between "corrected wind-tunnel data" and "in-flight" data is variable. The rear arc attenuation observed in flight is lower than that obtained in a "corrected" wind tunnel and there is a definite tendency for forward arc levels, including 90°, to be higher in flight than in the corresponding wind-tunnel situation. It can reasonably be argued that the thickness of the secondary flow, in the simulation test, is not large enough and that the test is irrelevant. However, we think that the very many differences existing between a model jet and that of a real engine are much more likely to be responsible for most of this discrepancy. Furthermore additional sources, which are not simulated in the model jet experiment, are liable to arise in flight from interactions between the jet and its unsteady environment. This is supported by the fact that the agreement between corrected "wind-tunnel data" and "in-flight" data is better on a vehicle such as the Bertin Aérotrain whose unsteady aerodynamic field is much weaker than that of any aircraft.

2. Relevance of a "Source Position at Reception Time" Geometry to a Wind-Tunnel Situation

The relevance of a "source position at reception time" geometry to a wind-tunnel situation is not new and has been used in the past by Lighthill[14] to study the propagation of sound in moving media. However, the concepts involved are not used freely in existing technology. Our objective here is to improve that situation by giving a clear comparison between flight and wind-tunnel situations in order to make this relevance obvious.

The model we adopt for a wind-tunnel situation is that of a source and an observer at rest in a uniform flow of Mach number $\underset{\sim}{M}_o$ that we assume homogeneous and infinite in all directions. In an ideal flight situation, the source moves uniformly with a Mach number $\underset{\sim}{M}_o$ in a homogeneous motionless unbounded medium. The distant sound field of both configurations can be analysed successfully using ray theory in which the wave propagation is described in terms of energy propagation paths and normals to wave-fronts.

The flight case illustrated by diagram (b) of Fig. 0 is analysed first. In this situation, sound reaching the fluid fixed observer O at time t when the source occupies the position $S''(x''_i)$ has been emitted when the source occupied the position $S(\overline{x_i})$. During the travel time $\frac{SO}{c_o}$ of the signal from S to O, the source has moved the distance $SS'' = M_o \overline{SO}$ such that $x''_i = \overline{x}_i - M_o c_o t_{emission}$ S", which is the source position at reception time, is then the source position in a Galilean frame. Wave-fronts are normal to SO. Ray path and wave-front normal are identical; phase and group velocity are the same.

The wind-tunnel configuration is described in diagram (a) of Fig. 0. Let S" be the source position in the flow. Sound reaching the observer O travels along the ray path S"O. But, due to convection, the direction $\underset{\sim}{n}$, the normal to the wave-fronts along which the acoustic wave propagates at speed c_o relative to the fluid, is such that the vector $(\underset{\sim}{M}_o + \underset{\sim}{n})$ gives the ray path orientation and also the velocity at which energy propagates, the group velocity. Therefore, in the absence of flow, the same wave intrinsically characterised by its wave-fronts, would reach the observer O at the same time provided the source were located at a position S (or the observer shifted to a position O_1). The time taken by the wave to travel from S" to O in the presence of flow, $\frac{\overline{SO}}{c_o}$, is equal to the time taken by the flow to drift the wave a distance SS", ie $\frac{\overline{SS''}}{M_o c_o}$. Therefore, $\overline{SS''} = M_o \overline{SO}$.

This analysis leads one to the following conclusions:

(i) The source position S" in a wind tunnel is relevant to a Galilean frame, ie to a "source position at reception time" geometry.

(ii) Although the wave propagation processes differ, flight and wind-tunnel configurations are formally equivalent but for the fact that in the wind-tunnel situation, the source is fixed relative to the observer. The Doppler effect on frequencies is then, of course, absent. This equivalence requires flow and source motions to be taken in opposite directions.

3. Flight Simulation in a Wind Tunnel with Microphones inside the Flow

The similarity between idealised wind-tunnel and flight situations pointed out earlier makes clear the validity of the simulation of flight in a wind tunnel with true field monitoring probes inside the flow. The radiation of sound in both situations is described by a common equation which is the far field solution of the wave equation $\Box^2\phi = Q$ expressed in a frame of reference moving with the source[15], namely:

$$\phi = \frac{1}{4\pi c_o^2 \bar{r}(1 + M_o \cos\bar{\theta})} \int_{v''} \left[Q(\underset{\sim}{\bar{x}},t) \right]'' dv''(\underset{\sim}{x''}) . \qquad (1)$$

Doubly primed quantities are evaluated in a frame of reference moving with the source (Galilean frame). The brackets [ ] designate the usual retarded time operation and bars apply to source co-ordinates at emission time, the observation angle $\bar{\theta}$ being taken relative to the direction opposite to that of source motion in a flight situation and relative to the direction of flow motion in a wind-tunnel configuration. ϕ is any quantity chosen to describe the sound field and Q an ad hoc source term.

The effect of motion is contained in the Doppler factor $(1 + M_o \cos\bar{\theta})$ and in the source term $[Q(\bar{x},t)]''$ which, in most cases and in the far field, is merely proportional to $[Q(x'',t)]$; the proportionality factor depends only on the speed of the source and the direction of observation. The "source effect" is the same in flight and in a wind tunnel; the formulation is indeed unique. From now on, $\int_{v''} [Q(\underset{\sim}{\bar{x}},t)]''dv''(x'')$ will be denoted as S and sound radiations in both flight and wind tunnel, with the microphones inside the flow, will then be described by the following equation:

$$\phi = \frac{S}{4\pi c_o^2 \bar{r}(1 + M_o \cos\bar{\theta})} . \qquad (2)$$

However, in spite of this apparent simplicity, a flight to wind-tunnel comparison is not quite straightforward. Indeed, flight data are usually expressed in terms of source co-ordinates at emission time (F,θ) whereas wind-tunnel data are naturally obtained in a "reception time" geometry (r'',θ''). Therefore, as illustrated in the following sketch, wind-tunnel data are fully comparable to flight data provided that:

$$r''_{W.T.} = r''_F \quad \text{and} \quad \theta''_{W.T.} = \theta''_F$$

or equivalently

$$\bar{r}_F = \bar{r}_{W.T.} \quad \text{and} \quad \bar{\theta}_F = \bar{\theta}_{W.T.}$$

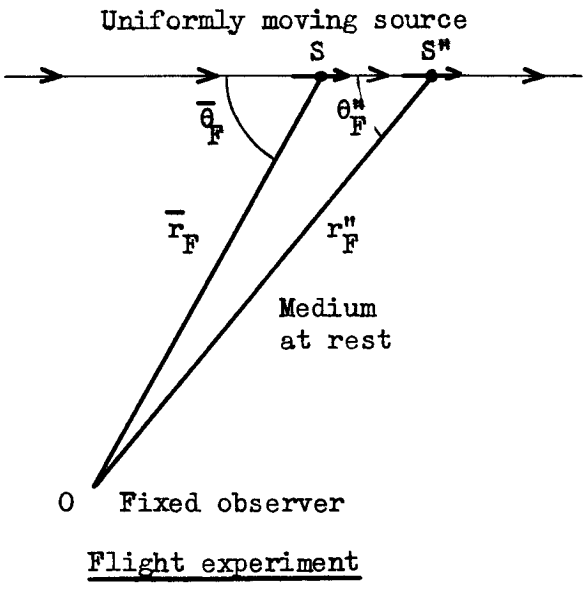

Flight experiment

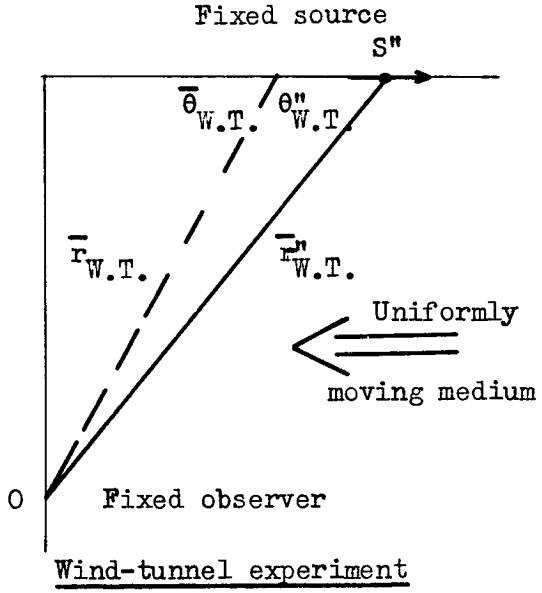

Wind-tunnel experiment

A practical way of performing wind-tunnel experiments would involve a choice of observation angles, θ'', relative to the source inside the flow so that they correspond to integer values of the observation angle at emission time $\bar{\theta}$ at which flight data is available. Wind-tunnel data so referred to $\bar{\theta}$ and $\bar{r}$ can then be compared unambiguously with flight data. The following expressions allow this angle and distance selection to be performed:

$$\tan \theta'' = \frac{\sin \bar{\theta}}{M_o + \cos \bar{\theta}} \qquad (3)$$

$$r'' = \bar{r}\left[(1 + M_o \cos \bar{\theta})^2 + M_o^2 \sin^2 \bar{\theta}\right]^{\frac{1}{2}}$$

$\theta''(\bar{\theta})$ and $20 \log \frac{r''}{r}(\bar{\theta})$ are plotted respectively in Figs. 1 and 2 in a Mach number range covering practical take-off, landing and fly-over cases.

4. Flight Simulation in a Wind Tunnel with Microphones outside the Flow

4.1 Sound transmission from a moving medium to a medium at rest. First approach

Our first approach of the problem of sound transmission through the interface separating a moving medium from a medium at rest is based on a general calculation by Howe[11,12]. Howe calculates the sound generated in the ambient atmosphere at rest by a point source uniformly moving at an arbitrary speed U_o in a uniform flow of arbitrary speed U_R. Howe's model is depicted in Fig. 3. The source moves along a stream line of the flow. The shear layer which separates the flow from the ambient atmosphere where the unsteady pressure is measured is assumed to be sharp, ie its thickness is small compared with the wavelength of the incident sound field. This implies that the axial spreading of the shear layer is neglected. Three different geometries are considered by Howe, a semi-infinite flow with a perfectly plane interface, a slab-shaped flow with two perfectly parallel and plane boundaries and a cylindrical flow of constant radius with an axisymmetric source moving along the axis of the cylinder. The mean-square pressure $\overline{p^2}$ in the far field of the source-flow system is given by the following formulae, each one relevant to a particular geometry. In the case

of a plane interface separating two semi-infinite media and of a source moving at a distance h from the boundary, the mean square pressure $\overline{p^2_{1p}}$ radiated in the fly-over plane is:

$$\overline{p^2_{1p}} = \frac{|S|^2}{8\pi^2 c_1^4 r^2} \frac{\sin^2\theta F^2_{1p}}{(1 + M_o \cos\theta)^2} \tag{4}$$

with

$$F_{1p} = \frac{\exp.\left\{ \frac{-2\pi h/\lambda}{|1+M_o\cos\theta|} \left| I_m\left\{ \left(\frac{c_o}{c_1}\right)^2 \left(1-M_R\cos\theta\right)^2 - \cos^2\theta \right\}^{\frac{1}{2}} \right| \right\}}{\left| \left[\left(\frac{c_o}{c_1}\right)^2 \left(1-M_R\cos\theta\right)^2 - \cos^2\theta \right]^{\frac{1}{2}} + \left(\frac{c_o}{c_1}\right)^2 \sin\theta \left(1-M_R\cos\theta\right)^2 \right|} .$$

The exponential is non-zero only inside the zone of silence; therefore it is only in that zone that the transmitted signal is frequency-dependent. In the case of a slab-shaped flow of thickness d and of a source moving at a distance h from the boundary seen by the observer, the mean-square pressure $\overline{p^2_{2p}}$ at an observation point located in the fly-over plane is:

$$F_{2p} = \left| \frac{e^{i\gamma_1 d} + R\, e^{i\gamma_1 (2d-h)}}{1 - R^2\, e^{2i\gamma_1 d}} \right| \tag{5}$$

γ_1 is the wave number inside the flow in the direction parallel to the flow:

$$\gamma_1 = \frac{2\pi/\lambda}{1 + M_o \cos\theta} \left[\left(\frac{c_o}{c_1}\right)^2 \left(1 - M_R\cos\theta\right)^2 - \cos^2\theta \right]^{\frac{1}{2}} \tag{6}$$

and

$$R = \frac{1 - Q}{1 + Q} \quad \text{with} \quad Q = \frac{\left(\frac{c_o}{c_1}\right)^2 \sin\theta \left(1 - M_R\cos\theta\right)^2}{\left[\left(\frac{c_o}{c_1}\right)^1 \left(1 - M_R\cos\theta\right)^2 - \cos^2\theta \right]^{\frac{1}{2}}} . \tag{7}$$

In the case of a circular jet of radius "a":

$$\overline{p^2_c} = \frac{|S|^2}{32\pi^2 c_1^4 (1 + M_o\cos\theta)^2 r^2} \left| F_c \right|^2 \tag{8}$$

with

$$F_c = \frac{J_o(Z_1) H_1(Z_1) - J_1(Z_1) H_o(Z_1)}{\left(\frac{c_o}{c_1}\right)^2 \frac{Z_o}{Z_1} \left(1 - M_R\cos\theta\right)^2 J_o(Z_1) H_1(Z_o) - J_1(Z_1) H_o(Z_o)}$$

and

$$Z_o = \frac{\sin\theta}{1 + M_o \cos\theta} \frac{2\pi a}{\lambda}$$

$$Z_1 = \frac{\mathrm{sgn}(1 - M_R \cos\theta)}{1 + M_o \cos\theta} \left| \left(\frac{c_o}{c_1}\right)^2 \left(1 - M_R \cos\theta\right)^2 - \cos^2\theta \right|^{\frac{1}{2}} \frac{2\pi a}{\lambda}$$

for angles outside the zone of silence.

J_o and J_1, and H_o and H_1 are respectively the Bessel and Hankel functions of the first kind, of order 0 and 1. In formulae (4) to (8), M_R and M_o are respectively the flow and source Mach numbers both referred to the speed of sound in the ambient atmosphere, c_o. c_1 is the speed of sound in the flow and λ is the wavelength of the incident sound at 90°. r and θ are the far field observation co-ordinates at emission time; θ is taken relative to the direction of flow motion, ie opposite to flight. S describes the nature and the strength of the source, it is identical to that of equation (2).

The factors F_{1p}, F_{2p} and F_c describe the effects of sound propagation in a moving medium and those due to an interface crossing. The multiple reflection process at flow boundaries which is of course absent in the case of a single shear layer, the sound transmission and the angular redistribution of acoustic energy associated with the refraction process are built into Howe's result and cannot be easily isolated.

The general expressions obtained by Howe can be applied to a wind-tunnel configuration by setting the source at rest inside the flow of Mach number $M_R = M_o$. Formulae (4) to (8) then read:

$$\left(\overline{p^2_{W.T.}}\right)_{1p} = \frac{|S|^2 \sin^2\theta}{8\pi^2 c_1^4 r^2} F_{1p}^2$$

with

$$F_{1p} = \frac{\exp\left\{-\frac{2\pi h}{\lambda}\left|I_m\left\{\left(\frac{c_o}{c_1}\right)^2\left(1 - M_o\cos\theta\right)^2 - \cos^2\theta\right\}^{\frac{1}{2}}\right|\right\}}{\left[\left(\frac{c_o}{c_1}\right)^2\left(1-M_o\cos\theta\right)^2 - \cos^2\theta\right]^{\frac{1}{2}} + \left(\frac{c_o}{c_1}\right)^2 \sin\theta\left(1-M_o\cos\theta\right)^2} \qquad (9)$$

in the case of a single plane boundary,

$$\left(\overline{p^2_{W.T.}}\right)_{2p} = F_{2p}^2 \left(\overline{p^2_{W.T.}}\right)_{1p}, \quad F_{2p} \text{ being given by equation (5) with}$$

now

$$\gamma_1 = \frac{2\pi}{\lambda}\left[\left(\frac{c_o}{c_1}\right)^2 \left(1 - M_o \cos\theta\right)^2 - \cos^2\theta\right]^{\frac{1}{2}} \qquad (10)$$

and

$$Q = \frac{(c_o/c_1)^2 \sin\theta (1 - M_o \cos\theta)^2}{\left[\left(\frac{c_o}{c_1}\right)^2 \left(1 - M_o \cos\theta\right)^2 - \cos^2\theta\right]^{\frac{1}{2}}} \qquad (11)$$

in the case of a slab,

$$\left(\overline{p^2_{W.T.}}\right)_c = |S|^2 \, |F_c|^2 / 32 \pi^2 c_1^4 r^2 \quad \text{with}$$

$$F_c = \frac{J_o(Z_1) H_1(Z_1) - J_1(Z_1) H_o(Z_1)}{\left(\frac{c_o}{c_1}\right)^2 \frac{Z_o}{Z_1} \left(1 - M_o \cos\theta\right)^2 J_o(Z_1) H_1(Z_o) - J_1(Z_1) H_o(Z_o)}, \qquad (12)$$

$$Z_o = \sin\theta \frac{2\pi a}{\lambda} \quad \text{and} \quad Z_1 = \left|\left(\frac{c_o}{c_1}\right)^2 \left(1 - M_o \cos\theta\right)^2 - \cos^2\theta\right|^{\frac{1}{2}} \frac{2\pi a}{\lambda}$$

in the case of a circular flow.

Our primary objective is to compare wind-tunnel mean-square pressure levels, $10 \log(\overline{p^2_{W.T.}})$, with the corresponding flight mean-square pressure levels, $10 \log(\overline{p^2_F})$. The far field pressure field $\overline{p^2_F}$ of a source moving at speed U_o in a medium at rest, in which the sound speed is c_o, is contained in equation (2):

$$\overline{p^2_F} = \frac{|S|^2}{32 \pi^2 c_o^4 \bar{r}^2 (1 + M_o \cos\bar{\theta})^2} \qquad (13)$$

where $\bar{r}$ and $\bar{\theta}$ are actually the observation distance and angle taken at emission time. Therefore, before being compared with in-flight sound levels, wind-tunnel levels have to be expressed in terms of the angle $\bar{\theta}$ characterising wave propagation in the flow in the "emission time" geometry. $\bar{\theta}$ actually characterises the "normal to wave-fronts" in the flow and is the angle of incidence on the interface. After refraction, wave-fronts emerge at the angle θ as illustrated by Fig.19. θ and $\bar{\theta}$ are related through Snell's law:

$$\cos\theta = \frac{\cos\bar{\theta}}{\frac{c_1}{c_o} + M_o \cos\bar{\theta}} . \qquad (14)$$

The angular transformation defined by equation (14) must then be performed on formulae (9)-(12) to facilitate a wind tunnel to flight comparison. Noting that. in the transformation, $\sin\theta$ and $(1 - M_o \cos\theta)$ become respectively

$$\frac{\left(\frac{c_1}{c_o} + M_o \cos\bar{\theta}\right)^2 - \cos^2\bar{\theta}}{\frac{c_1}{c_o} + M_o \cos\bar{\theta}} \quad \text{and} \quad \frac{c_1/c_o}{\frac{c_1}{c_o} + M_o \cos\bar{\theta}},$$

we find finally after some algebra that:

$$\left(\overline{p^2_{W.T.}}\right)_{1p} = \frac{|S|^2}{8\pi^2 c_1^4 r^2} \frac{\left(\frac{c_1}{c_o} + M_o \cos\bar{\theta}\right)^2 - \cos^2\bar{\theta}}{\left[\sin\bar{\theta} + \frac{\left[\left(\frac{c_1}{c_o} + M_o \cos\bar{\theta}\right)^2 - \cos^2\bar{\theta}\right]^{\frac{1}{2}}}{\left(\frac{c_1}{c_o} + M_o \cos\bar{\theta}\right)^2}\right]^2} \qquad (15)$$

in the case of a single plane interface,

$$\left(\overline{p^2_{W.T.}}\right)_{2p} = \left| \frac{e^{iy_1 h} + R\, e^{iy_1(2d-h)}}{1 - R^2 e^{2iy_1 d}} \right|^2 \left(\overline{p^2_{W.T.}}\right)_{1p} \qquad (16)$$

with now

$$y_1 = \frac{2\pi}{y} \frac{\sin\bar{\theta}}{\frac{c_1}{c_o} + M_o \cos\bar{\theta}}$$

and

$$R = \frac{\sin\bar{\theta} - \frac{\left[\left(\frac{c_1}{c_o} + M_o \cos\bar{\theta}\right)^2 - \cos^2\bar{\theta}\right]^{\frac{1}{2}}}{\left(\frac{c_1}{c_o} + M_o \cos\bar{\theta}\right)^2}}{\sin\bar{\theta} + \frac{\left[\left(\frac{c_1}{c_o} + M_o \cos\bar{\theta}\right)^2 - \cos\bar{\theta}\right]^{\frac{1}{2}}}{\left(\frac{c_1}{c_o} + M_o \cos\bar{\theta}\right)^2}} \qquad (17)$$

in the case of a slab and

$$\left(\overline{p^2_{W.T.}}\right)_c = \frac{|S|^2 \sin^2\bar{\theta}}{32\pi^2 c_1^4 r^2} \left(\frac{\left[J_o(Z_1) H_1(Z_1) - J_1(Z_1) H_o(Z_1)\right]^2}{\frac{\left[\left(\frac{c_1}{c_o} + M_o\cos\bar{\theta}\right)^2 - \cos^2\bar{\theta}\right]^{\frac{1}{2}}}{\left(\frac{c_1}{c_o} + M_o\cos\bar{\theta}\right)^2} J_o(Z_1)H_1(Z_o) - \sin\bar{\theta} J_1(Z_1)H_o(Z_o)} \right)^2 \qquad (18)$$

with

$$Z_o = \frac{2\pi a}{\lambda} \frac{\left[\left(\frac{c_1}{c_o} + M_o \cos\bar{\theta}\right)^2 - \cos^2\bar{\theta}\right]^{\frac{1}{2}}}{\frac{c_1}{c_o} + M_o \cos\bar{\theta}} \quad \text{and} \quad Z_1 = \frac{2\pi a}{\lambda} \frac{\sin\bar{\theta}}{\frac{c_1}{c_o} + M_o \cos\bar{\theta}}$$

in the case of a circular flow.

The numerical computation of $\left(p^2_{W.T.}\right)_c$ is not easy because of the presence of Bessel and Hankel functions. When the argument of these functions is very large, this is the high frequency limit, a simpler expression is obtained by using asymptotic expressions, namely:

$$J_o(Z) = \sqrt{\frac{2}{\pi Z}} \cos\left(Z - \frac{\pi}{4}\right), \quad J_1(Z) = \sqrt{\frac{2}{\pi Z}} \sin\left(Z - \frac{\pi}{4}\right)$$

$$H_o(Z) = \sqrt{\frac{2}{\pi Z}}\, e^{i(Z-\pi/4)}, \quad H_1(Z) = -i\, H_o(Z).$$

After some algebra we find that in the high frequency limit, equation (18) reads:

$$\left(\overline{p^2_{W.T.}}\right)_c = \frac{|S|^2}{32\pi^2 c_1^4 r^2} \frac{\sin\bar{\theta}\left[\left(\frac{c_1}{c_o} + M_o\cos\bar{\theta}\right)^2 - \cos^2\bar{\theta}\right]^{\frac{1}{2}} \left|e^{2i(Z-Z_o)}\left(1+i\cot\left(Z_1 - \frac{\pi}{4}\right)\right)\right|^2}{\left|\sin\bar{\theta} + i\frac{\left[\left(\frac{c_1}{c_o} + M_o\cos\bar{\theta}\right)^2 - \cos^2\bar{\theta}\right]^{\frac{1}{2}}}{\left(\frac{c_1}{c_o} + M_o\cos\bar{\theta}\right)^2} \cot\left(Z_1 - \frac{\pi}{4}\right)\right|^2}$$

and finally

$$\left(\overline{p^2_{W.T.}}\right)_c = \frac{|S|^2}{8\pi^2 c_1^4 r^2} \frac{\sin\bar{\theta}\left[\left(\frac{c_1}{c_o} + M_o\cos\bar{\theta}\right)^2 - \cos^2\bar{\theta}\right]^{\frac{1}{2}}}{\sin^2\bar{\theta}\sin^2\left(Z_1 - \frac{\pi}{4}\right) + \frac{\left(\frac{c_1}{c_o} + M_o\cos\bar{\theta}\right)^2 - \cos^2\bar{\theta}}{\left(\frac{c_1}{c_o} + M_o\cos\bar{\theta}\right)^4} \cos^2\left(Z_1 - \frac{\pi}{4}\right)}. \tag{19}$$

These results permit us to make two significant observations. Firstly, whatever the geometry of the interface, $\bar{\theta}$ is limited to the range $[0, \bar{\theta}_T]$ with

$$\bar{\theta}_T = \cos^{-1}\left(-\frac{c_1/c_o}{1+M_o}\right).$$

$\bar{\theta}$ is actually the limiting angle for total reflection of sound at the interface. A wave impinging on the interface with the incident angle $\bar{\theta}_T$ emerges out of the flow at $\theta = 180°$. Waves such that $\bar{\theta} > \bar{\theta}_T$ are then trapped inside the flow and will never get to the observer located outside of it. Therefore, flight simulation in a wind tunnel is only possible in the range of incidence

angles $[0, \bar{\theta}_T]$ when the microphones are in the ambient atmosphere. The range $[\bar{\theta}_T, 180°]$ of forward arc angles is not accessible to measurement at least for the low Mach numbers considered here. Secondly, wind-tunnel corrections are frequency-dependent because the multiple reflection process already mentioned imposes a definite modal structure on the field.

4.2 Sound transmission from a moving medium to a medium at rest. Second approach

The first approach to the problem did not allow to discriminate between the various physical mechanisms contributing to the general phenomenon of sound transmission through a sharp interface between two media in relative motion. These mechanisms will now be studied separately using the concepts of ray acoustics. The model is the same as that of Howe, illustrated in Fig. 3, but we now treat it in the high frequency limit. In that case, a wave is defined by the normal to its front and by the direction along which energy actually propagates. Three phenomena have to be investigated. Firstly, there is a transmission loss at the interface crossing due to impedance mismatch. Secondly, the wave-fronts are distorted by the refraction phenomenon; this distortion is a function of the interface geometry; we call it the "wave curvature effect". Thirdly, when several boundaries are present, a multiple reflection phenomenon is expected due to the bouncing of waves from one boundary to the other.

4.2.1 Transmission loss

The transmission loss is classically determined by the boundary conditions at the interface, namely the conservation of pressure and normal particle displacement. Morse and Ingard[9] give the transmission coefficient for pressure, T say, as:

$$T = \frac{2\rho_o c_o^2 \sin 2\bar{\theta}}{\rho_o c_o^2 \sin 2\bar{\theta} + \rho_1 c_1^2 \sin 2\theta} ,$$

where as previously $\bar{\theta}$ and θ are the angles characterising the wave-front normal respectively in the moving medium and in the ambient medium at rest.

If static pressures are assumed to be the same in both media (this is implicitly assumed in Howe's calculation) then, for gases with a constant ratio of specific heats, $\rho_o c_o^2 = \rho_1 c_1^2$. This relation together with equation (14) allows one to express T in terms of c_1/c_o, M_o and $\bar{\theta}$ only:

$$T = \frac{2 \sin \bar{\theta}}{\sin \bar{\theta} + \dfrac{\left[\left(\dfrac{c_1}{c_o} + M_o \cos \bar{\theta}\right)^2 - \cos^2 \bar{\theta}\right]^{\frac{1}{2}}}{\left(\dfrac{c_1}{c_o} + M_o \cos \bar{\theta}\right)^2}} . \qquad (20)$$

4.2.2 Wave curvature effects

Let us consider a bundle of rays emitted by a point source S fixed in a uniform medium as illustrated in Fig. 4. This bundle illuminates a surface $\Delta\Sigma$ of the "flow/ambient medium" interface. On crossing the interface, the rays are re-directed in the motionless atmosphere so that the shape of the

bundle is distorted. After transmission, the wave-fronts can be characterised by their radii of curvature, R_1 and R_2, in two principal directions of the interface. These radii of curvature are shown in Fig. 5. Since the group velocity is constant, the conservation of the acoustic energy contained in the emergent bundle reads: $E\Delta S$ = constant, where E is the acoustic energy density and ΔS a cross-section of the bundle. In a medium at rest, the acoustic energy density E, is related to the mean-square pressure, $\overline{p^2}$, by the following relation:

$$E = \frac{\overline{p^2}}{\rho_o c_o^2} .$$

The mean-square pressure, $\overline{p_K^2}$, at a point K located immediately below the illuminated surface element $\Delta\Sigma$ is then related to that, $\overline{p_o^2}$, at an observation point O located a distance r from K and on the same ray, through the following expression:

$$\overline{p_K^2}\, R_1 R_2 = \overline{p_o^2}\, (R_1 + r)(R_2 + r). \qquad (21)$$

The mean-square pressure $\overline{p_{\bar{K}}^2}$, at a point $\bar{K}$ located immediately above the surface $\Delta\Sigma$ differs from $\overline{p_K^2}$ only through the transmission loss coefficient given by equation (20) so that:

$$\overline{p_K^2} = T^2\, \overline{p_{\bar{K}}^2} .$$

Therefore the mean-square pressures outside and inside the flow are related through the following expression:

$$\overline{p_o^2} = \frac{R_1 R_2}{(R_1 + r)(R_2 + r)}\, T^2\, \overline{p_{\bar{K}}^2}$$

Now $\overline{p_{\bar{K}}^2}$ is given by equation (2) in terms of the "emission time" co-ordinates, $\bar{r}$ and $\bar{\theta}$, of point $\bar{K}$ so that:

$$\overline{p_{\bar{K}}^2} = \frac{|S|^2}{32\pi^2 c_1^4\, \bar{r}^2 \left(1 + M_o \frac{c_o}{c_1} \cos\bar{\theta}\right)^2} . \qquad (22)$$

As stated before, the source term S needs not be specified. It is the same in flight and wind-tunnel situations so that it will therefore cancel out in the final wind-tunnel to flight comparison. The final expression for $\overline{p_o^2}$ is then:

$$\overline{p_o^2} = \frac{|S|^2\, T^2}{32\pi^2\, c_1^4\, \bar{r}^2 \left(1 + M_o \frac{c_o}{c_1} \cos\bar{\theta}\right)^2} \frac{R_1 R_2}{(R_1 + r)(R_2 + r)} , \quad M_o = \frac{U_o}{c_o} . \qquad (23)$$

Far enough from the interface, ie $\{r >> R_1, R_2\}$, $\overline{p_o^2}$ represents the far field wind-tunnel mean-square pressure $\overline{p_{W.T.}^2}$ obtained by Howe and then assumes the simple form:

$$\overline{p^2_{W.T.}} = \frac{|S|^2 T^2}{32\pi^2 c_1^4 r^2 \left(1 + M_o \frac{c_o}{c_1} \cos \bar{\theta}\right)^2} \frac{R_1 R_2}{\bar{r}^2} \qquad (24)$$

The quantity $\alpha = \frac{R_1 R_2}{\bar{r}^2}$ describes the wave curvature effect. We shall now evaluate it for the plane and the circular geometries. The principal directions characterising these two geometries are the direction of fluid motion and the direction normal to it and tangent to the interface. It is obvious that the radius of curvature in the direction of fluid motion, R_1 say, is the same for both geometries; we then evaluate that first.

R_1 is determined by a procedure illustrated in the following sketch. Two rays emitted by a point source S in the plane normal to the interface and parallel to $\underset{\sim}{U}_o$ appear, after refraction, to come from a point C_1. R_1 is the apparent distance, C_1B, travelled in the flow.

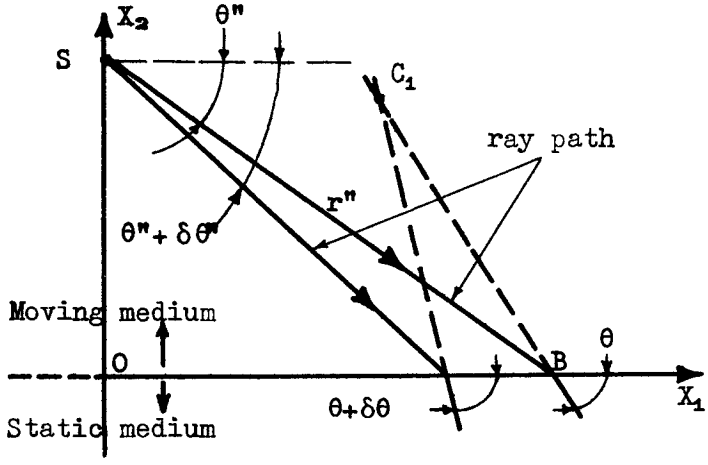

The co-ordinates of the centre of curvature, c_1, are:

$$C_1 \left| \begin{array}{l} \sin\theta \cos\theta \dfrac{\partial X}{\partial \theta} + X \\ -\sin^2\theta \dfrac{\partial X}{\partial \theta} \end{array} \right.$$

with $X = OB = r'' \cos\theta''$

and $r'' = SB$

so that $R_1 = \left| \sin\theta \dfrac{\partial X}{\partial \theta} \right|$

$\dfrac{\partial X}{\partial \theta}$ is evaluated as follows:

$$\frac{\partial X}{\partial \theta} = -r'' \sin\theta'' \frac{\partial \theta''}{\partial \theta} + \cos\theta'' \frac{\partial r''}{\partial \theta}$$

with $\dfrac{\partial r''}{\partial \theta} = -\dfrac{\partial \theta''}{\partial \theta} r'' \cot\theta''$ because $r'' \sin\theta'' = (r''+\delta r'')\sin(\theta''+\delta\theta'')$.

Therefore, $$\frac{\partial X}{\partial \theta} = -\frac{r''}{\sin\theta''} \frac{\partial \theta''}{\partial \theta}$$

and $$\frac{R_1}{r''} = \left| \frac{\sin\theta}{\sin\theta''} \frac{\partial \theta''}{\partial \theta} \right|. \qquad (25)$$

Using the second of equations (3) and noting that the Mach number to be considered is actually $\left(M_o \frac{c_o}{c_1}\right)$, one obtains the ratio:

$$\frac{R_1}{\bar{r}} = \left| \frac{\sin\theta}{\sin\theta''} \frac{\partial\theta''}{\partial\theta} \right| \left[1 + 2 M_o \frac{c_o}{c_1} \cos\bar{\theta} + \left(M_o \frac{c_o}{c_1}\right)^2 \right]^{\frac{1}{2}} \qquad (26)$$

θ characterises the wave-fronts in the medium at rest, $\bar{\theta}$ the wave-fronts in the moving medium, θ'' the acoustic ray, or direction of energy propagation, in the moving medium. A more compact expression for $\frac{R_1}{\bar{r}}$ is obtained if equation (14) is used together with the relation between θ'' and $\bar{\theta}$ given by the first of equations (3). This gives:

$$\frac{\sin\theta}{\sin\theta''} = \frac{\sin\theta}{\sin\bar{\theta}} \left[1 + 2 M_o \frac{c_o}{c_1} \cos\bar{\theta} + \left(M_o \frac{c_o}{c_1}\right)^2 \right]^{\frac{1}{2}},$$

$$\frac{\sin\theta}{\sin\bar{\theta}} = \frac{c_1/c_o}{(c_1/c_o + M_o \cos\bar{\theta})^2} \frac{\partial\bar{\theta}}{\partial\theta},$$

$$\frac{\partial\theta''}{\partial\theta} = \frac{1 + M_o(c_o/c_1)\cos\bar{\theta}}{1 + 2 M_o(c_o/c_1)\cos\bar{\theta} + (M_o c_o/c_1)^2} \frac{\partial\bar{\theta}}{\partial\theta} \quad \text{and consequently:}$$

$$\frac{R_1}{\bar{r}} = \frac{1}{c_1/c_o + M_o \cos\bar{\theta}} \left(\frac{\partial\bar{\theta}}{\partial\theta}\right)^2 \qquad (27)$$

$\frac{R_1}{\bar{r}}$ is plotted in Fig. 6 as a function of $\bar{\theta}$ for a set of values of M_o and $c_o = c_1$.

R_2 is anticipated not to be the same in both geometries. Indeed, in the case of a circular interface, all planes containing the flow axis on which the source is located are fly-over planes. Then, the curvature effect does not depend on the polar co-ordinate ϕ in a plane normal to $\underset{\sim}{U}_o$, so that ϕ is conserved across the boundary ($\phi = \bar{\phi}$). This is not true for the plane interface that we shall study first. The circular case will be derived straightforwardly from the more general plane case. The radius of curvature, R_2 ray, in the direction normal to $\underset{\sim}{U}_o$ and parallel to a plane interface can be determined in a way similar to that used to determine R_1. We shall concentrate on the fly-over plane and define ϕ so that $\phi = 0$ in that plane as shown in Fig. 5. Let us consider a ray characterised in the flow by the angles θ'' and ϕ'' and the corresponding wave-front normal defined by the angles $\bar{\theta}$ and $\bar{\phi}$. After refraction, the ray and the wave-front normal are both defined by

the angles θ and ϕ. The components of the wave-number along the principal directions of the interface are conserved across the interface. In the direction of fluid motion, this conservation law leads to the well-known equation (14). In the other principal direction, it gives (11) the following less familar relation:

$$\sin\theta \sin\phi = \frac{\sin\bar{\theta}\sin\bar{\phi}}{\frac{c_1}{c_0} + M_0 \cos\bar{\theta}} . \qquad (28)$$

This equation together with equation (14) allows a complete determination of the actual ray path after refraction when the ray is slightly out of the fly-over plane. Let us project two rays whose wave-fronts are characterised by $(\bar{\phi} = 0; \bar{\theta})$ and $(\delta\phi; \bar{\theta})$ in the flow and by $(\phi = 0; \theta)$ and $(\delta\phi; \theta)$ in the ambient medium on the plane (x_2, x_3) normal to $\underset{\sim}{U}_0$. The result of this projection is illustrated in the following sketch:

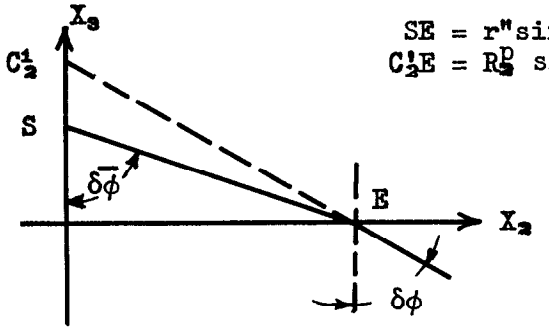

$SE = r''\sin\theta'' = \bar{r}\sin\bar{\theta}$

$C_2^1E = R_2^p \sin\theta$

By analogy with expression (25), we have:

$$\frac{R_2^p \sin\theta}{\bar{r}\sin\bar{\theta}} = \frac{\partial\bar{\phi}}{\partial\phi} \qquad (29)$$

In the fly-over plane, $\phi = \bar{\phi} = 0$ and $\frac{\partial\bar{\phi}}{\partial\phi}$ is given from equation (28) by:

$$\frac{\partial\bar{\phi}}{\partial\phi} = \frac{\sin\theta}{\sin\bar{\theta}}\left(\frac{c_1}{c_0} + M_0\cos\bar{\theta}\right).$$

The second radius of curvature for a plane interface and for an observer located in the fly-over plane is then:

$$\frac{R_2^p}{\bar{r}} = \frac{c_1}{c_0} + M_0\cos\bar{\theta}. \qquad (30)$$

In the case of a circular interface, the expression for the second radius of curvature, R_2^c say, results from equation (29) by noting that now $\phi \equiv \bar{\phi}$, so that

$$\frac{R_2^c}{\bar{r}} = \frac{\sin\bar{\theta}}{\sin\theta} \qquad \text{or equivalently}$$

$$\frac{R_2^c}{\bar{r}} = \frac{c_0}{c_1}\left(\frac{c_1}{c_0} + M_0\cos\bar{\theta}\right)^2 \frac{\partial\theta}{\partial\bar{\theta}} . \qquad (31)$$

In the fly-over plane, the curvature effect attached to a plane interface is described by the following equation:

$$\alpha^p = \left(\frac{\partial\bar{\theta}}{\partial\theta}\right)^2 \qquad (32)$$

If the interface is circular, the curvature effect is given by:

$$\alpha^c = \left(1 + M_o \frac{c_o}{c_1} \cos \bar{\theta}\right) \frac{\partial \bar{\theta}}{\partial \theta} \qquad (33)$$

$\frac{R_2^p}{r}$, $\frac{R_2^c}{r}$, α^p and α^c are plotted respectively in Figs. 7 to 10, as a function of $\bar{\theta}$, for a set of values of M_o and $c_1 = c_o$.

4.2.3 Multiple reflection effect

The multiple reflection mechanism is illustrated in Fig. 11. The main difference between the slab and the circular flow cases as far as that mechanism is concerned is that the jet axis is actually a focus line in the circular case. Indeed any ray originating from a source located on the axis will cross again the jet axis after it has undergone a reflection at the flow boundary whatever its initial orientation. However, for both geometries, reflected waves can be divided into two families. The first family includes waves that are initially emitted towards the interface seen by the observer and, therefore, undergo an even number of reflections before being transmitted. The second one includes those that are initially emitted towards the hidden interface and, therefore, undergo an odd number of reflections; they are primed in Fig. 11. The signal received in a direction θ by a far field microphone is then the sum of a doubly infinite number of signals. Each of them undergoes the same curvature effect characterised by the factor α^p or α^c according to the geometry. If the distance travelled by the waves inside the jet is neglected in comparison with that travelled in the ambient medium after transmission, this is the far field limit, then the pressure attached to the n^{th} transmitted wave is related to that attached to the first one by $p_n = \zeta^{2(n-1)} p_1$ for the first family and $p_n' = \zeta^{2(n-1)} p_1'$ for the second family. ζ is a complex number accounting for the reflection loss and the phase shift involved in traversing the jet. The total pressure signal is then:

$$p_T = \sum_{n=1}^{\infty} (p_n + p_n') = \frac{p_1 + p_1'}{1 - \zeta^2}. \qquad (34)$$

This general result is now applied to particular geometries. In the case of a slab thickness d, the source being located a distance h from the boundary seen by the observer, we have

$$\zeta = R\, e^{i\gamma_1 d} \quad \text{and} \quad p_1' = R\, p_1\, e^{2i\gamma_1 (d-h)}$$

where γ_1 is the axial wave-number inside the flow (see equation (16)), and R is the reflection coefficient. R is related to T, given by equation (19), by the pressure continuity equation $R = T - 1$. The total pressure is then:

$$(p_T)_{2p} = \frac{1 + R\, e^{2i\gamma_1 (d-h)}}{1 - R^2\, e^{2i\gamma_1 d}} (p_1)_{2p}. \qquad (35)$$

If the source is equidistant from the boundaries, then $h = d/2$ and

$$(p_T)_{2p} = \frac{(p_1)_{2p}}{1 - R\, e^{i\gamma_1 d}}. \qquad (36)$$

In the case of a circular jet of radius "a", the source being on the axis, $\zeta = i R\, e^{2i\gamma_1 a}$ and $p_1' = - i R\, e^{2i\gamma_1 a} p_1$. The $-\pi/2$ phase shift

is brought in by the crossing of the jet axis which acts as a focus line. This is a classical result of geometrical optics[16]. The total pressure is then:

$$(p_T)_c = \frac{(p_i)_c}{1 + i\,R\,e^{2iy_1 a}}. \qquad (37)$$

It is interesting to note that if waves are damped during their propagation so that y_1 is complex and $I_m(y_1) > 0$, then when $|y_1 a| \to \infty$ the total pressure p_T tends to p_i whatever the geometry. If we now consider that transmitted waves are uncorrelated due to the fact that in a realistic situation the interface is randomly defined then the pressure signals added in mean square and phase shifts can be ignored. We find then that for both geometries:

$\overline{p_T^2} = \dfrac{\overline{p_i^2} + \overline{p'^2_i}}{1 - \zeta^4}$; ζ is now a real number equal to the reflection coefficient R. Moreover, $\overline{p'^2_i} = R^2\,\overline{p_i^2}$ so that:

$$\overline{p_T^2} = \frac{\overline{p_i^2}}{1 - R^2}. \qquad (38)$$

4.2.4 General expressions and comparison with the results obtained through the first approach

The various effects contributing to the transmission of sound through the interface separating two media in relative motion are now brought together. The mean-square pressure $(\overline{p^2_{W.T.}})$ measured by a microphone located in the far field of the "source-interface" system is given by the following formulae: - in the case of a single plane boundary, the observer lying in the fly-over plane:

$$(\overline{p^2_{W.T.}})_{1p} = \frac{\alpha^p\,|S|^2\,T^2}{32\,\pi^2 c_1^4\,r^2\left(1 + M_o\,\dfrac{c_o}{c_1}\cos\bar{\theta}\right)^2} \qquad (39)$$

- in the case of a slab of thickness d, the source lying at a distance h from the boundary nearest the observer located in the fly-over plane:

$$(\overline{p^2_{W.T.}})_{2p} = (\overline{p^2_{W.T.}})_{1p}\left|\frac{1 + R\,e^{2iy_1(d-h)}}{1 - R^2\,e^{2iy_1 d}}\right|^2 \qquad (40)$$

if reflected waves are correlated,

$$(\overline{p^2_{W.T.}})_{2p} = (\overline{p^2_{W.T.}})_{1p}\,\frac{1}{1 - R^2} \qquad (41)$$

if reflected waves are uncorrelated.

- in the case of a circular jet of radius "a",

$$(\overline{p^2_{W.T.}})_c = \frac{\alpha^c\,|S|^2\,T^2}{32\pi^2 c_1^4 r^2\left|1 + iRe^{2iy_1 a}\right|^2\left(1 + M_o\dfrac{c_o}{c_1}\cos\bar{\theta}\right)^2} \qquad (42)$$

if reflected waves are correlated and

$$\left(\overline{p^2_{W.T.}}\right)_c = \left(\overline{p^2_{W.T.}}\right)_{1p} \frac{\sin \bar{\theta}}{(1 - R^2)\left[\left(\frac{c_1}{c_o} + M_o \cos \bar{\theta}\right)^2 - \cos^2 \bar{\theta}\right]^{\frac{1}{2}}} \qquad (43)$$

if reflected waves are uncorrelated.

α^p, α^c and T are respectively given by equations (32), (33) and (20); $R = T - 1$; r is the distance travelled by waves in the ambient medium and M_o is the flow Mach number referred to the speed of sound in the ambient medium, c_o. c_1 is the speed of sound in the flow.

It is then easy to check that equations (39) and (40) are respectively identical to equations (15) and (16) obtained from Howe's calculation. Equation (42) does not look very much like equation (19) which is the asymptotic expression of equation (18) in the high frequency limit. However, after some algebra, they were found to be identical. Therefore, both approaches give the same answer in the high frequency limit.

The second approach not only makes possible a separate quantification of the various effects involved but allows one to release the far field condition by taking a full account of the distance dependence shown in equation (23). The main findings of this second approach are tabulated in Figs. 12 and 13.

4.3 Comparison between far field sound radiations in a wind tunnel and in flight

Formulae (39) to (43) give the mean-square pressure levels in the ambient medium at rest in terms of the "emission time" angle $\bar{\theta}$ characterising wave-front normals. They can then be directly compared with the sound radiated in flight expressed in "emission time" co-ordinates. If the source is assumed to move at speed U_o in a still atmosphere where sound propagates at speed c_o, then, the mean-square pressure $\overline{p^2_F}$ say, is:

$$\overline{p^2_F} = \frac{|S|^2}{32 \pi^2 c_o^4 \bar{r}^2 \left(1 + M_o \cos \bar{\theta}\right)^2} \quad , \quad M_o = \frac{U_o}{c_o} \quad ,$$

where the "source to observer" distance at emission time, $\bar{r}$, is chosen equal to the distance, r, travelled by waves in the ambient medium in the wind-tunnel situation. The quantity $10 \log \frac{\overline{p^2_F}}{\overline{p^2_{W.T.}}}$ represents the correction to be added to wind-tunnel data so as to make it relevant to flight, all sound levels being expressed in decibels. The various expressions for $C = \frac{\overline{p^2_F}}{\overline{p^2_{W.T.}}}$ according to the geometry and to the assumption made to evaluate the multiple reflection effect are given below.

In the case of a single plane boundary:

$$C^{1p} = \left(\frac{c_1}{c_o}\right)^4 \frac{\left[\sin\bar{\theta} + \dfrac{[(c_1/c_o + M_o\cos\bar{\theta})^2 - \cos^2\bar{\theta}]^{\frac{1}{2}}}{(c_1/c_o + M_o\cos\bar{\theta})^2}\right]^2}{4(1 + M_o\cos\bar{\theta})^2\left[\left(\dfrac{c_1}{c_o} + M_o\cos\bar{\theta}\right)^2 - \cos\bar{\theta}\right]} . \qquad (44)$$

The quantity $10 \log C^{1p}(\bar{\theta})$ is plotted in Fig. 14 for $c_1 = c_o$ and various values of M_o.

In the case of a slab:

$$C^{2p} = \left|\frac{1 - R^2 e^{2iy_1 d}}{1 + R e^{2iy_1(d-h)}}\right|^2 C^{1p} \qquad (45)$$

if reflected waves are correlated, and

$$C^{2p} = (1 - R^2)\, C^{1p} \qquad (46)$$

if reflected waves are uncorrelated.

The frequency dependence of C^{2p} as given by equation (45) is illustrated in Fig. 15 for $c_o = c_1$, $h = d/2$ and $M_o = 0.4$ at various angles $\bar{\theta}$. This shows that the amplitude of the oscillations becomes very large only in the forward arc when the limiting angle for total reflection is approached. The effect of multiple uncorrelated reflection described by equation (46) turns out to be negligible; this is due to the fact that $R^2 \ll 1$ in a very wide range of angles; R^2 goes to 1 at the limiting angle for total reflection but this increase is extremely sudden.

In the case of a circular jet:

$$C^c = \left(\frac{c_1}{c_o}\right)^4 \frac{\left|\sin\bar{\theta}\, J_1(Z_1)H_o(Z_o) - \dfrac{[(c_1/c_o + M_o\cos\bar{\theta})^2 - \cos^2\bar{\theta}]^{\frac{1}{2}}}{(c_1/c_o + M_o\cos\bar{\theta})^2} J_o(Z_1)H_1(Z_o)\right|^2}{\sin^2\bar{\theta}(1 + M_o\cos\bar{\theta})^2\left|J_o(Z_1)H_1(Z_1) - J_1(Z_1)H_o(Z_1)\right|^2} \qquad (47)$$

if the reflected waves are correlated and whatever the frequency; Z_o and Z_1 are given by equation (18). The frequency dependence of C^c is illustrated in Fig. 16 for $c_o = c_1$, $M_o = 0.4$ and various angles $\bar{\theta}$. Again, oscillations are very large only at high observation angles. In the high frequency limit and when multiple reflections are neglected (total damping of reflected waves):

$$C^c = C^c_{H.F.} = C^{1p} \frac{\left[\left(\dfrac{c_1}{c_o} + M_o\cos\bar{\theta}\right)^2 - \cos^2\bar{\theta}\right]^{\frac{1}{2}}}{\sin\bar{\theta}} \qquad (48)$$

$10 \log C^c_{H.F.}(\bar{\theta})$ is plotted in Fig. 17 for $c_o = c_1$ and a set of values of M_o. Multiple correlated reflections bring in the extra factor $\left|1 + i R e^{2iy_1 a}\right|^2$ which makes C^c oscillate with changing frequency in the way shown in Fig. 16 at large values of a/λ. Multiple uncorrelated

reflections introduce the extra factor $(1 - R^2)$ which again is negligible except very near to the limiting angle for total reflection where R tends to 1.

The correction factor 10 log C is always positive in the forward arc and negative in the rear arc. Therefore, in the forward arc, sound levels measured in a simulated flight situation are smaller than those corresponding to real flight. The situation is reversed in the rear arc. 10 log C = 0 at $\bar{\theta} = 90°$, whatever the geometry, the frequency or the assumption made to evaluate the multiple reflection effect. The correction factor is smaller for a circular jet than for a slab.

Multiple reflections make the correction factor oscillate unless phase shifts are neglected in which case the correction factor is no longer frequency-dependent and the effect of multiple reflections is altogether negligible.

The choice of a practical factor is rather difficult. The circular geometry is more relevant to a real situation so we definitely recommend the use of the results obtained for that geometry. As far as jet noise studies are concerned, the oscillations brought in by multiple reflections are very unlikely to be present because the signal is a broad-band noise and the interface position is random. A good approximation then consists of taking $C^c_{H.F.}$ as the basic correction factor. At low frequencies, the full correction factor C^c as given by equation (47) should be used. However, as shown in Fig. 16, at low frequencies C^c does not deviate significantly from its high frequency value as given by $C^c_{H.F.}$. Therefore, the error made by using $C^c_{H.F.}$ whatever the frequency can probably be considered as acceptable.

4.4 Correction method

The practical application of the correction factors obtained in para. 4.3 implies that experimental wind-tunnel data can be obtained in terms of the angle $\bar{\theta}$ which as a matter of fact is not measurable. The geometrical parameters measurable in a wind-tunnel situation are the distance of the source from the observer, R say, and the geometrical angle of observation Θ. All angles and distances involved are defined in Fig. 19. In this paragraph, we assume that $c_0 = c_1$, a condition which is effectively satisfied in practice. Θ and $\bar{\theta}$ are then related through the three following equations:

$$\sin(\Theta - \theta) = \frac{a}{R} \frac{\sin(\theta'' - \theta)}{\sin \theta''} \qquad (49),$$

$$\cos \theta = \frac{\cos \bar{\theta}}{1 + M_0 \cos \theta} \qquad (50) \quad \text{and} \quad \tan \theta'' = \frac{\sin \bar{\theta}}{\cos \bar{\theta} + M_0} \qquad (51)$$

$\Theta(\bar{\theta})$ is plotted in Figs. (20) to (24) for various values of a/R and M_0 relevant to practical situations. Curves are stopped at the angle $\Theta_L = \sin^{-1} a/R$ because in a configuration such that $\Theta < \Theta_L$ the observer would be inside the flow.

An astigmatism correction can be introduced in order to take into account the distance dependence of sound pressure outside of the flow as expressed by equation (23). According to that equation,

$$\overline{p^2_{W.T.}} \sim \frac{1}{r^2\left(1 + \frac{R_1}{r}\right)\left(1 + \frac{R_2}{r}\right)}$$

where r is the distance the wave travels in the ambient medium before it reaches the microphone, R_1 and R_2 being the radii of curvature calculated in para. 4.2.2. If wind-tunnel data are made relevant to a flight situation characterised by an "emission time""source observer" distance equal to the geometrical distance R, then we must add to wind-tunnel data a correction equal, in decibels, to:

$$\delta_d = 10 \log \left\{ \frac{r^2}{R^2}\left(1 + \frac{R_1}{\bar{r}}\,\frac{\bar{r}}{r}\right)\left(1 + \frac{R_2}{\bar{r}}\,\frac{\bar{r}}{r}\right)\right\} \qquad (52)$$

where $\frac{R_1}{\bar{r}}$ is given by equation (27) and $\frac{R_2}{\bar{r}}$ by equation (30) or (31) according to the geometry of the interface.

$\frac{r}{R}$ and $\frac{\bar{r}}{r}$ are implicitly related to $\bar{\theta}$ through the following expressions:

$$\frac{r}{R} = \left[\left(\sin\Theta - \frac{a}{R}\right)^2 + \left(\cos\Theta - \frac{a}{R}\cot\theta''\right)^2\right]^{\frac{1}{2}}$$

and

$$\frac{\bar{r}}{r} = \frac{a/R}{\sin\theta''\left[(M_o + \cos\bar{\theta})^2 + \sin^2\bar{\theta}\right]^{\frac{1}{2}}\frac{r}{R}}$$

$\Theta(\bar{\theta})$ and $\theta''(\bar{\theta})$ are given by equations (49) to (51). The astigmatism correction, δ_d, is plotted against $\bar{\theta}$ in Figs. 25 to 29 for a plane interface and in Figs. 30 to 34 for a circular interface, for various values of h/R or a/R and M_o.

The application of the correction method is easy. Let $N_{W.T.}$ denote the overall sound pressure level, in decibels, measured in a wind-tunnel configuration characterised by a/R, Θ and M_o. This level is actually relevant to an emission angle $\bar{\theta}$, in flight, which can be determined from one of the Figs. 10 to 24. The predicted flight level N_F, at an "emission time" distance R, is then:

$$N_F(\bar{\theta}) = N_{W.T.}(\bar{\theta}) + 10 \log C(\bar{\theta}) + \delta_d(\bar{\theta}) \qquad (53)$$

where $10 \log C(\bar{\theta})$ is the theoretical correction for interface crossing determined and discussed in para. 4.3.

An example of application is shown in Fig. 35 in which an arbitrary wind-tunnel field shape is shown before and after correction assuming $a/R = 0.02$ and $M_o = 0.3$.

4.5 Experimental coaxial jet data and comparison with existing in-flight data

Some experiments on "jet noise/mean flow" interaction have been conducted in the anechoic chamber of C.E.Pr. (Centre d'Essais de Propulseurs, Saclay, France) on a model scale coaxial jets configuration. The objective was to determine the features of the acoustic data, measured in the ambient atmosphere at rest, with and without secondary flow. The theoretical corrections for refraction determined earlier will be applied to the data obtained with the secondary flow. Then, simulated flight data, before and after correction, will be compared with real flight data.

The biggest possible secondary nozzle diameter, $\phi_2 = 280$ mm, has been chosen. The primary nozzle diameter, ϕ_1, has been fixed at 58.6 mm; the area ratio, about 23, is rather small but the fundamental requirement that the noise sources of the primary jet are embedded inside the potential core of the secondary flow is met except for the very low frequency sound emitted far downstream. This is shown in Fig. 36 which depicts the mixing zones for two typical primary flows and a secondary flow of Mach number $M_0 = 0.3$. The distance between the exit planes of the two nozzles, $e = 150$ mm, has been determined as a compromise between the necessity of fulfilling this embedding condition and that of having an acceptable forward arc shadow zone for high frequency sound due to the presence of the secondary nozzle. The measurement distance was $R = 6$ m. The distance "a" appearing in our model cannot be defined very precisely in a real situation but it is certainly well approximated by the secondary nozzle diameter ϕ_2 so that a/R is chosen equal to 0.02.

The primary and secondary jet conditions have been chosen in order to simulate existing in-flight data made available to us by Rolls-Royce BED and SNECMA. This includes in-flight tests on the HS125, Canberra and Concorde aircraft and simulated flight tests on the Rolls-Royce Spinning Rig and on the Bertin Aérotrain.

Typical field shapes and spectra at 90° as measured at C.E.Pr. with and without secondary flow are presented in Figs. 37 and 38 respectively for a subsonic and a supersonic primary jet. Amazingly enough, the secondary flow provokes an overall level decrease whatever the angle. This effect is bigger in the rear arc, ie at small angles relative to the flows directions, than in the forward arc. It actually affects all frequencies. This result, although already observed by other authors[17,18], is most interesting. Indeed, these field shapes and spectra are quite different from those measured in a real flight situation. This is especially true at high forward arc angles where an amplification is usually observed!

The refraction corrections for a cylindrical interface (assuming a negligible multiple reflection effect) have been applied to these wind-tunnel results. Figures 39 to 42 depict the "flight to static" comparisons; three different possible comparisons are illustrated in each set of curves. The first one concerns the flight tests (aircraft, Spinning Rig or Aérotrain), the second one the coaxial jets experiment without correcting the "secondary flow on" field shape and finally the results obtained after the correction has been applied. The agreement between "flight-static" and "wind-tunnel (corrected) - static" overall levels is variable. It is rather poor in the cases of real flight (Figs. 39 and 40b) and the Spinning Rig (Fig. 40a) but much better in the case of the Aérotrain whatever the engine (Figs. 41 and 42). This is thought to be due to the fact that the relative velocity effect observed in the rear arc is bigger on the Aérotrain than on aircraft.

Our corrections which tend to enhance this effect in the rear arc, as shown in Fig. 35, then improve the situation in the case of the Aérotrain but make it worse in the other cases. In the forward arc, the agreement is bad when the amplification observed in real flight is high, ie on aircraft and on the Spinning Rig. It is better in the case of the Aérotrain because the forward arc amplification is not very large, even at supersonic jet speeds, and because a slight attenuation is actually measured at 90°.

On one hand, one can argue that it is surprising to find a good agreement between a criticisable model scale experiment on clean jets involving theoretical corrections obtained from an oversimplified shear layer model and a full-scale engine experiment where many noise sources are present. Then any agreement can only be fortuitous and this kind of comparison can be considered as meaningless.

On the other hand, if the simulation is admitted as acceptable in spite of the limited thickness of the secondary flow and if the corrections for refraction are fully relevant, then the results suggest that the additional noise sources present in a full-scale situation are weaker on the Aérotrain than on aircraft. This can be explained by the fact that the J85 engine propelling the Aérotrain was equipped with a long lined exhaust pipe and is therefore expected to radiate less internal or excess noise than any of the engines propelling the aircraft considered in this paper.

Furthermore, the effect of engine setting on its sound radiation might explain to some extent the observed phenomenon. This effect is neither well documented nor understood yet but noise generation mechanisms of the kind described in Ref. 19 might well play a significant role. Indeed, they involve the noisy interaction between the jet and its environment, the latter being expected to be much more unsteady on any aircraft than on the Aerotrain. The possible importance of engine mounting is supported by the fact that similar results are obtained on the Aérotrain equipped with two different engines.

The situation may be further confused by real atmosphere long distance propagation effects where the sound may be subject to significant interaction with atmospheric turbulence. This might be more pronounced in flight because of the longer distances travelled by the sound on its journey from the aircraft to the ground, and on the Spinning Rig because the sound travels in the vicinity of the jet wake left by previous jet passages past the observation point.

5. Conclusion

Some requirements for the valid simulation in a wind tunnel of the effects of flight have been highlighted. A formal equivalence between an ideal wind-tunnel experiment conducted with a constant velocity uniform flow and a constant velocity flight experiment has been shown to exist. In practice problems arise only because of the presence of shear layers separating the wind-tunnel flow from the ambient atmosphere and from the necessarily limited smoothness and size of the simulation flow.

In the case of microphones placed outside the flow, it has been shown how important it is to correct for the various effects accompanying the refraction of sound through the shear layer. The corrections are based on a model of negligible shear-layer thickness. The angular distortion of the sound field depends on the relative position of the source, the interface and the observer and on the flow Mach number; however, it does not depend on the geometry of the interface provided that the observer is in the fly-over plane. The difference between the angles defining the wave-front

normals inside and outside the flow is particularly large at low and high angles relative to the flow direction. It increases when the microphone gets nearer to the interface and when the flow Mach number increases. It is non-zero at 90° but, in the range of flow Mach numbers and geometries relevant to practical situations, the angle shift at 90° does not exceed a few degrees. The simulation is limited by the forward arc angle from which the incident waves start being trapped inside the flow; this angle is equal to 135° at a flow Mach number of 0.4. The main effect affecting sound levels at interface crossing is the "wave curvature effect". This effect is larger for a plane interface than for a circular one. However, it is dependent of the source - interface - observer geometry. There is no effect at 90° but the correction increases on both sides of 90° and, when the flow Mach number increases, attains several decibels at low and high angles. For example, the correction is about -5 dB at 130° for a Mach number of 0.4, all for a circular interface. There is also an astigmatism effect which depends on the source - interface - observer geometry and on the flow Mach number. In practical situations, this effect becomes significant only at very low angles relative to the direction of the flow. If the multiple reflections at the interface are fully correlated, and this is very unlikely to be true in practice, the corrections oscillate when the frequency of the incident sound changes; these oscillations are large only close to the forward arc limiting angle for total reflection. When the frequency dependence is assumed irrelevant, these corrections provoke a decrease of the noise levels and a stretching of the sound field in the rear arc. Forward arc levels are increased but the sound field at high angles is limited by the angle from which total reflection starts; levels at 90° are practically unchanged.

The comparison of wind-tunnel and in-flight experimental results gives a variable agreement from which it can be argued that the model chosen to determine the correction for refraction is oversimplified. Indeed, the shear layer is turbulent, not plane and not necessarily thin on the wavelength scale as assumed in the model. It can also be argued that, in a full-scale flight experiment, the noise sources other than the mixing jet flow are likely to be due not only to excess noise sources whose sound is flight-amplified but also to in-flight interactions between the jet and/or its sound and the unsteady aerodynamic field created by the aircraft or the turbulence encountered with atmosphere on the sound's relatively long path to a ground observer.

References

No.	Author	Title, etc.
1	W. Smith	The use of a rotating arm facility to study flight effect on jet noise. Paper presented to the 2nd International Symposium on Air Breathing Engines, Sheffield. (1974).
2	J.R. Jacques and P. Thomas	Caractérisation de l'Aérotrain 02 en tant que moyen d'etude expérimentale de l'influence de la vitesse de vol sur le bruit d'ejection. SNECMA internal report. (1973).
3	R.W. Paterson, P.G. Vogt and W.M. Foley	Design and development of the United Aircraft Research Laboratories acoustic research tunnel. AIAA Paper 72-1005. (1972).
4	A. Roussel and J.P. Duponchel	Etude de l'influence de l'étendue de la zone source sur la détermination du champ sonore d'un jet de tuyère convergente. SNECMA Report, YKA No. 865. (1975).
5	H.S. Ribner	Reflection, transmission and amplification of sound by a moving medium. Journal of the Acoustical Society of America, 29, No. 4, 435-441. (1957).
6	J.W. Miles	On the reflection of sound at an interface of relative motion. Journal of the Acoustical Society of America, 29, No. 2, 226-228. (1957).
7	B.H.K. Lee and D.J. Jones	Transmission of upstream sound through a subsonic jet. AIAA Paper 73-630. (1973).
8	G.G. Steinmetz and J.J. Singh	Reflection and transmission of acoustic waves from a moving layer. NASA TN D-6673. (1972).
9	P.M. Morse and U. Ingard	Theoretical Acoustics (Chapter 11, 711). McGraw Hill Book Company Inc. (1968).
10	R.K. Amiet	Correction of open jet wind-tunnel measurements for shear layer refraction. AIAA Paper No. 75-532. (1975).
11	M.S. Howe	Application of energy conservation to the solution of radiation problems involving uniformly convected source distributions. Journal of Sound and Vibration 43, No. 1, pp.77-86. (1975).
12	M.S. Howe	Acoustic radiation from an axisymmetric source in a circular jet. Cambridge Noise Research Unit Memorandum No. 31. (1974).
13	J.E. Ffowcs Williams	Sound production at the edge of a steady flow. Journal of Fluid Mechanics, 66, Pt. 4, pp.791-816. (1974).

References (Contd.)

No.	Author	Title, etc.
14	M.J. Lighthill	The fourth annual Fairey lecture: The propagation of sound through moving fluids. Journal of Sound and Vibration, 24, Pt. 4, pp.471-492. (1972).
15	C.L. Morfey	The sound field of sources in motion. Journal of Sound and Vibration, 23, Pt. 3, pp.291-295. (1972).
16	A. Sommerfeld	Lectures on Theoretical Physics, Vol. IV, Optics, Chapter 6. Academic Press. (1964).
17	U. Von Glahn, O. Grossbeck and J. Goodykoontz	Velocity decay and acoustic characteristics of various nozzle geometries in forward flight. AIAA Paper No. 73-629. (1973).
18	A.B. Packman, K.W. Ng and R.W. Paterson	Effect of simulated forward flight on subsonic jet exhaust noise. AIAA Paper 75-869. (1975).
19	J.R. Jacques	The acoustic response of a nozzle flow to an externally applied low frequency pressure field. Journal of Sound and Vibration, 41, Pt. 1, pp.13-32. (1975).

Acknowledgments

This work has been done under the direction of Prof. Ffowcs Williams while the author was a member of the Cambridge Noise Research Unit on secondment from SNECMA (Société Nationale d'Etude et de Construction de Moteurs d'Aviation, France). The author wishes to thank Dr. M.S. Howe for many stimulating discussions, Mrs. J. Broadway, M. R. Siot at the Centre d'Essais de Propulseurs, France, and Mm. M. Julliand and S. Monot at SNECMA for their technical assistance. In-flight data are presented by courtesy of Rolls-Royce, BED and SNECMA. This is gratefully acknowledged.

COMPARISON OF WIND-TUNNEL AND FLIGHT CONFIGURATIONS

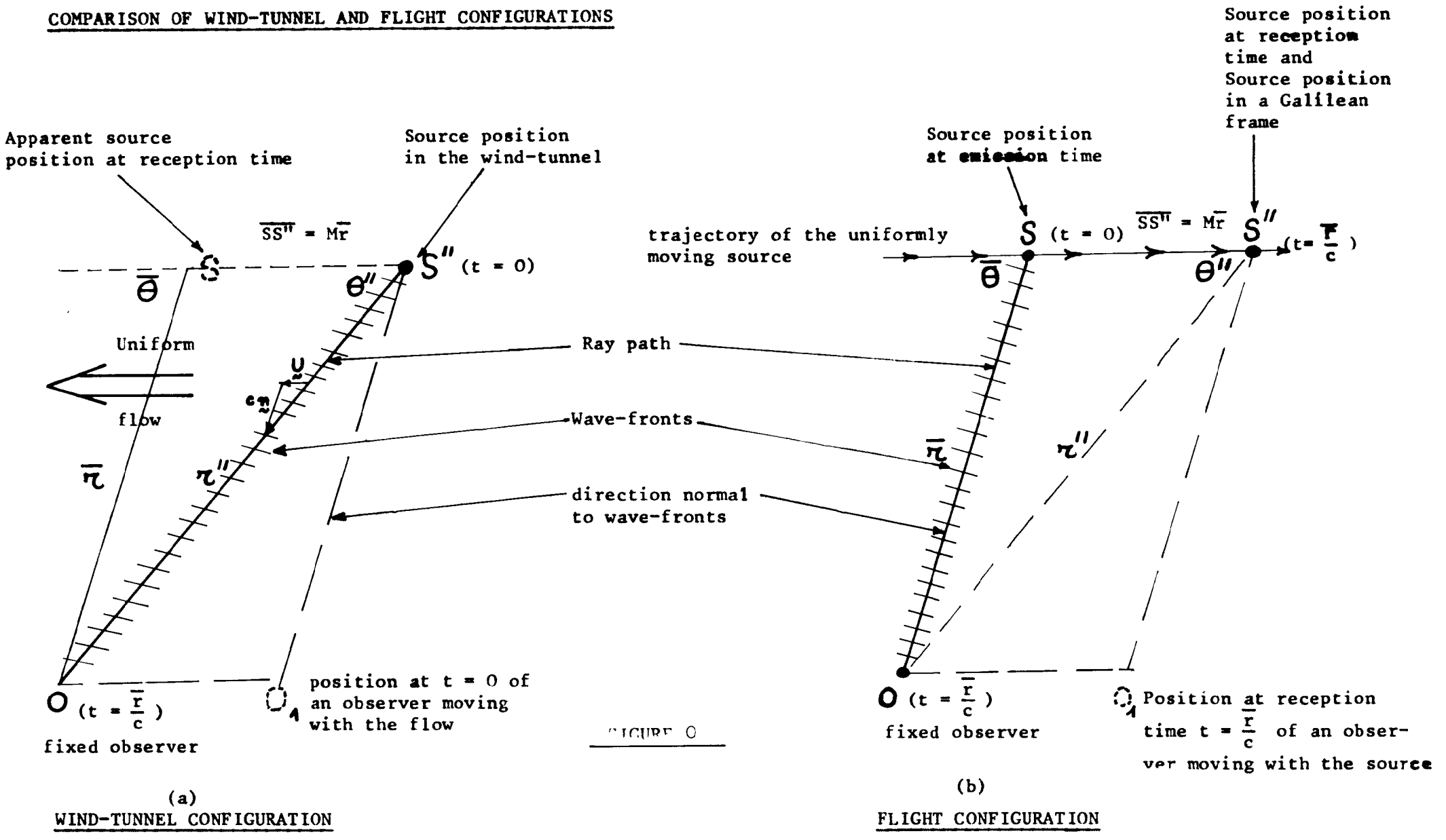

FIGURE 0

"MICROPHONE INSIDE THE FLOW" TECHNIQUE. RELATION BETWEEN WIND-TUNNEL, AND FLIGHT OBSERVATION ANGLES.

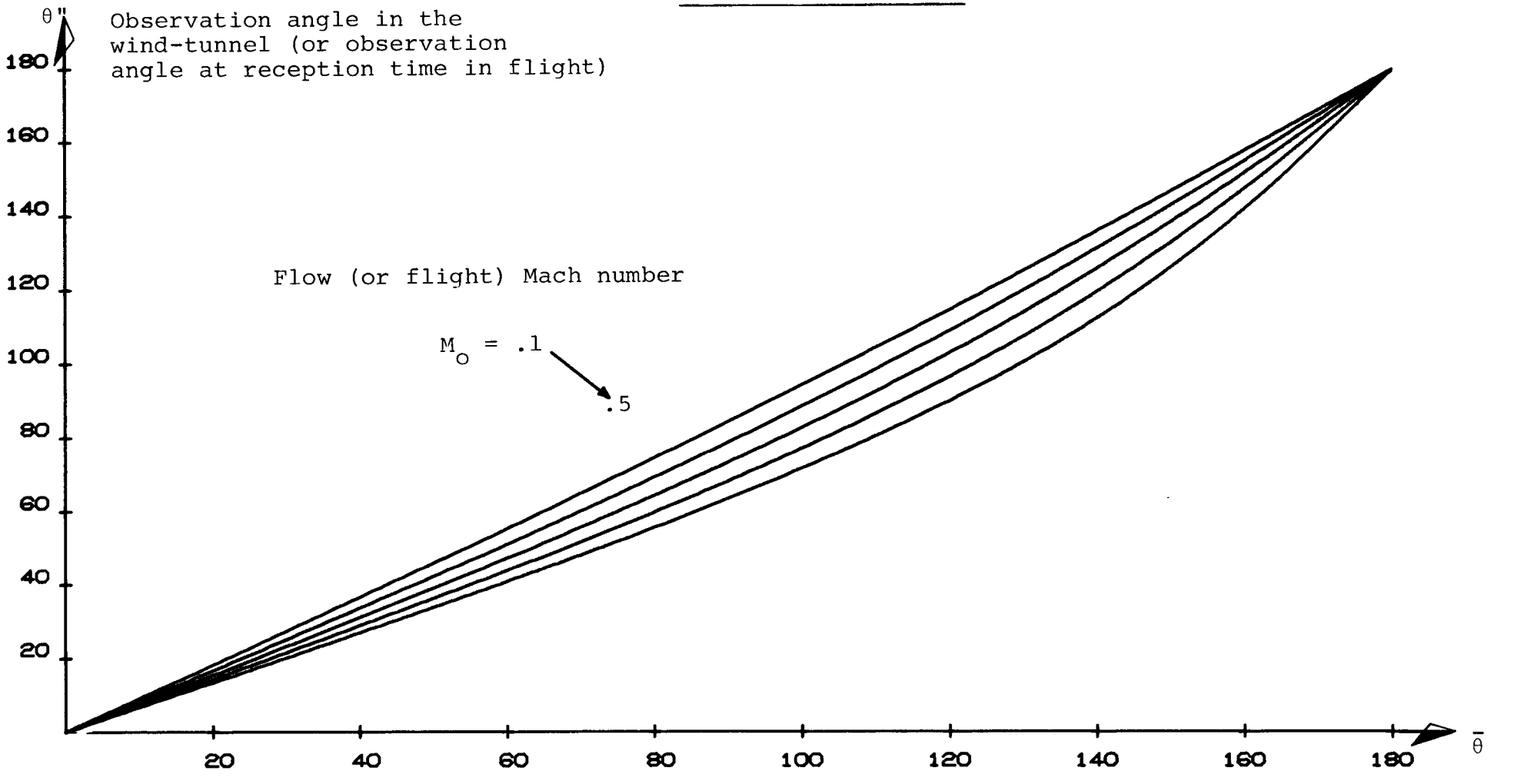

FIGURE 1

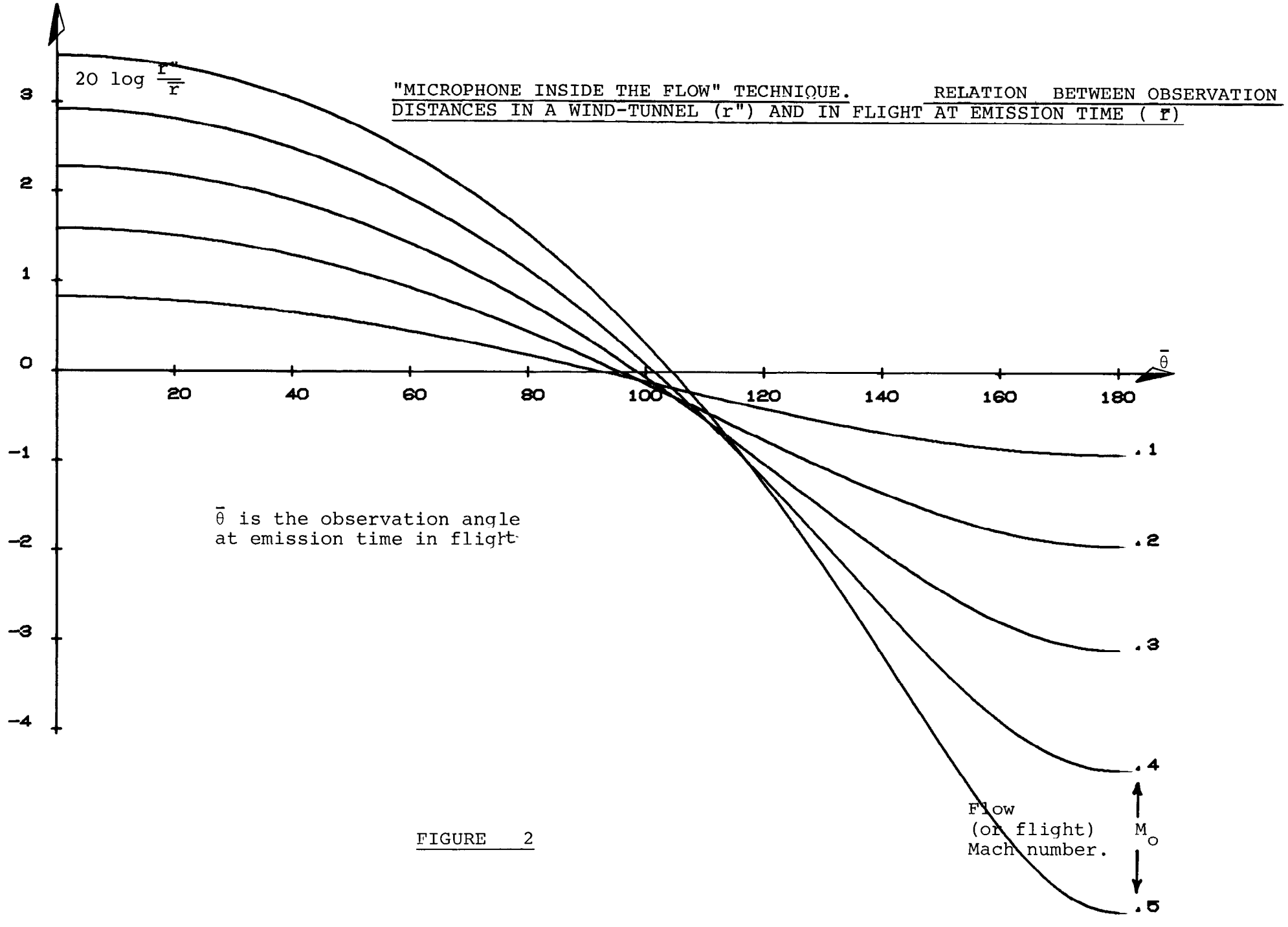
"MICROPHONE INSIDE THE FLOW" TECHNIQUE. RELATION BETWEEN OBSERVATION DISTANCES IN A WIND-TUNNEL (r") AND IN FLIGHT AT EMISSION TIME (r)
20 log r"/r
3
2
1
0
-1
-2
-3
-4
20
40
60
80
100
120
140
160
180
θ̄
.1
.2
.3
.4
.5
θ̄ is the observation angle at emission time in flight
Flow (or flight) Mach number.
M_o

FIGURE 2

ILLUSTRATION OF HOWE'S MODEL

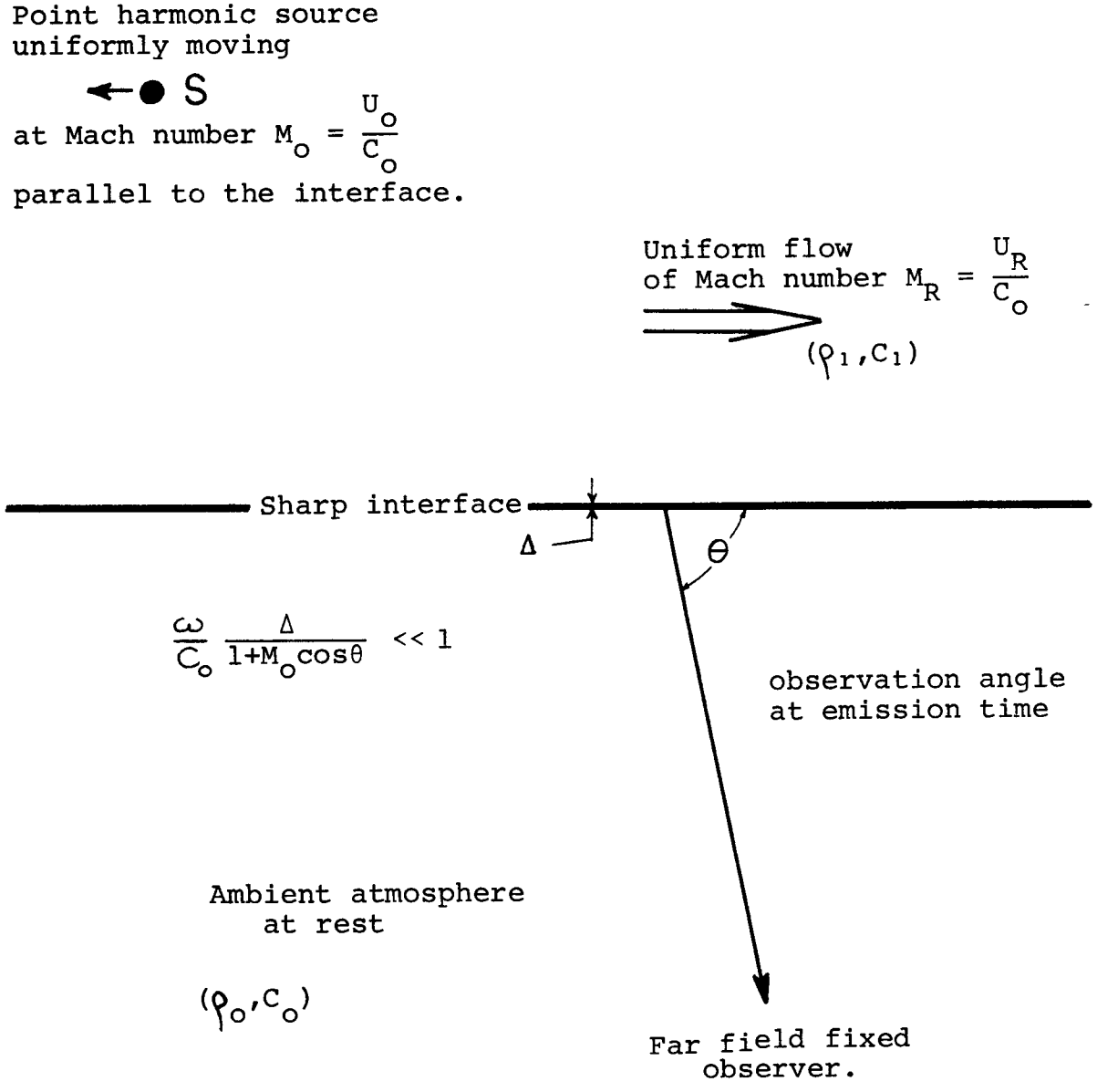

Figure 3

SOUND TRANSMISSION THROUGH THE PLANE BOUNDARY

BETWEEN A MOVING MEDIUM AND A MEDIUM AT REST

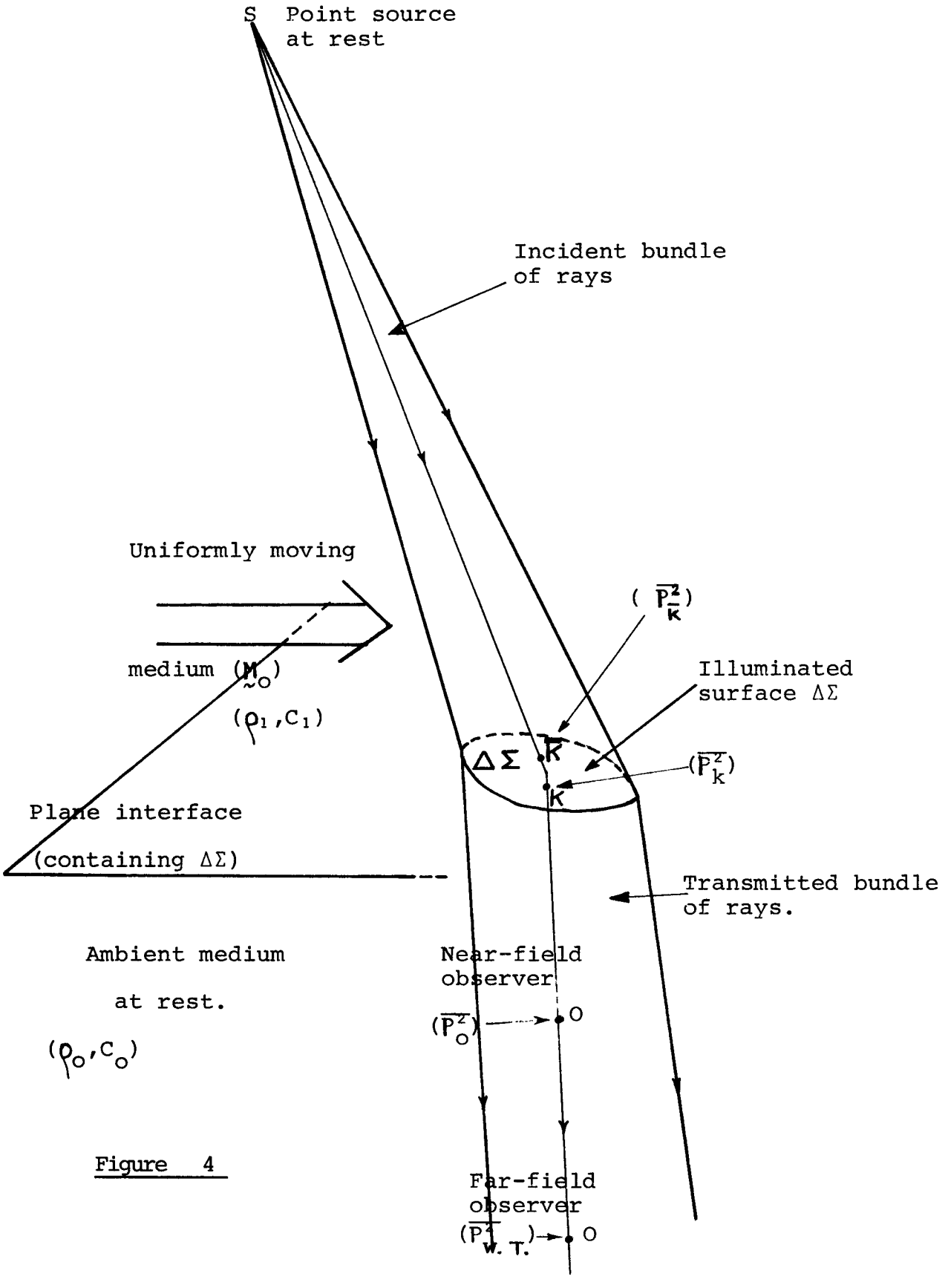

Figure 4

CURVATURE EFFECT - ILLUSTRATION FOR A PLANE INTERFACE

AND AN OBSERVER LOCATED IN THE FLY-OVER PLANE.

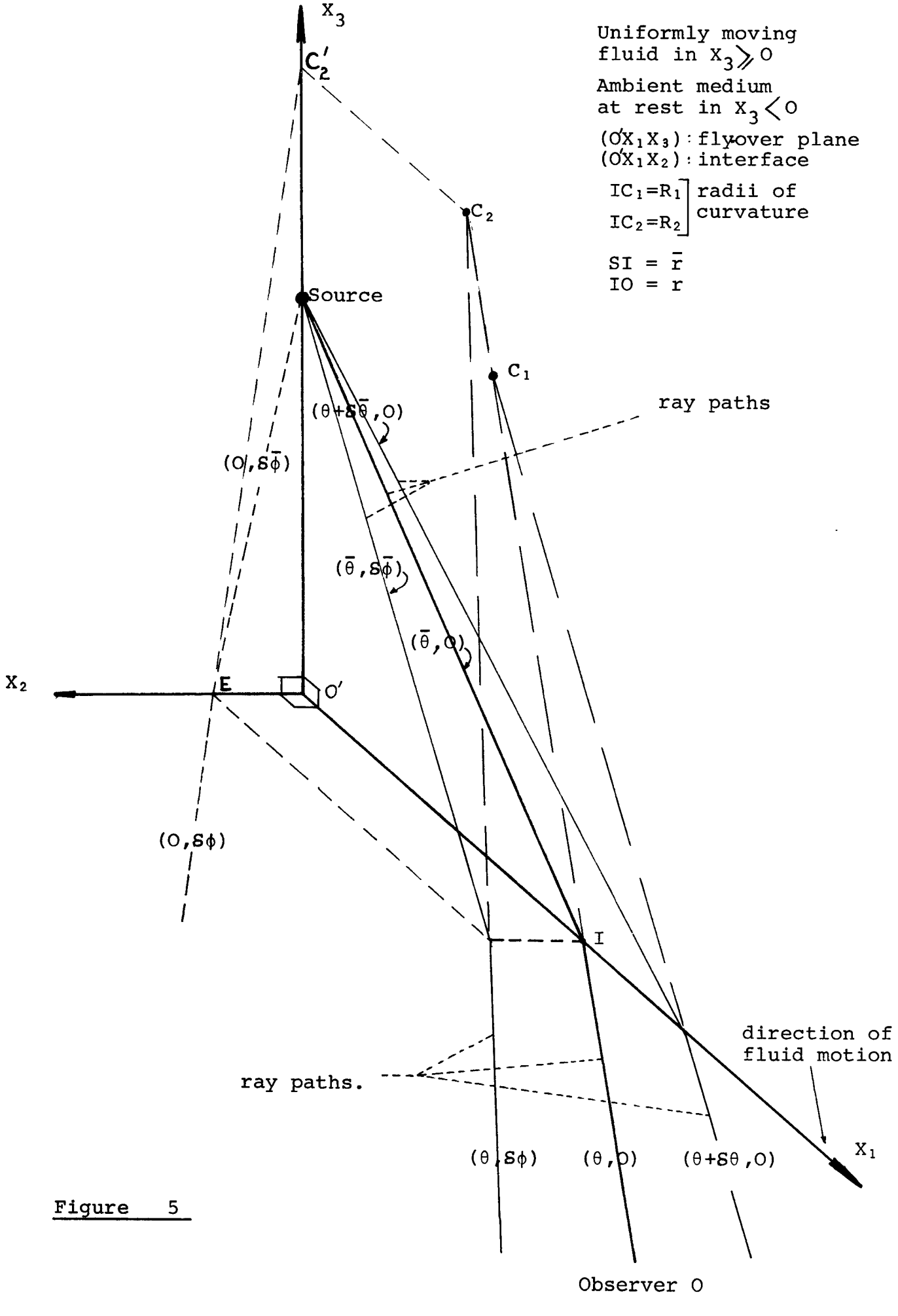

Figure 5

RADIUS OF CURVATURE IN THE DIRECTION OF THE FLOW

PLANE OR CIRCULAR INTERFACE

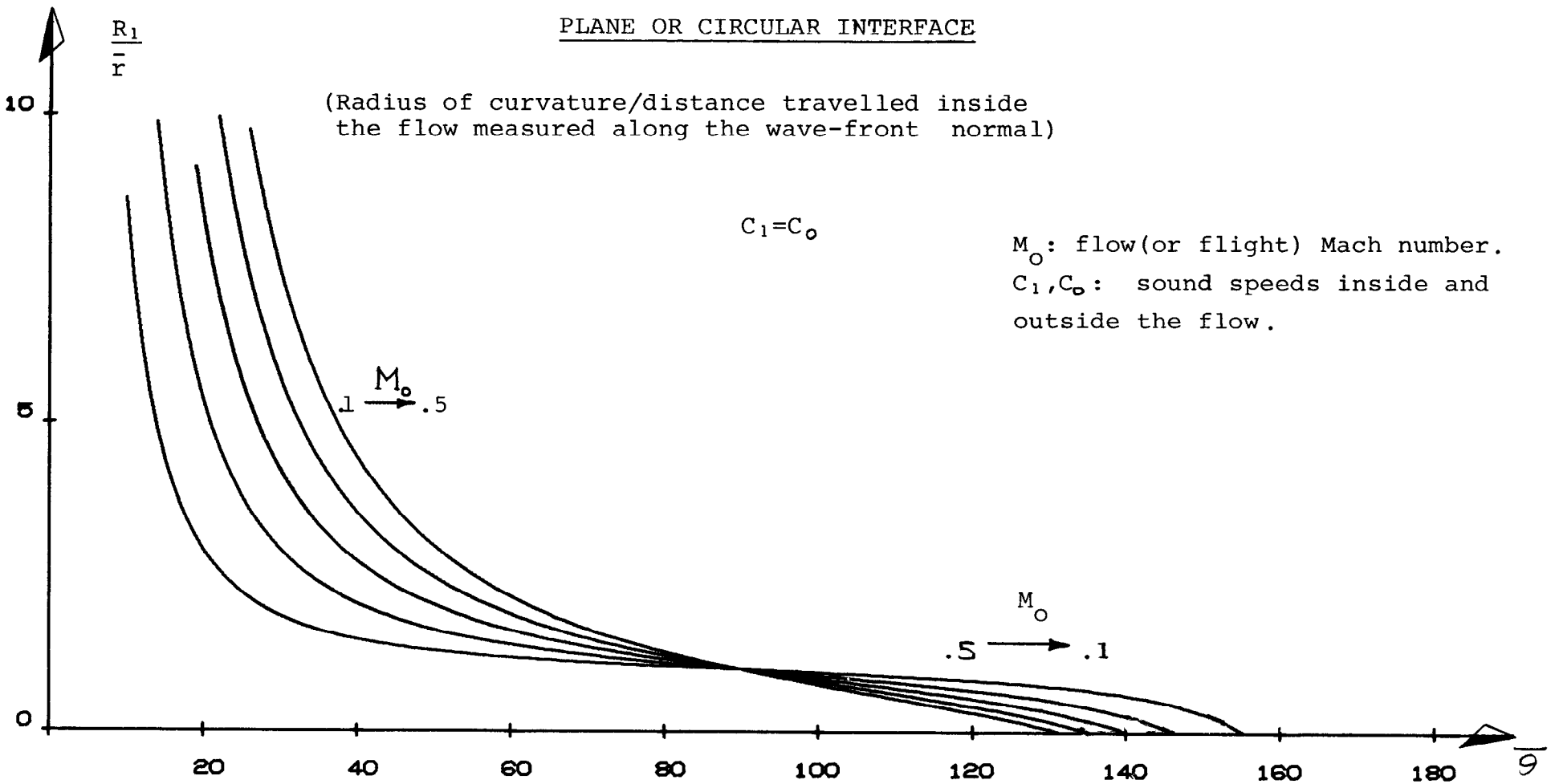

M_o: flow(or flight) Mach number.
C_1, C_o: sound speeds inside and outside the flow.

Angle of the wave-front normals inside the flow relative to the direction of flow (or observation angle at emission time in flight).

FIGURE 6

RADIUS OF CURVATURE IN THE DIRECTION NORMAL TO THE FLOW AND PARALLEL TO A PLANE INTERFACE

M_o, flow (or flight) Mach number.
C_1, C_o: sound speeds inside and outside the flow.

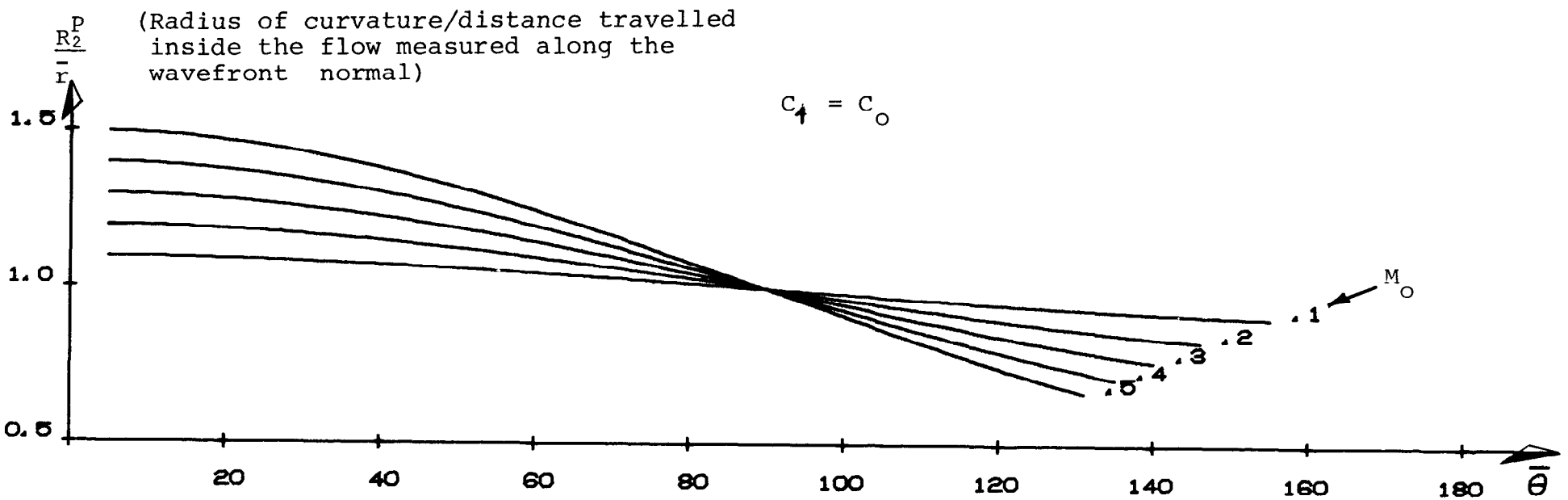

Angle of the wave-front normals inside the flow relative to the direction of flow (or observation angle at emission time in flight)

FIGURE 7

RADIUS OF CURVATURE IN THE DIRECTION NORMAL TO THE FLOW AND TANGENT TO A CIRCULAR INTERFACE

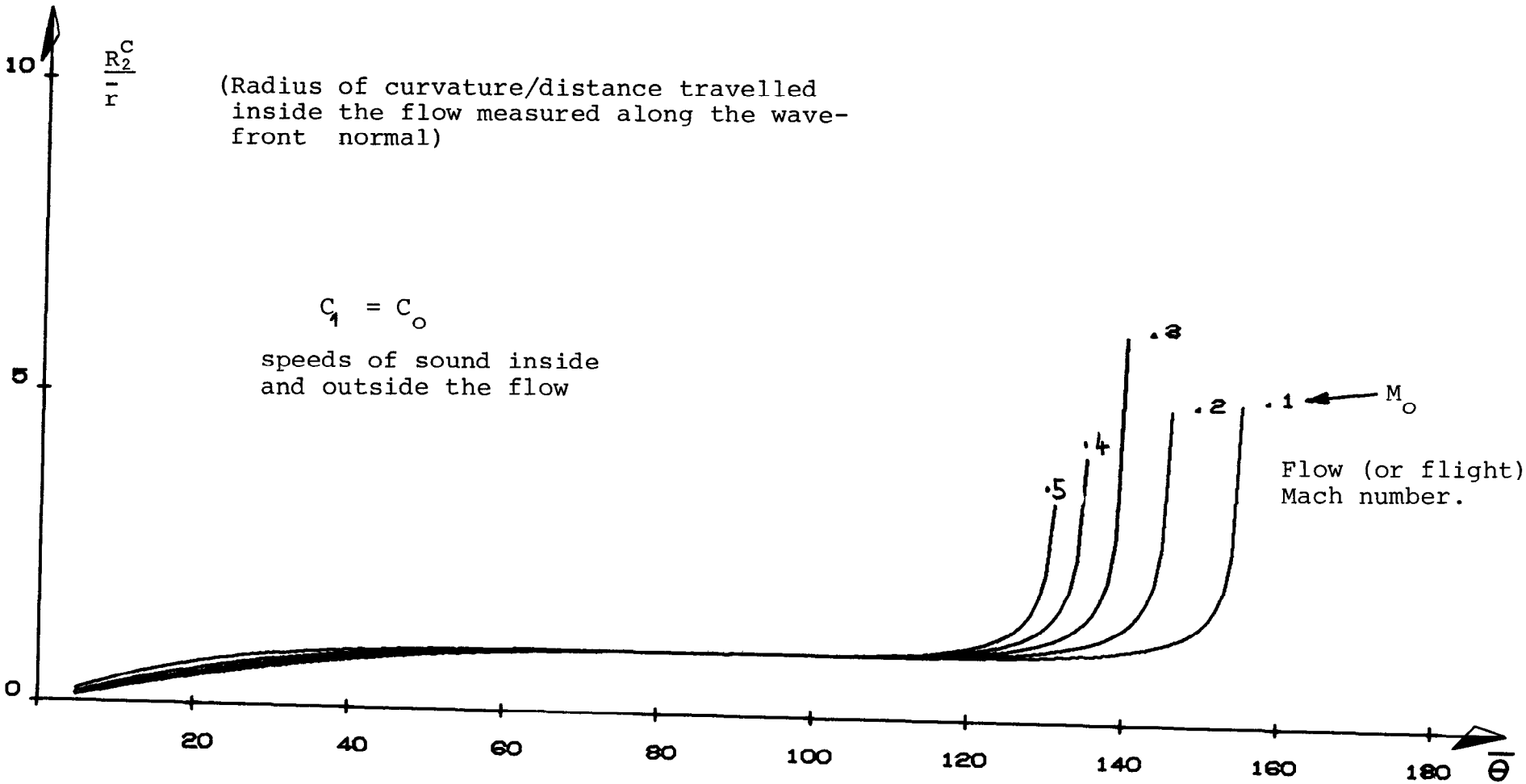

FIGURE 8

"WAVE CURVATURE EFFECT" FOR A PLANE INTERFACE AND A FLY-OVER OBSERVER.

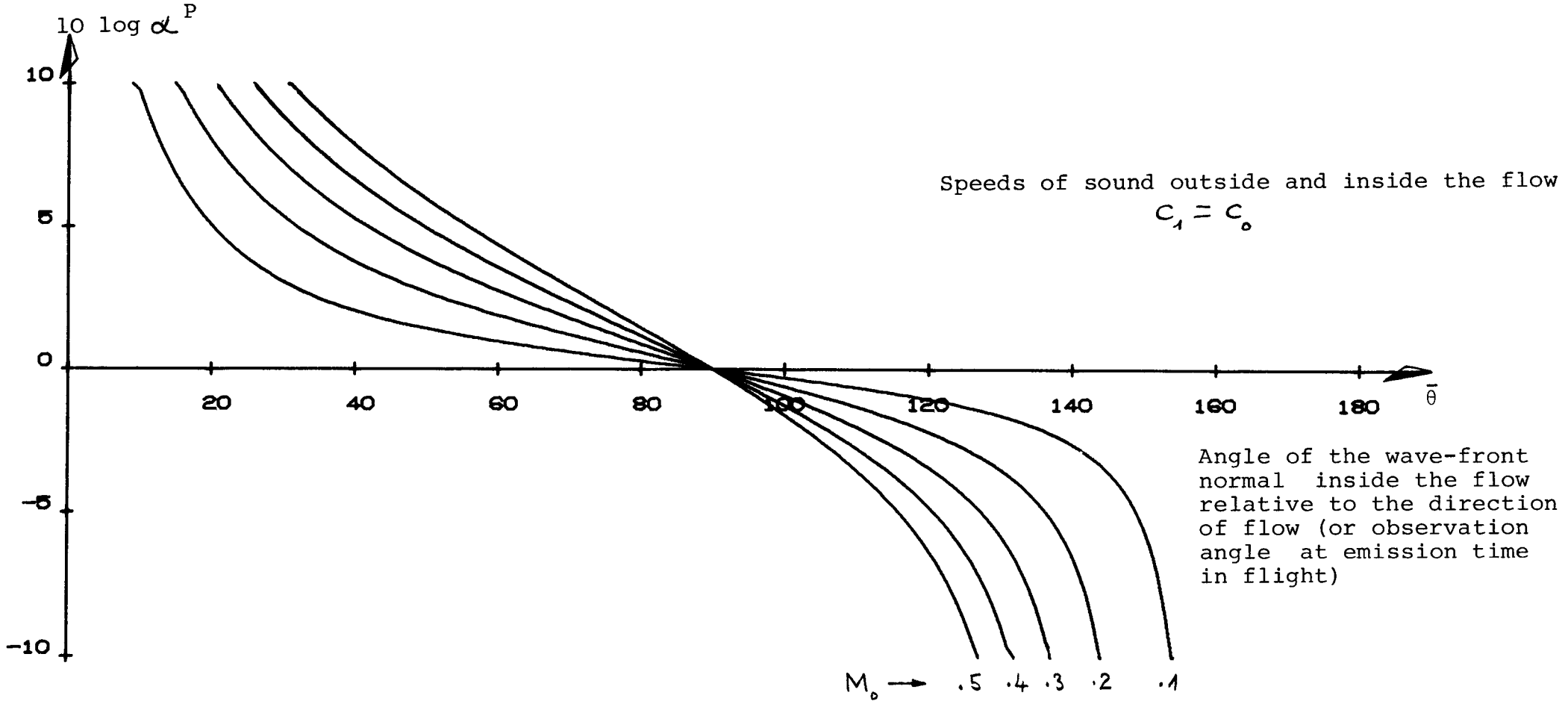

Figure 9

$\alpha^P = \frac{R_1 R_2^P}{\bar{r}^2}$; R_1, R_2^P are the radii of curvature respectively in the directions parallel and normal to the flow, $\bar{r}$ is the distance travelled inside the flow measured along the wave-front normal.

"WAVE CURVATURE EFFECT" FOR A CIRCULAR INTERFACE.

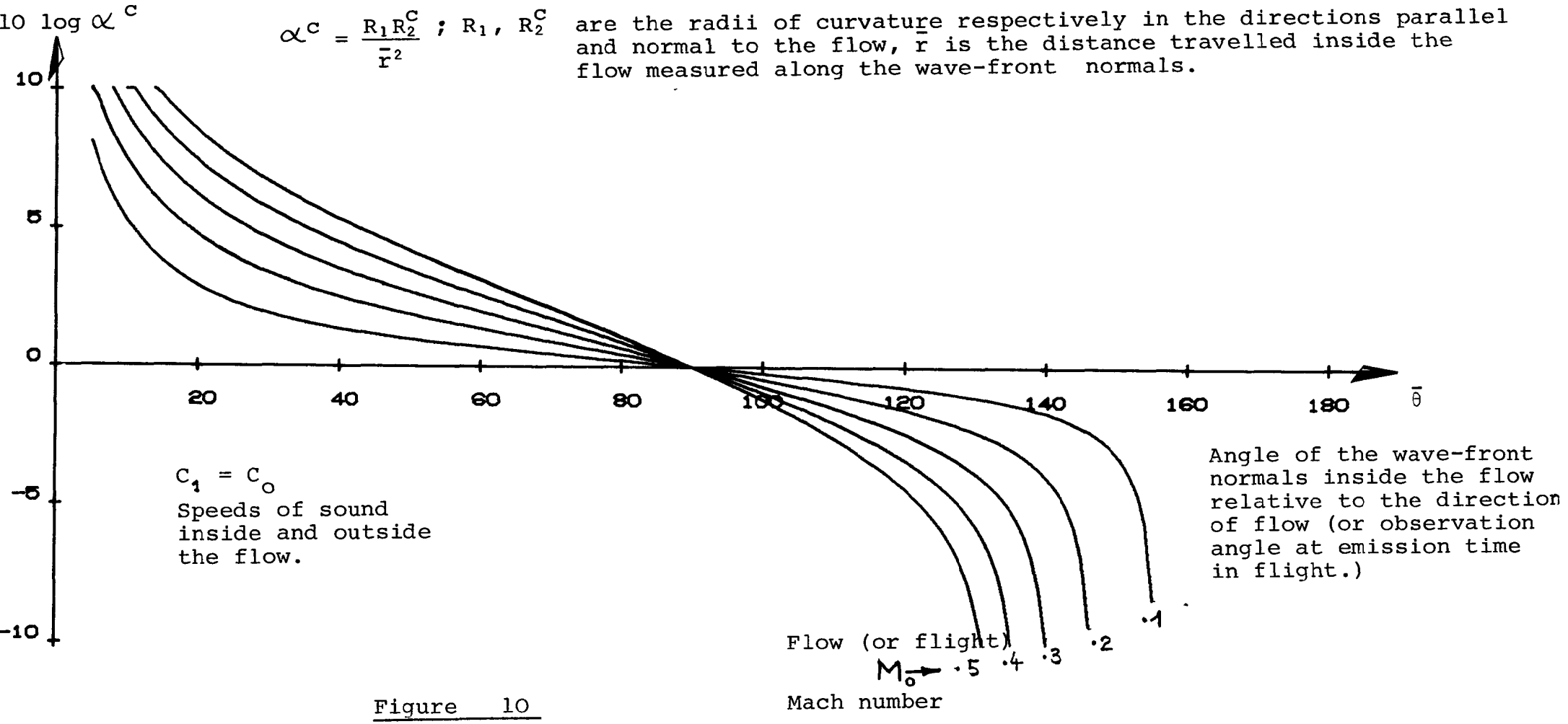

$\alpha^c = \frac{R_1 R_2^c}{\bar{r}^2}$; R_1, R_2^c are the radii of curvature respectively in the directions parallel and normal to the flow, $\bar{r}$ is the distance travelled inside the flow measured along the wave-front normals.

Figure 10

ILLUSTRATION OF THE MULTIPLE REFLECTION MECHANISM.

PLANE (FLY-OVER PLANE) AND CIRCULAR GEOMETRIES

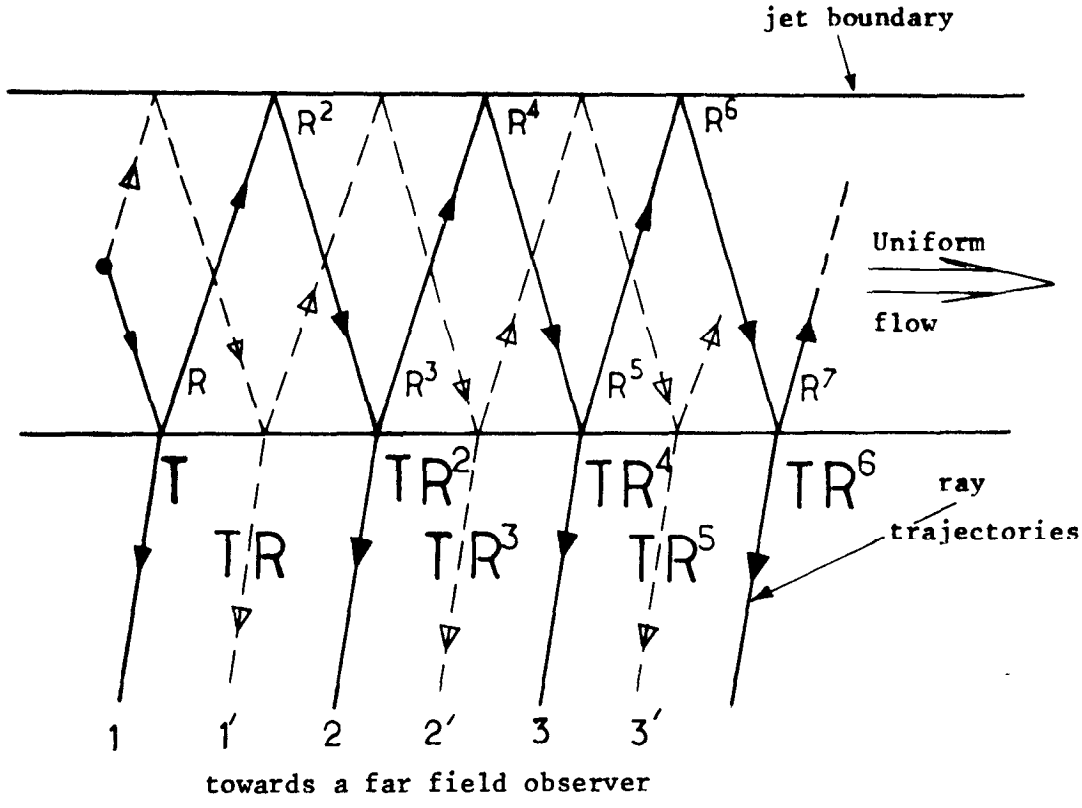

R and T are respectively the reflection and transmission coefficients for a plane wave, R = T - 1. The factor α describing the "wave curvature effect" which equally affects the transmitted waves has been deliberately omitted.

FIGURE 11

WIND-TUNNEL TO FLIGHT COMPARISON

(far field wind-tunnel observer)

PLANE GEOMETRY

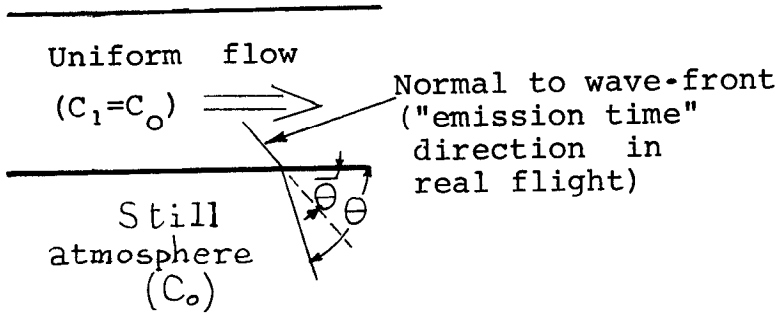

$$\frac{\overline{P_F^2}}{\overline{P_{W.T.}^2}} = \frac{1}{\mathcal{C}\alpha}$$

	Transmission loss and multiple reflections. $\mathcal{C}$	Wave curvature effect α
Multiple reflections totally damped	T^2	$\left(\frac{\partial \bar{\theta}}{\partial \theta}\right)^2$
Multiple reflections taken in and reflected waves assumed correlated	$\frac{T^2}{\lvert 1-(T-1)e^{i\gamma_1 d}\rvert^2}$	$\left(\frac{\partial \bar{\theta}}{\partial \theta}\right)^2$
Multiple reflections taken in but reflected waves assumed uncorrelated	$\frac{T}{2-T}$	$\left(\frac{\partial \bar{\theta}}{\partial \theta}\right)^2$

$$\cos\theta = \frac{\cos\bar{\theta}}{1 + M_o \cos\bar{\theta}} \quad \text{(Snell's law)}$$

T is the transmission coefficient for pressure

d is the slab thickness

$$\gamma_1 = \frac{\sin\bar{\theta}}{1+M_o\cos\bar{\theta}} \quad \frac{2\pi}{\lambda}$$

Figure 12

WIND-TUNNEL TO FLIGHT COMPARISON

(far field wind-tunnel observer)

CIRCULAR INTERFACE

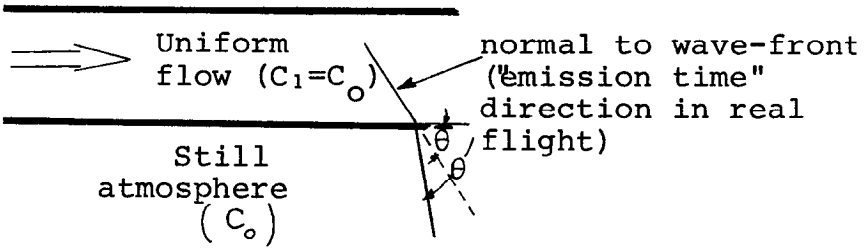

$$\frac{\overline{P_F^2}}{\overline{P_{W.T.}^2}} = \frac{1}{\mathcal{C}\alpha}$$

	Transmission loss and multiple reflections $\mathcal{C}$	Wave curvature effect α
Multiple reflections totally damped	T^2	$(1+M_o\cos\bar{\theta})\,\frac{\partial\bar{\theta}}{\partial\theta}$
Multiple reflections taken in and reflected waves assumed correlated	$\frac{T^2}{\lvert 1+i(T-1)e^{i\overline{\gamma_1 2a}}\rvert^2}$	$(1+M_o\cos\bar{\theta})\,\frac{\partial\bar{\theta}}{\partial\theta}$
Multiple reflections taken in but reflected waves assumed uncorrelated	$\frac{T}{2-T}$	$(1+M_o\cos\bar{\theta})\,\frac{\partial\bar{\theta}}{\partial\theta}$

$$\cos\theta = \frac{\cos\bar{\theta}}{1+M_o\cos\bar{\theta}} \qquad \text{(Snell's law)}$$

T is the transmission coefficient for pressure,

a is the jet radius,

$$\gamma_1 = \frac{\sin\bar{\theta}}{1+M_o\cos\bar{\theta}}\,\frac{2\pi}{\lambda}$$

Figure 13

SOUND LEVEL CORRECTIONS TO CONVERT WIND-TUNNEL MEASUREMENTS TO FREE FLIGHT

PLANE INTERFACE CASE

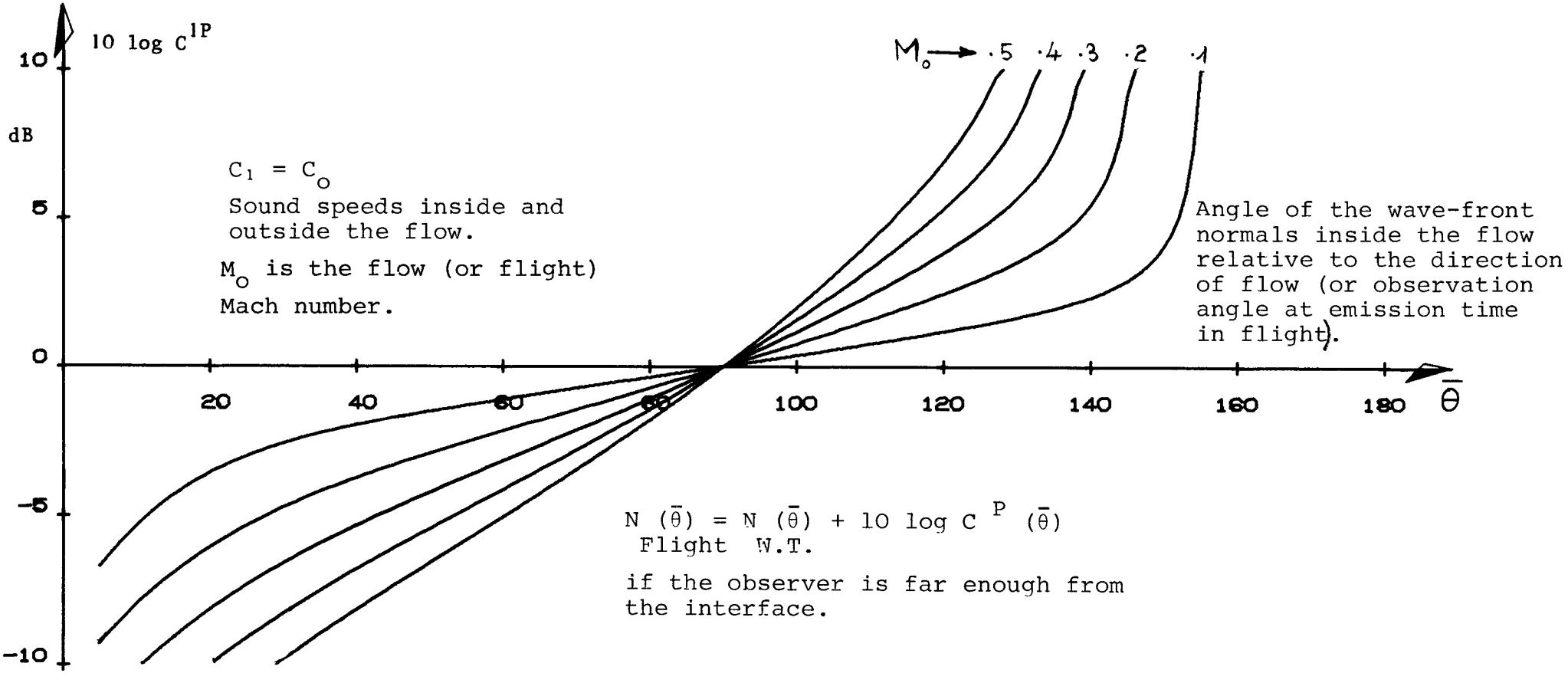

$C_1 = C_o$

Sound speeds inside and outside the flow.

M_o is the flow (or flight) Mach number.

Angle of the wave-front normals inside the flow relative to the direction of flow (or observation angle at emission time in flight).

$$N_{Flight}(\bar{\theta}) = N_{W.T.}(\bar{\theta}) + 10 \log C^{P}(\bar{\theta})$$

if the observer is far enough from the interface.

Figure 14

EFFECT OF MULTIPLE REFLECTIONS ON SOUND LEVEL CORRECTIONS TO CONVERT WIND-TUNNEL MEASUREMENTS TO FREE FLIGHT FOR A PLANE INTERFACE AND A FLOW MACH NUMBER M_o = .4 .

h is the source-interface distance, λ the wavelength of the incident sound and $\bar{\theta}$ the "emission time" observation angle in flight.

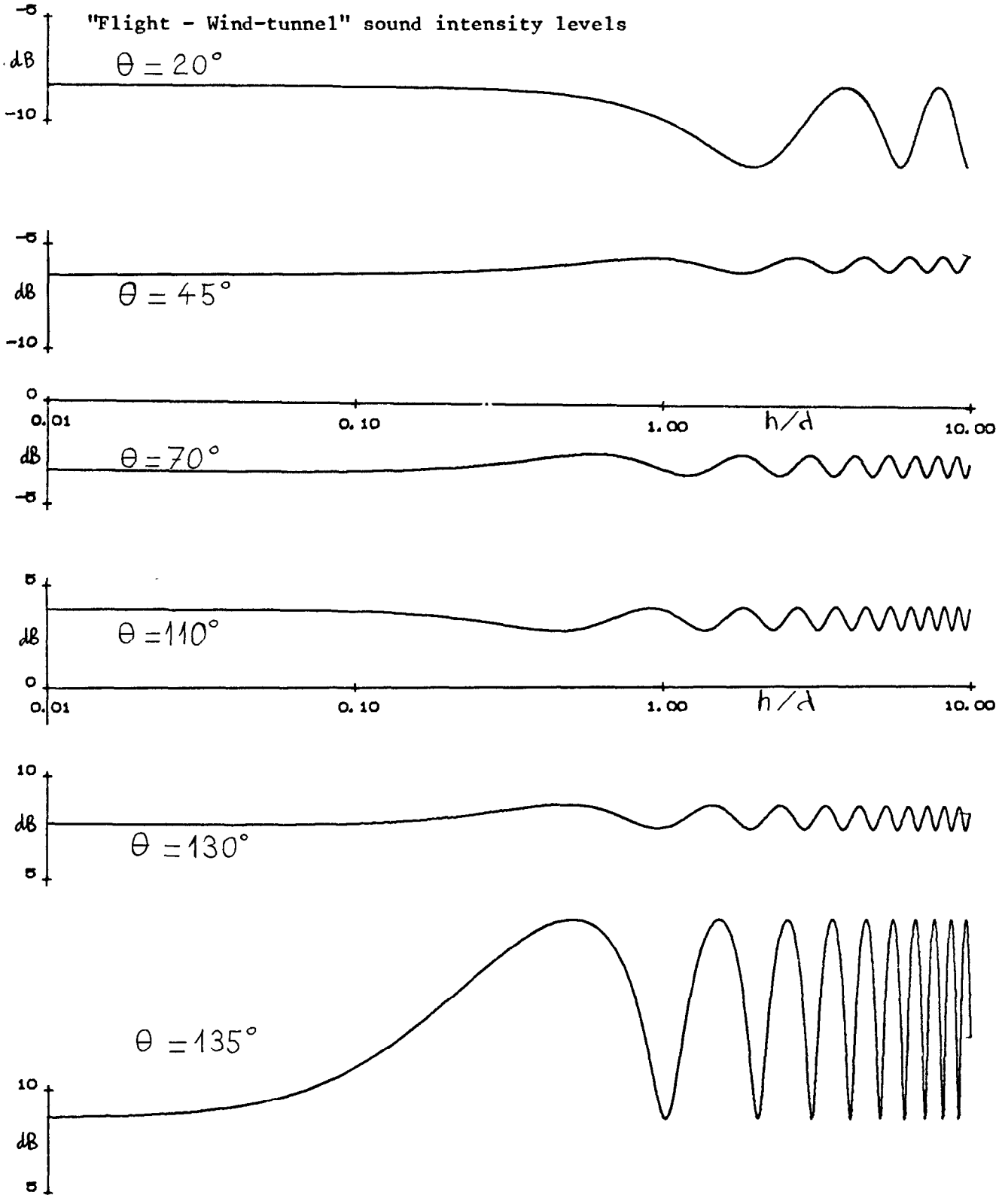

FIGURE 15

EFFECT OF MULTIPLE REFLECTIONS ON SOUND LEVEL CORRECTIONS TO CONVERT WIND-TUNNEL MEASUREMENTS TO FREE FLIGHT FOR A CIRCULAR INTERFACE AND A FLOW MACH NUMBER M_o = .4 .

"a" is the flow radius, λ the wavelength of the incident sound and $\bar{\theta}$ the "emission time" observation angle in flight.

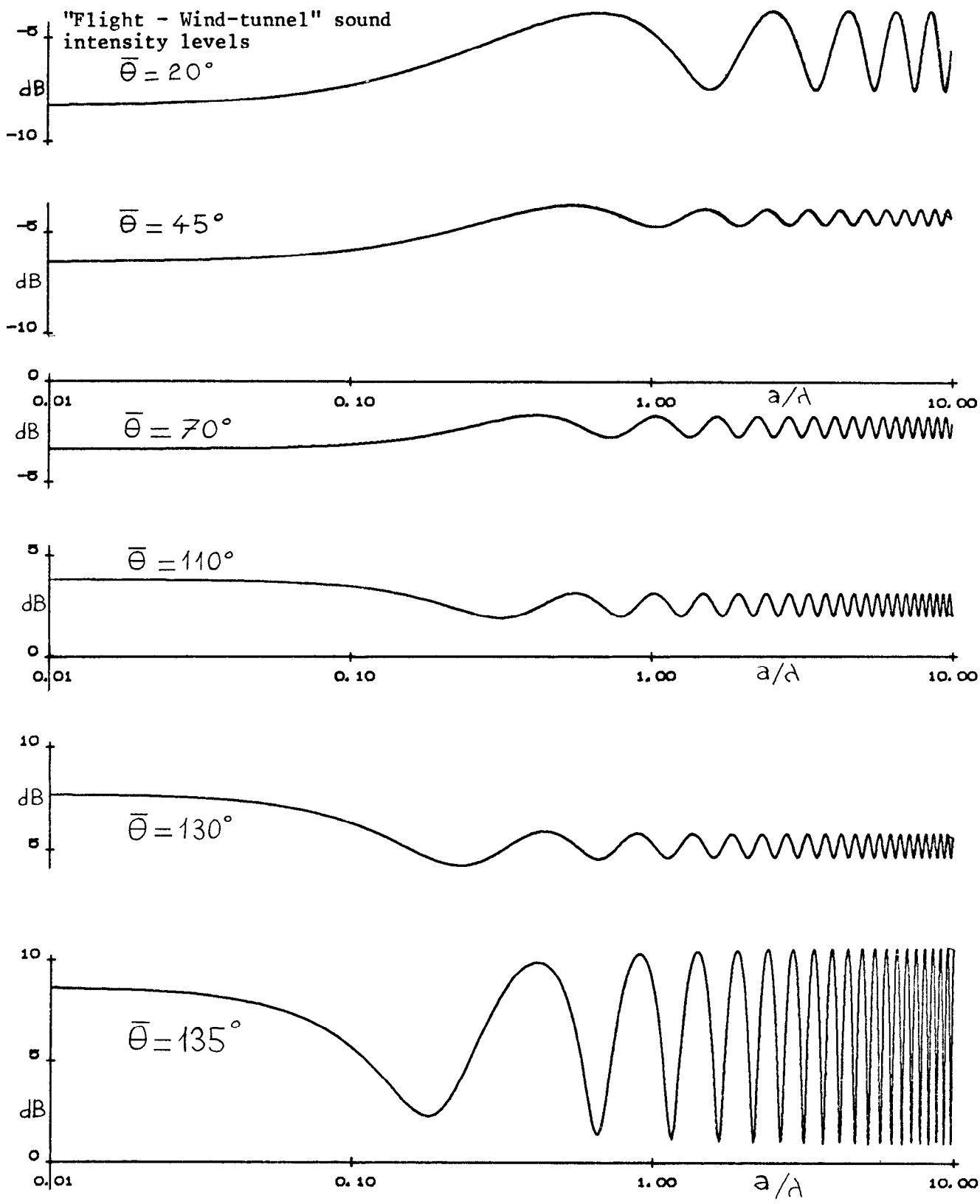

FIGURE 16

SOUND LEVEL CORRECTIONS TO CONVERT WIND-TUNNEL MEASUREMENTS

TO FREE FLIGHT.

CIRCULAR INTERFACE CASE

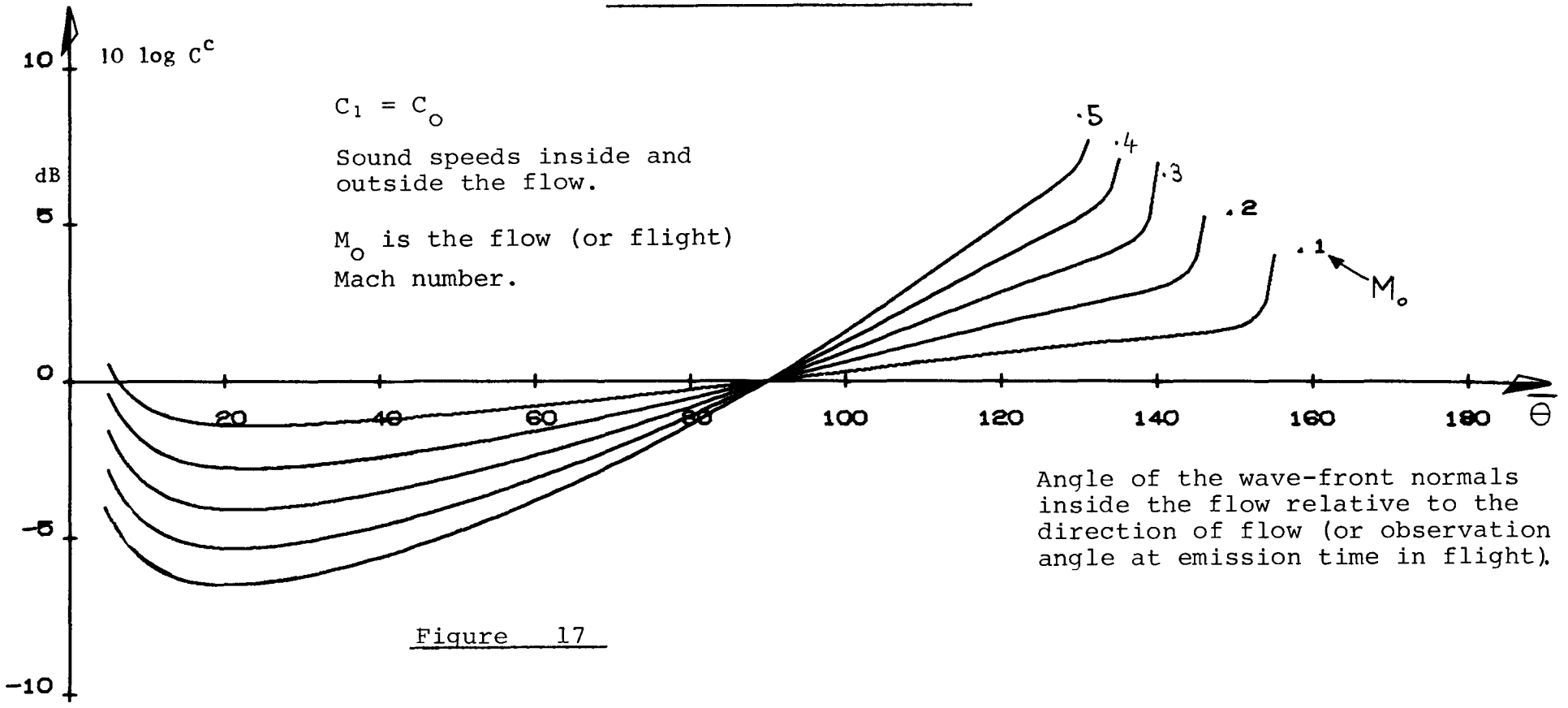

Figure 17

$N(\bar{\theta}) = N(\bar{\theta}) + 10 \log C^c$

Flight W.T.

if the observer is far enough from the interface.

INFLUENCE OF INTERFACE GEOMETRY

ON SOUND LEVEL CORRECTION

(FAR-FIELD OBSERVER)

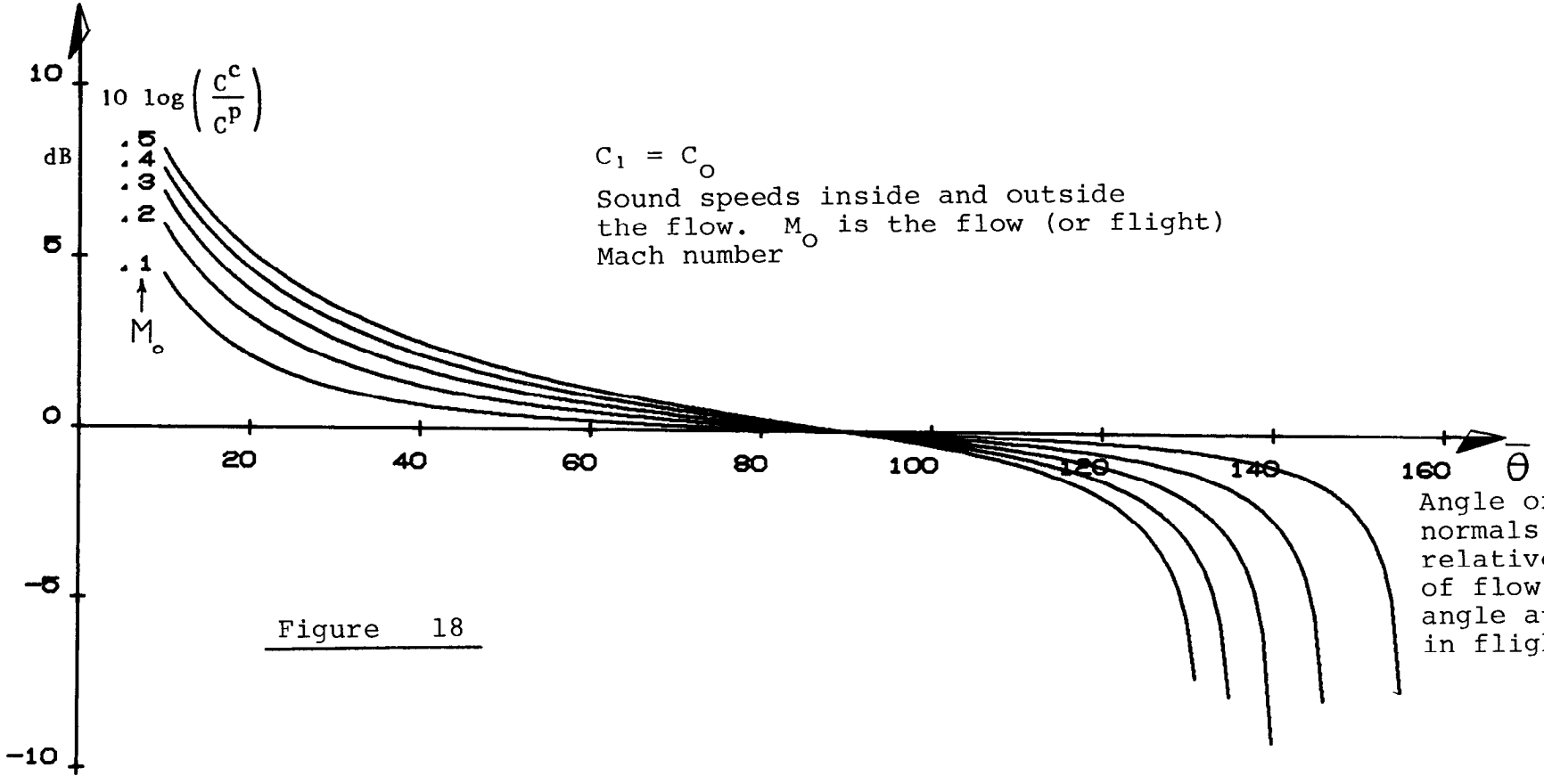

$C_1 = C_o$

Sound speeds inside and outside the flow. M_o is the flow (or flight) Mach number

Angle of the wave-front normals inside the flow relative to the direction of flow (or observation angle at emission time in flight).

Figure 18

10 log C^C and 10 log C^P are the sound level corrections to convert wind-tunnel measurements to free flight respectively for a circular interface and for a plane interface.

GEOMETRY OF A WIND-TUNNEL CONFIGURATION

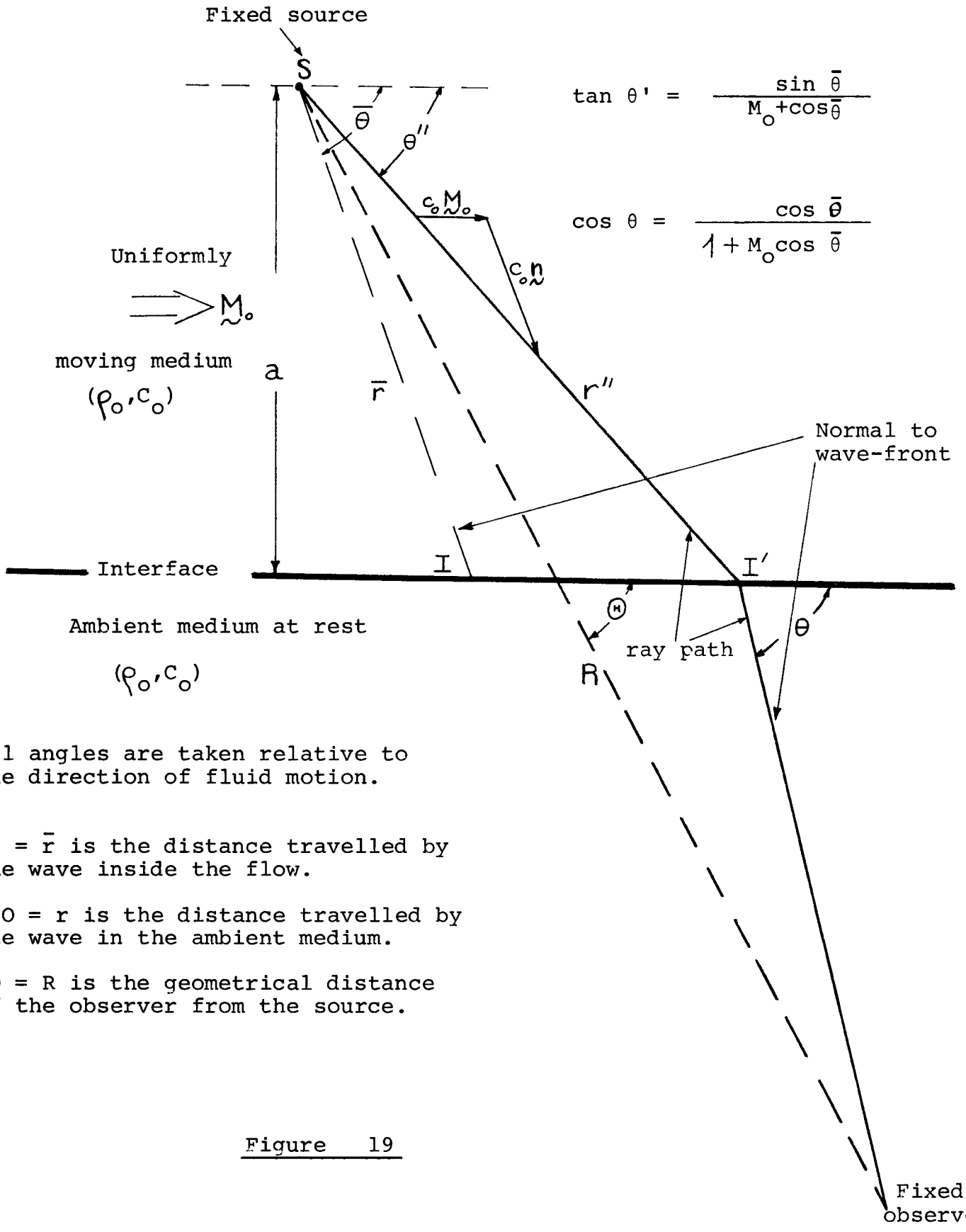

$$\tan \theta' = \frac{\sin \bar{\theta}}{M_o + \cos \bar{\theta}}$$

$$\cos \theta = \frac{\cos \bar{\theta}}{1 + M_o \cos \bar{\theta}}$$

All angles are taken relative to the direction of fluid motion.

SI = $\bar{r}$ is the distance travelled by the wave inside the flow.

I'O = r is the distance travelled by the wave in the ambient medium.

SO = R is the geometrical distance of the observer from the source.

Figure 19

ANGULAR CORRECTION TO CONVERT WIND-TUNNEL MEASUREMENTS TO REAL FLIGHT

PLANE OR CIRCULAR INTERFACE

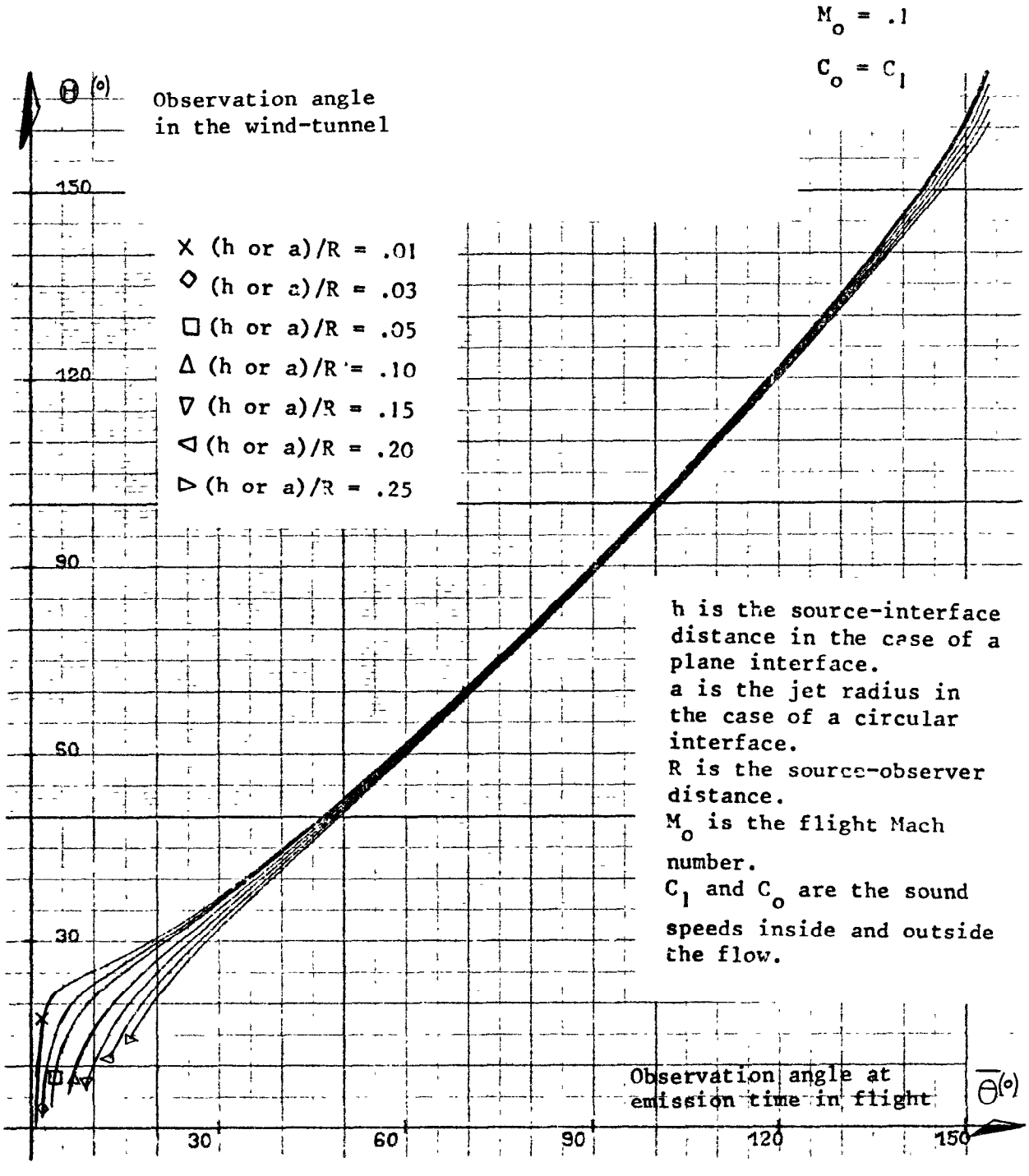

FIGURE 20

ANGULAR CORRECTION TO CONVERT WIND-TUNNEL MEASUREMENTS TO REAL FLIGHT

PLANE OR CIRCULAR INTERFACE

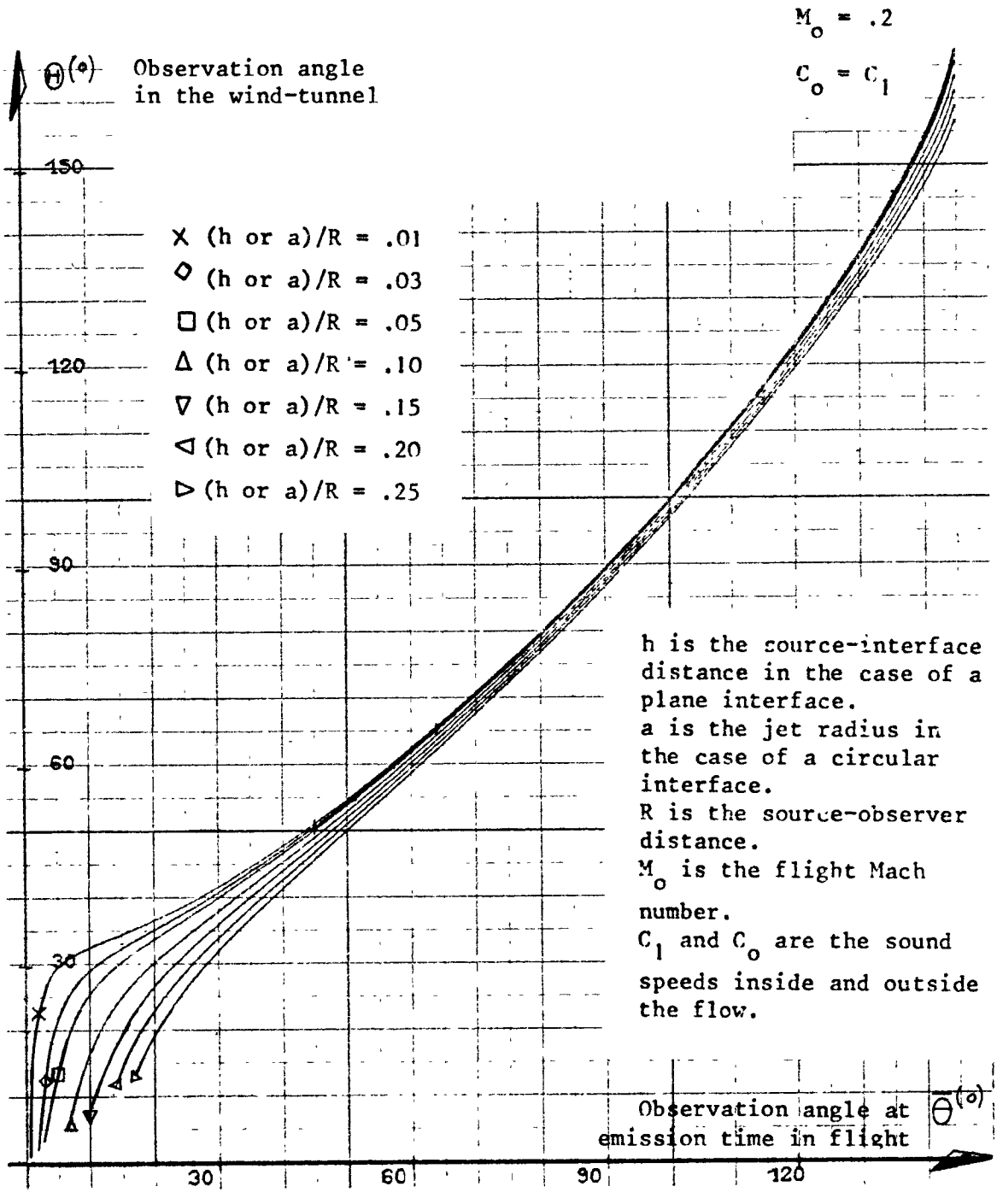

FIGURE 21

ANGULAR CORRECTION TO CONVERT WIND-TUNNEL MEASUREMENTS TO REAL FLIGHT

PLANE OR CIRCULAR INTERFACE

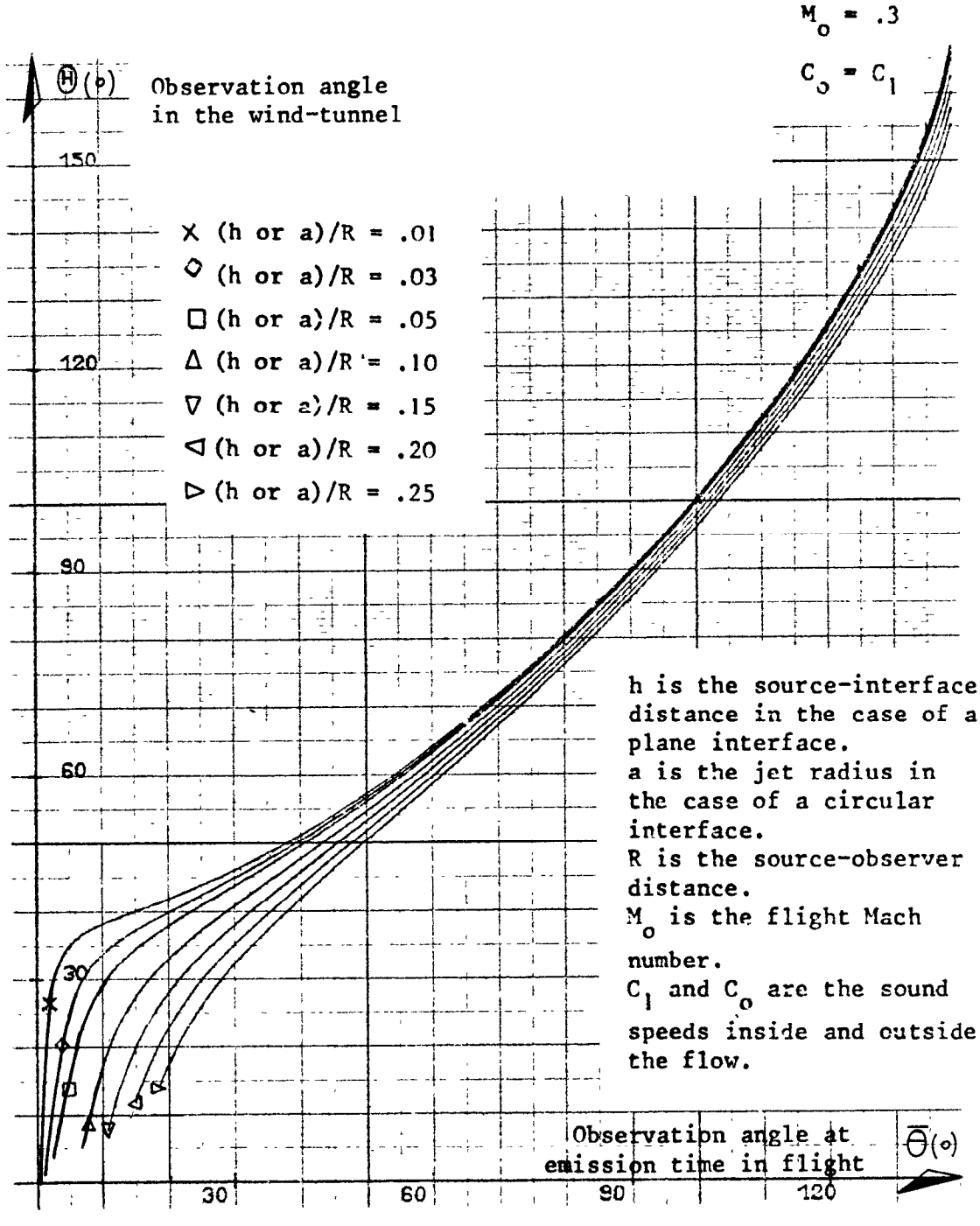

FIGURE 22

ANGULAR CORRECTION TO CONVERT WIND-TUNNEL MEASUREMENTS TO REAL FLIGHT

PLANE OR CIRCULAR INTERFACE

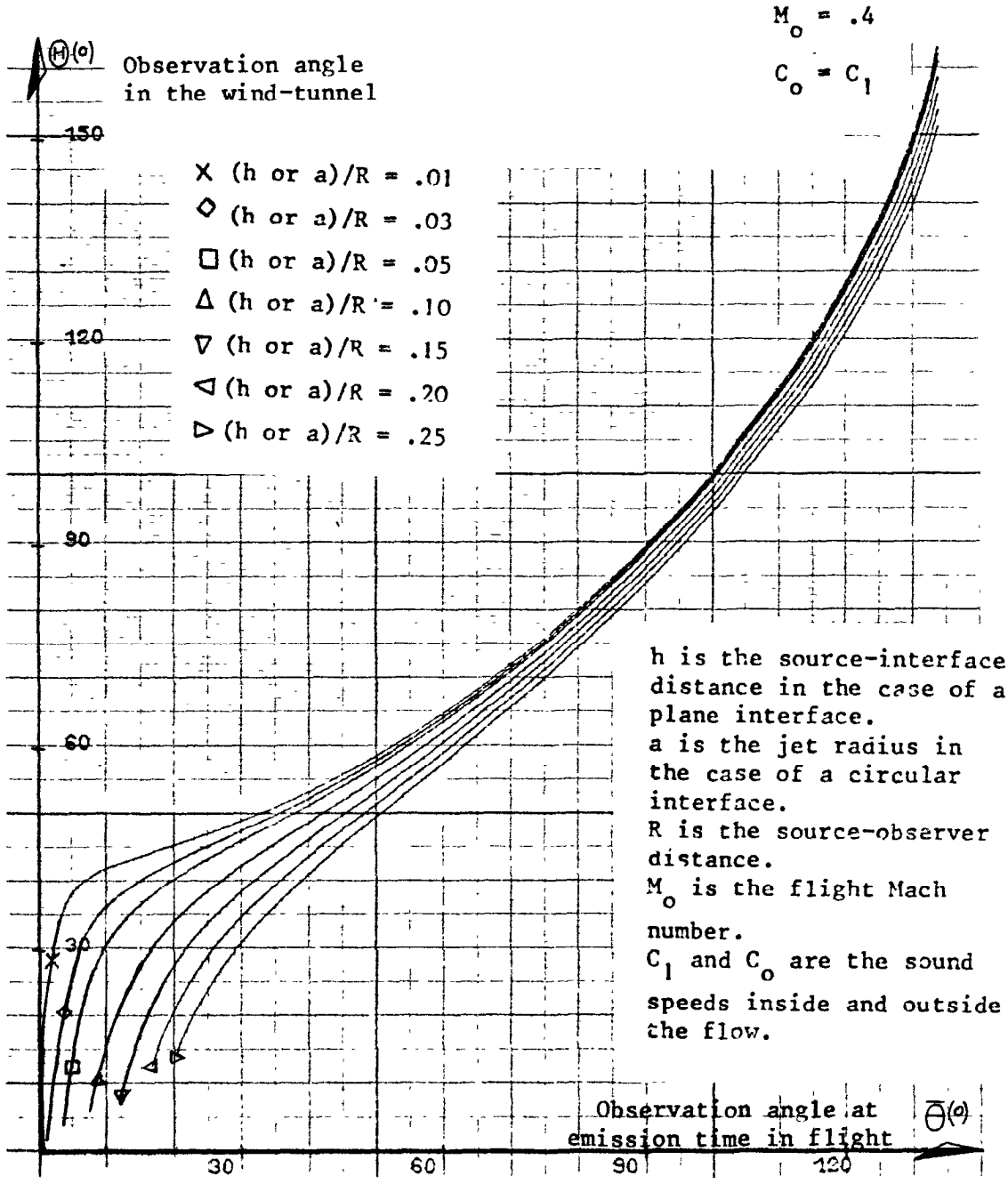

FIGURE 23

ANGULAR CORRECTION TO CONVERT WIND-TUNNEL MEASUREMENTS TO REAL FLIGHT

PLANE OR CIRCULAR INTERFACE

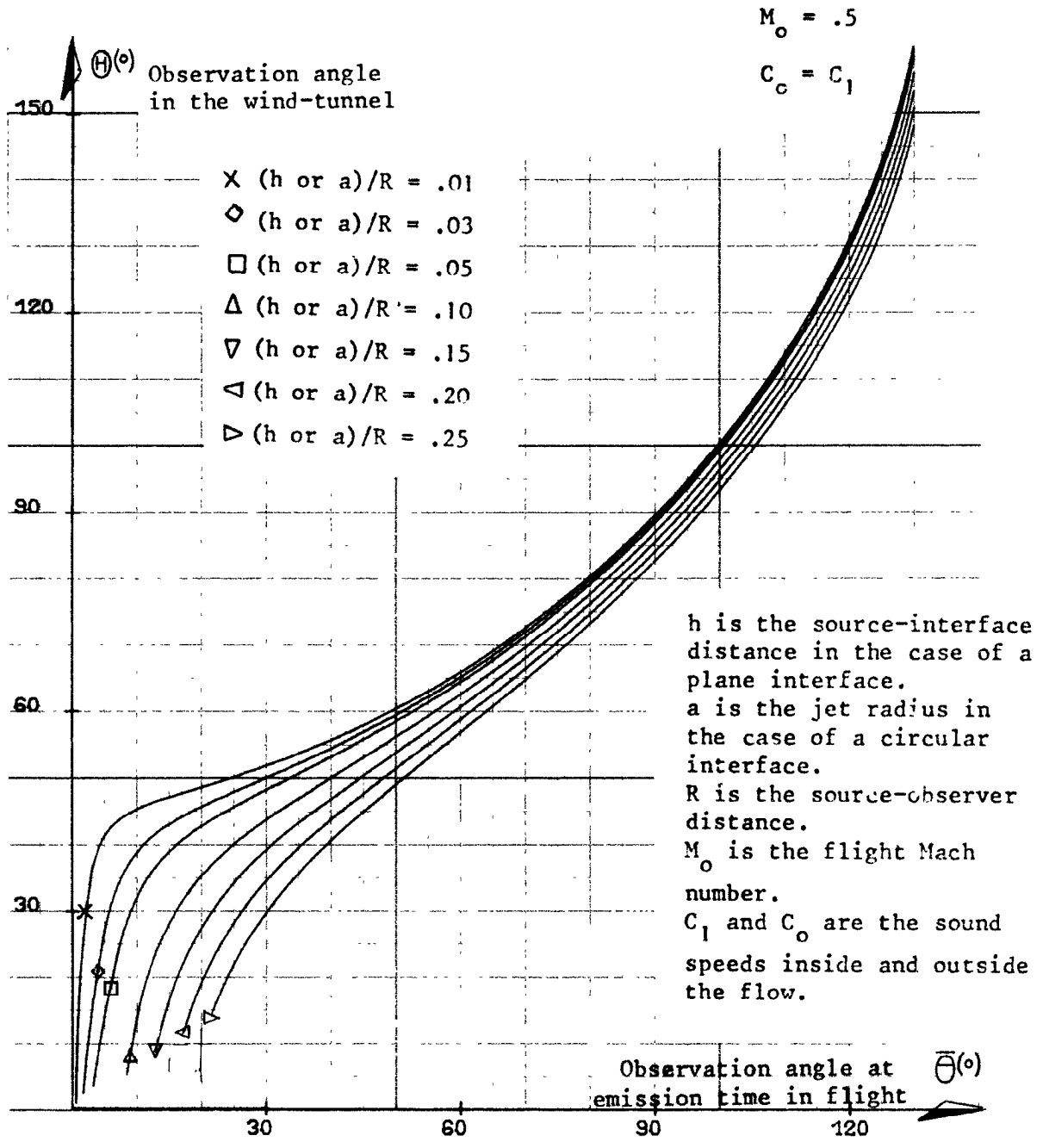

FIGURE 24

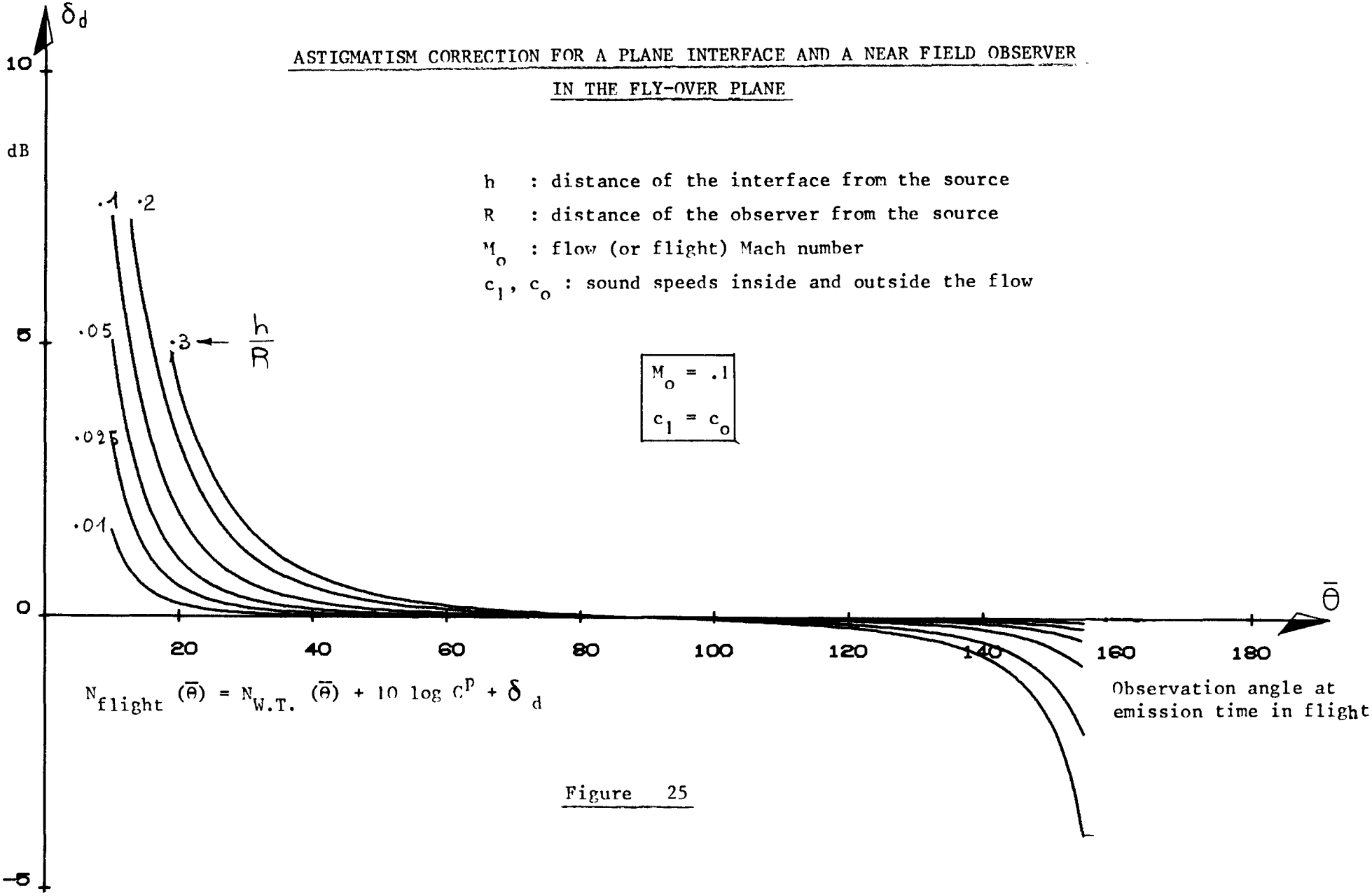
ASTIGMATISM CORRECTION FOR A PLANE INTERFACE AND A NEAR FIELD OBSERVER IN THE FLY-OVER PLANE
h : distance of the interface from the source
R : distance of the observer from the source
M_o : flow (or flight) Mach number
c_1, c_o : sound speeds inside and outside the flow
M_o = .1
c_1 = c_o
δ_d
10
dB
5
0
-5
.1
.2
.3
.05
.025
.01
h/R
20
40
60
80
100
120
140
160
180
θ̄
N_flight (θ̄) = N_W.T. (θ̄) + 10 log C^p + δ_d
Observation angle at emission time in flight

Figure 25

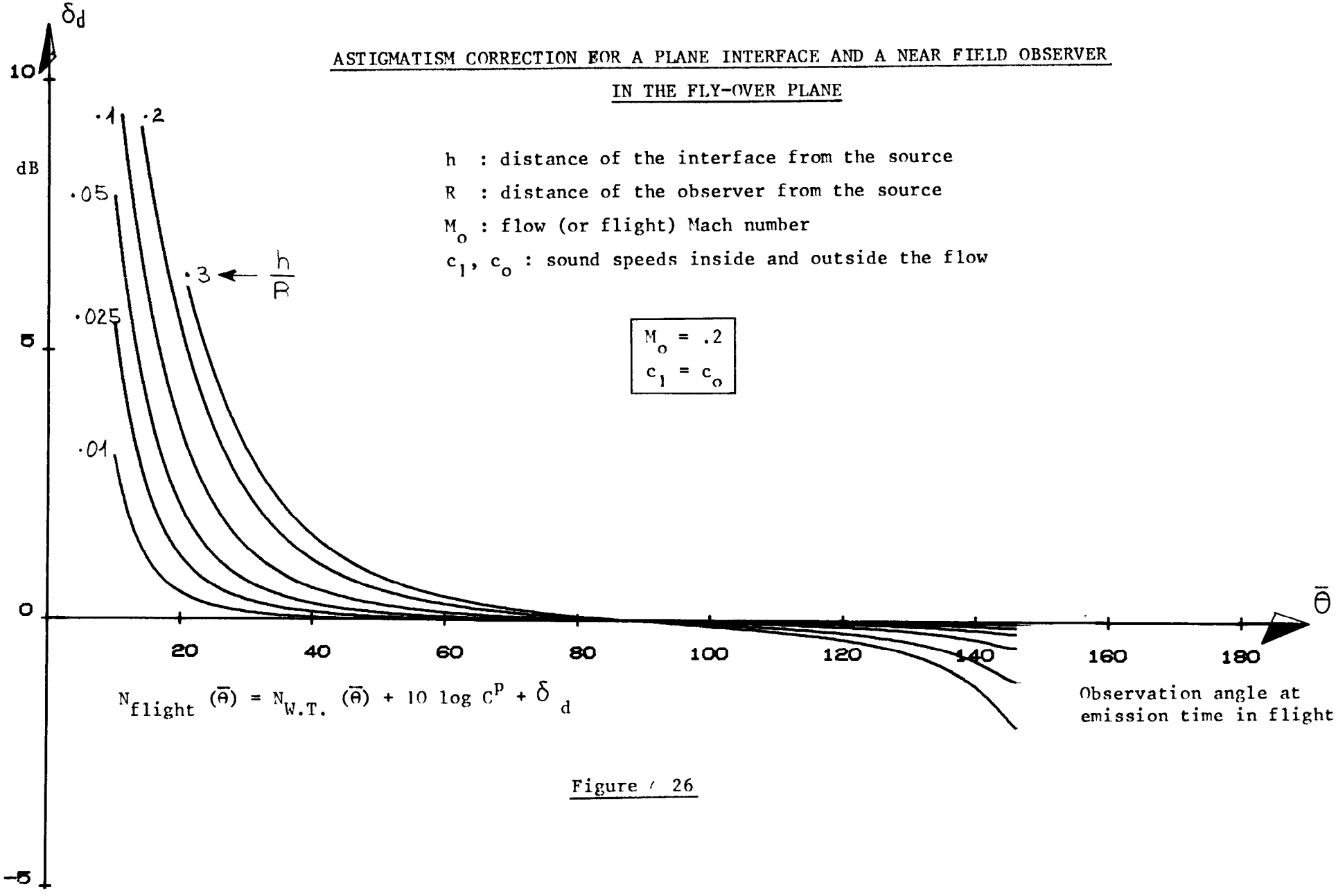

ASTIGMATISM CORRECTION FOR A PLANE INTERFACE AND A NEAR FIELD OBSERVER IN THE FLY-OVER PLANE

h : distance of the interface from the source

R : distance of the observer from the source

M_o : flow (or flight) Mach number

c_1, c_o : sound speeds inside and outside the flow

$M_o = .2$

$c_1 = c_o$

Figure / 26

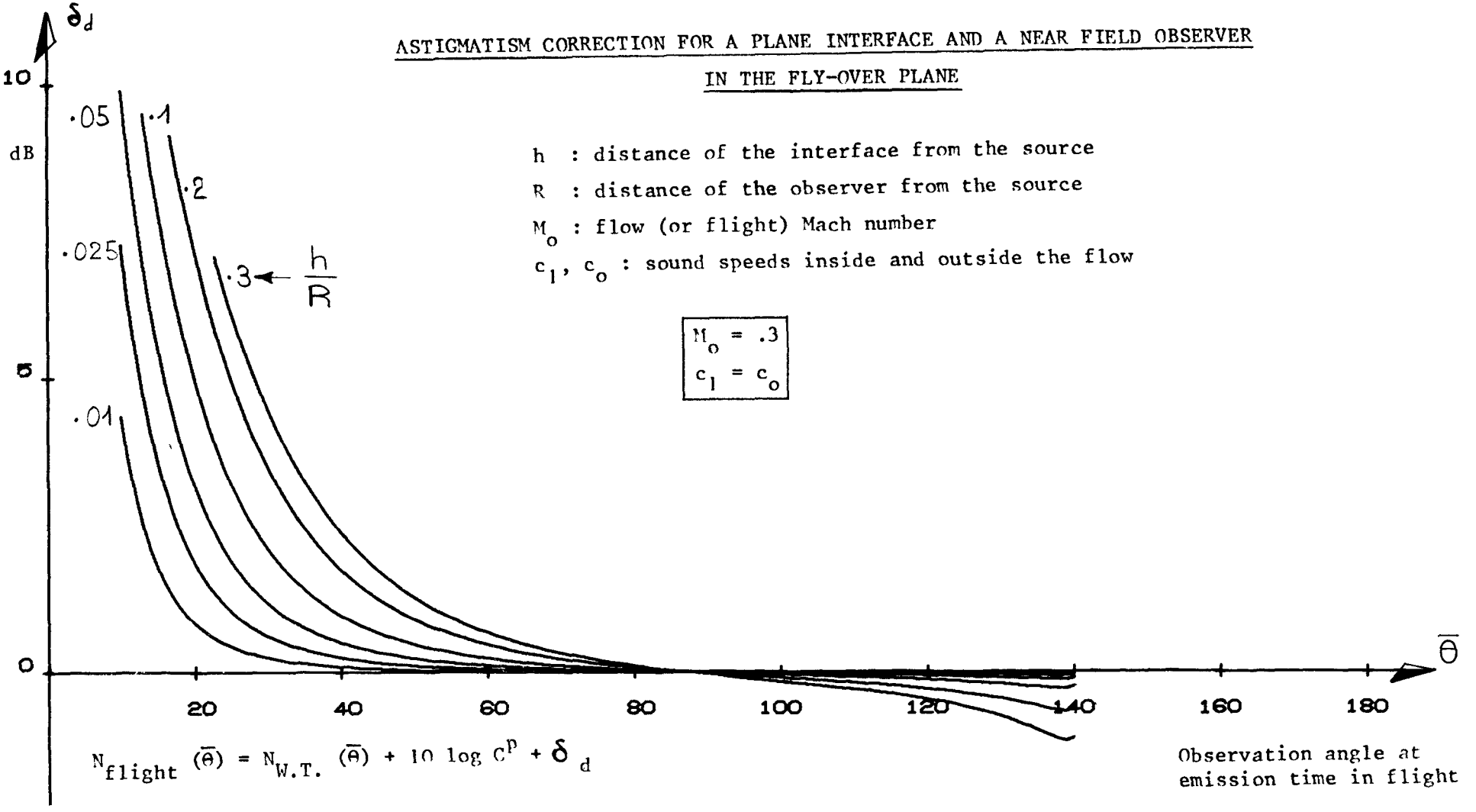
ASTIGMATISM CORRECTION FOR A PLANE INTERFACE AND A NEAR FIELD OBSERVER
IN THE FLY-OVER PLANE
h : distance of the interface from the source
R : distance of the observer from the source
M_o : flow (or flight) Mach number
c_1, c_o : sound speeds inside and outside the flow
$M_o = .3$
$c_1 = c_o$
δ_d
dB
10
5
0
.05
.1
.2
.3 ← h/R
.025
.01
20
40
60
80
100
120
140
160
180
$\bar{\theta}$
$N_{flight}(\bar{\theta}) = N_{W.T.}(\bar{\theta}) + 10 \log C^p + \delta_d$
Observation angle at emission time in flight

Figure 27

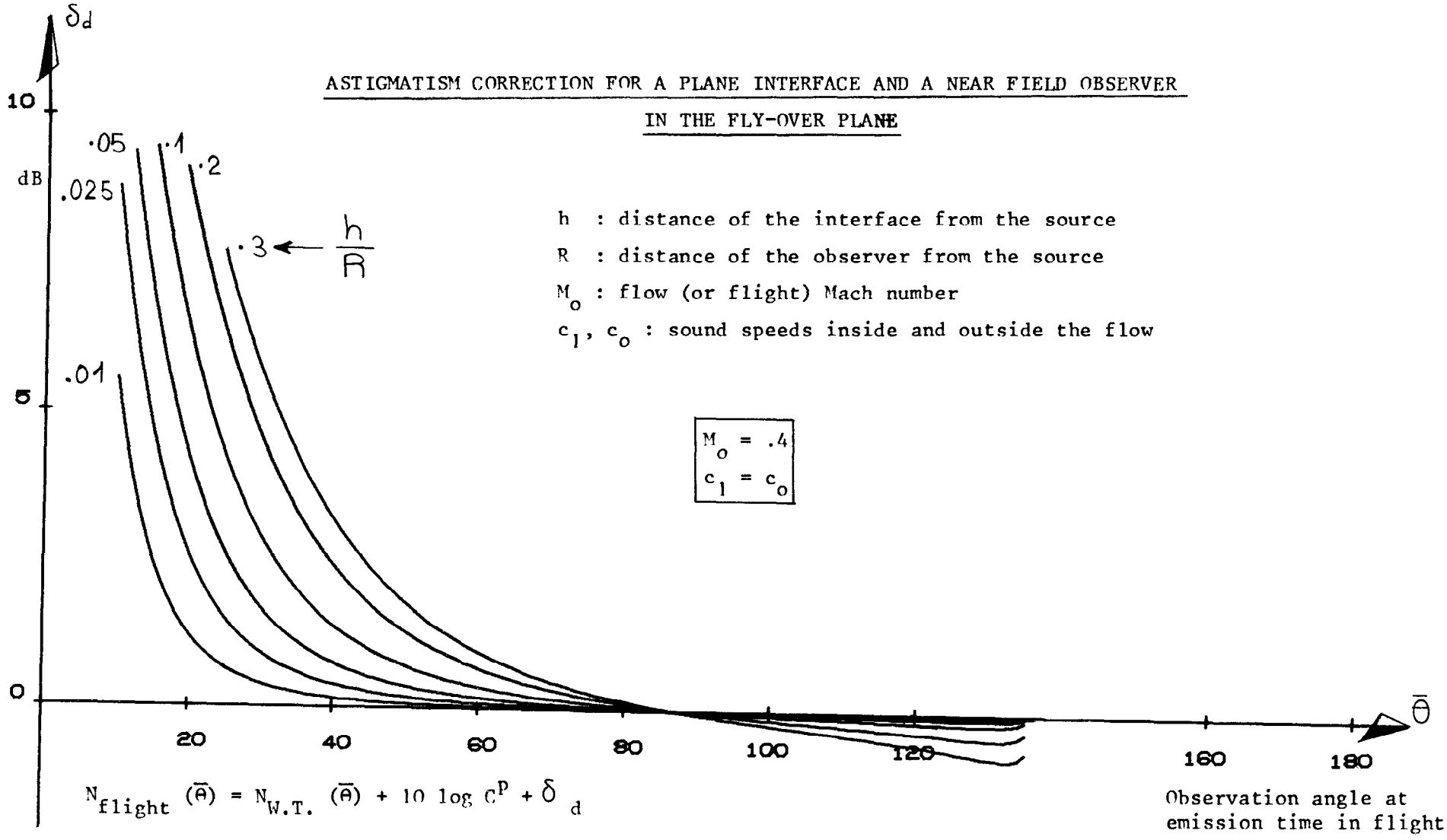

ASTIGMATISM CORRECTION FOR A PLANE INTERFACE AND A NEAR FIELD OBSERVER IN THE FLY-OVER PLANE

h : distance of the interface from the source

R : distance of the observer from the source

M_o : flow (or flight) Mach number

c_1, c_o : sound speeds inside and outside the flow

$M_o = .4$

$c_1 = c_o$

Figure 28

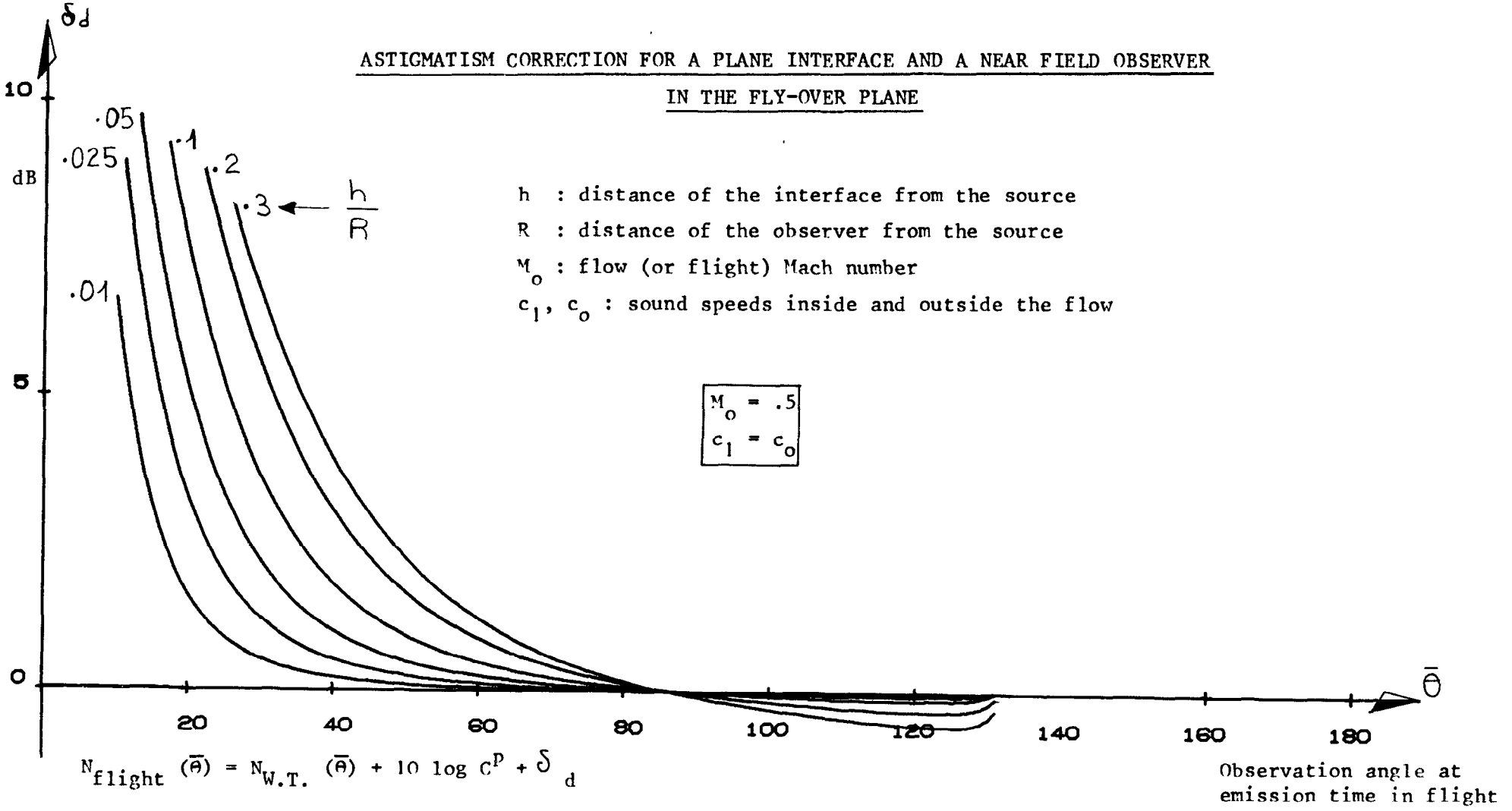
ASTIGMATISM CORRECTION FOR A PLANE INTERFACE AND A NEAR FIELD OBSERVER
IN THE FLY-OVER PLANE
δd
10
dB
5
0
.05
.025
.01
.1
.2
.3
h/R
h : distance of the interface from the source
R : distance of the observer from the source
M0 : flow (or flight) Mach number
c1, c0 : sound speeds inside and outside the flow
M0 = .5
c1 = c0
20
40
60
80
100
120
140
160
180
θ̄
N flight (θ̄) = N W.T. (θ̄) + 10 log C^p + δ d
Observation angle at emission time in flight

Figure 29

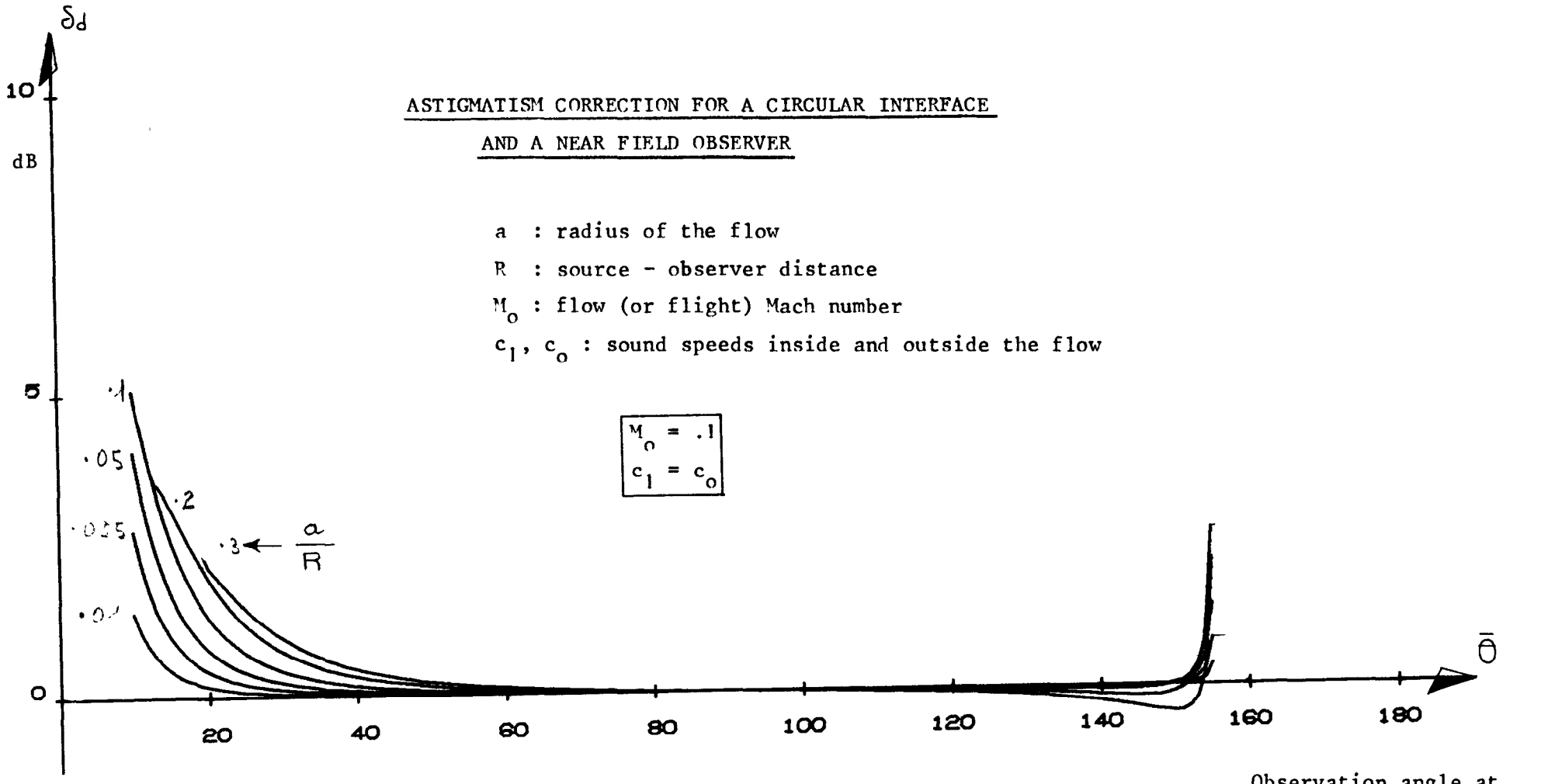
ASTIGMATISM CORRECTION FOR A CIRCULAR INTERFACE
AND A NEAR FIELD OBSERVER
a : radius of the flow
R : source - observer distance
M_o : flow (or flight) Mach number
c_1, c_o : sound speeds inside and outside the flow
$M_o = .1$
$c_1 = c_o$
δ_d
dB
10
5
0
.1
.05
.2
.3
$\frac{a}{R}$
20
40
60
80
100
120
140
160
180
$\bar{\theta}$
$N_{flight}(\bar{\theta}) = N_{W.T.}(\bar{\theta}) + 10 \log c^c + \delta_d$
Observation angle at emission time in flight

Figure 30

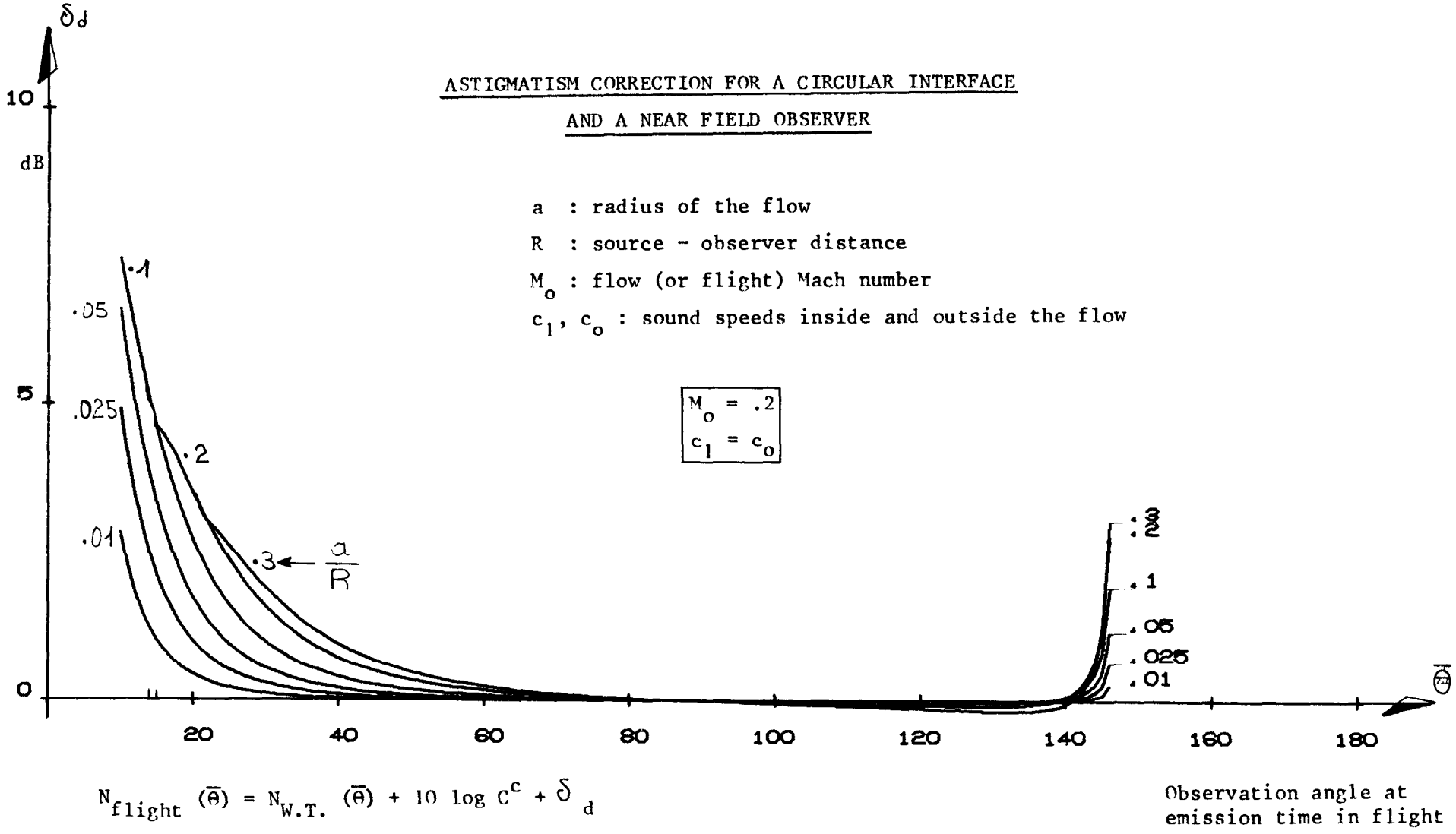
ASTIGMATISM CORRECTION FOR A CIRCULAR INTERFACE
AND A NEAR FIELD OBSERVER
a : radius of the flow
R : source - observer distance
M_o : flow (or flight) Mach number
c_1, c_o : sound speeds inside and outside the flow
$M_o = .2$
$c_1 = c_o$
δ_d
10
dB
5
0
.1
.05
.025
.01
.2
.3
$\frac{a}{R}$
.3
.2
.1
.05
.025
.01
20
40
60
80
100
120
140
160
180
$\bar{\theta}$
$N_{flight}(\bar{\theta}) = N_{W.T.}(\bar{\theta}) + 10 \log C^c + \delta_d$
Observation angle at emission time in flight

Figure 31

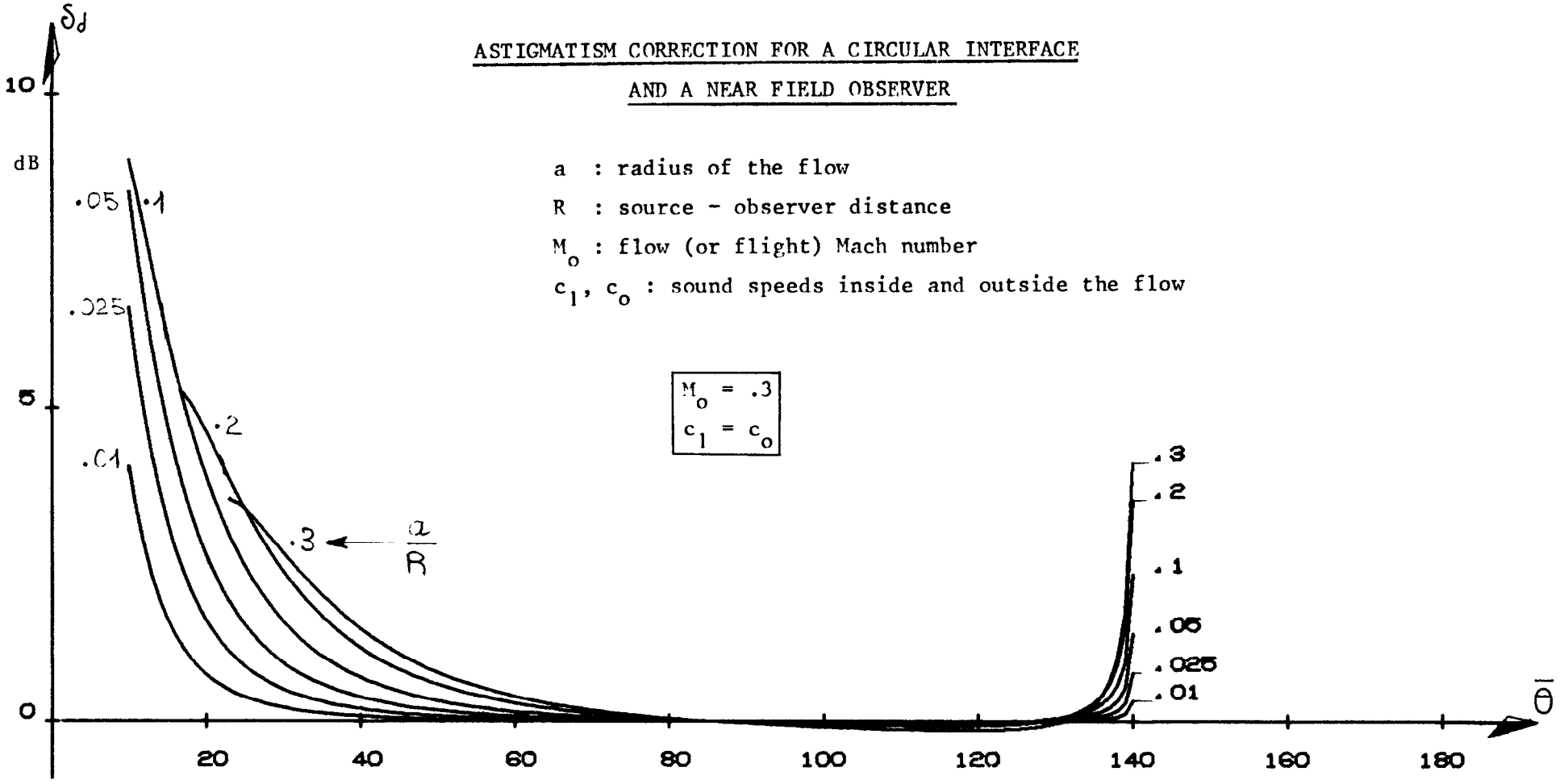

ASTIGMATISM CORRECTION FOR A CIRCULAR INTERFACE

AND A NEAR FIELD OBSERVER

a : radius of the flow

R : source - observer distance

M_o : flow (or flight) Mach number

c_1, c_o : sound speeds inside and outside the flow

$M_o = .3$

$c_1 = c_o$

$N_{flight}(\bar{\theta}) = N_{W.T.}(\bar{\theta}) + 10 \log c^c + \delta_d$

Observation angle at emission time in flight

Figure 32

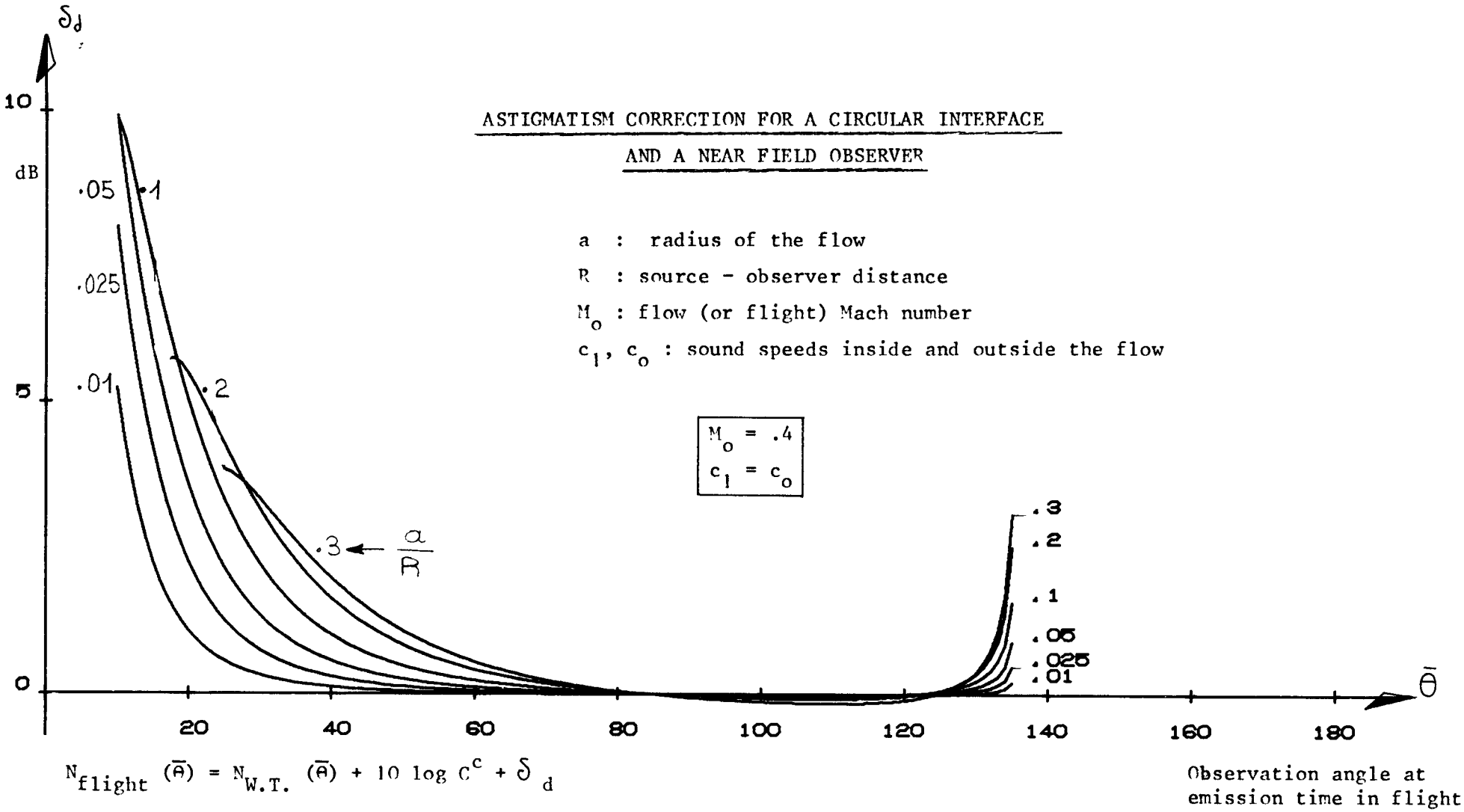

ASTIGMATISM CORRECTION FOR A CIRCULAR INTERFACE AND A NEAR FIELD OBSERVER

a : radius of the flow

R : source - observer distance

M_o : flow (or flight) Mach number

c_1, c_o : sound speeds inside and outside the flow

Figure 33

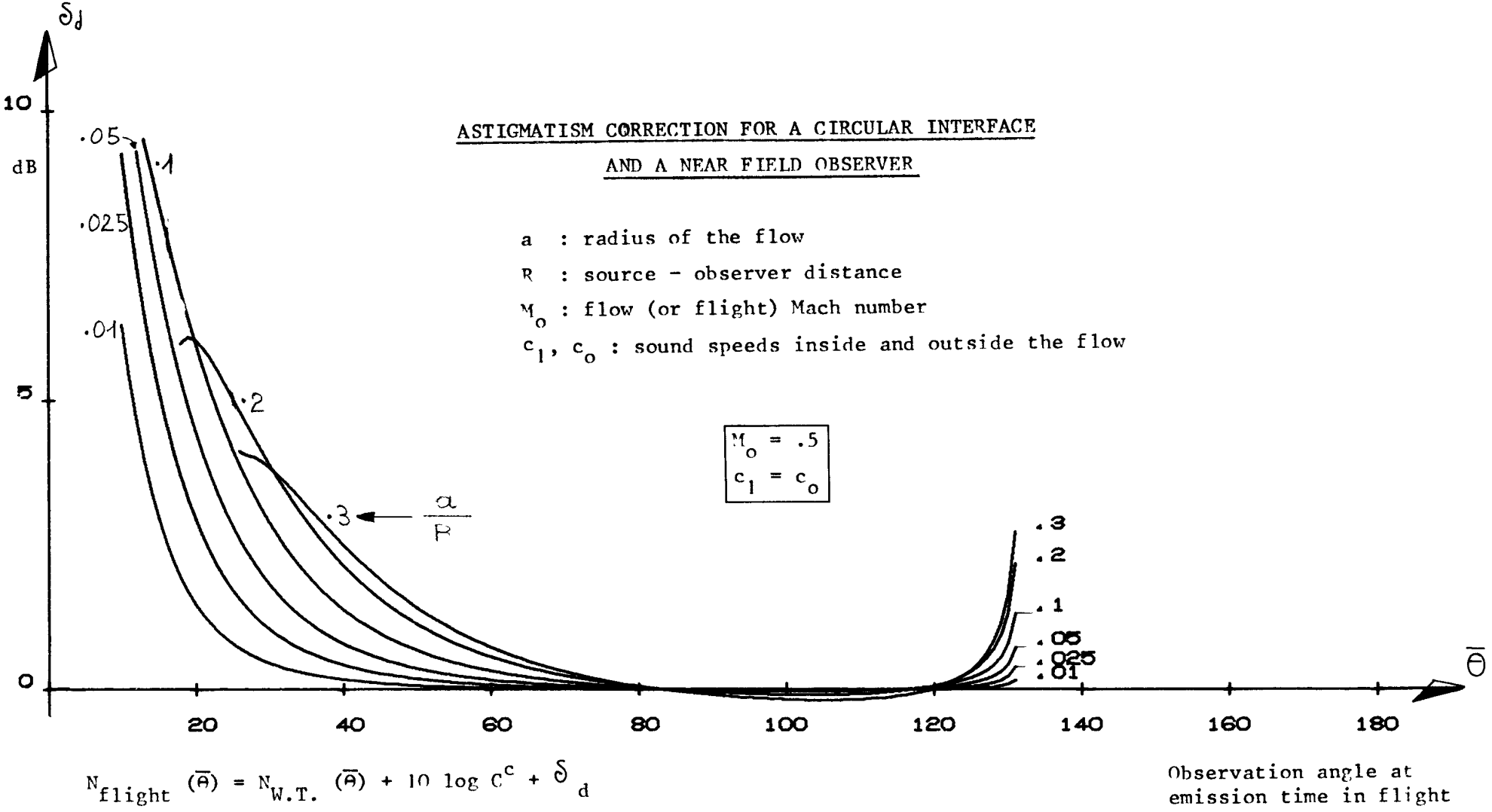
ASTIGMATISM CORRECTION FOR A CIRCULAR INTERFACE
AND A NEAR FIELD OBSERVER
a : radius of the flow
R : source - observer distance
M_o : flow (or flight) Mach number
c_1, c_o : sound speeds inside and outside the flow
$M_o = .5$
$c_1 = c_o$
δ_d
dB
10
5
0
.05
.1
.025
.01
.2
.3
$\frac{a}{R}$
.3
.2
.1
.05
.025
.01
$\bar{\Theta}$
20
40
60
80
100
120
140
160
180
$N_{flight}(\bar{\Theta}) = N_{W.T.}(\bar{\Theta}) + 10 \log C^c + \delta_d$
Observation angle at emission time in flight

Figure 34

EXAMPLE OF APPLICATION OF THE CORRECTION METHOD

TO A TYPICAL WIND-TUNNEL FIELD SHAPE

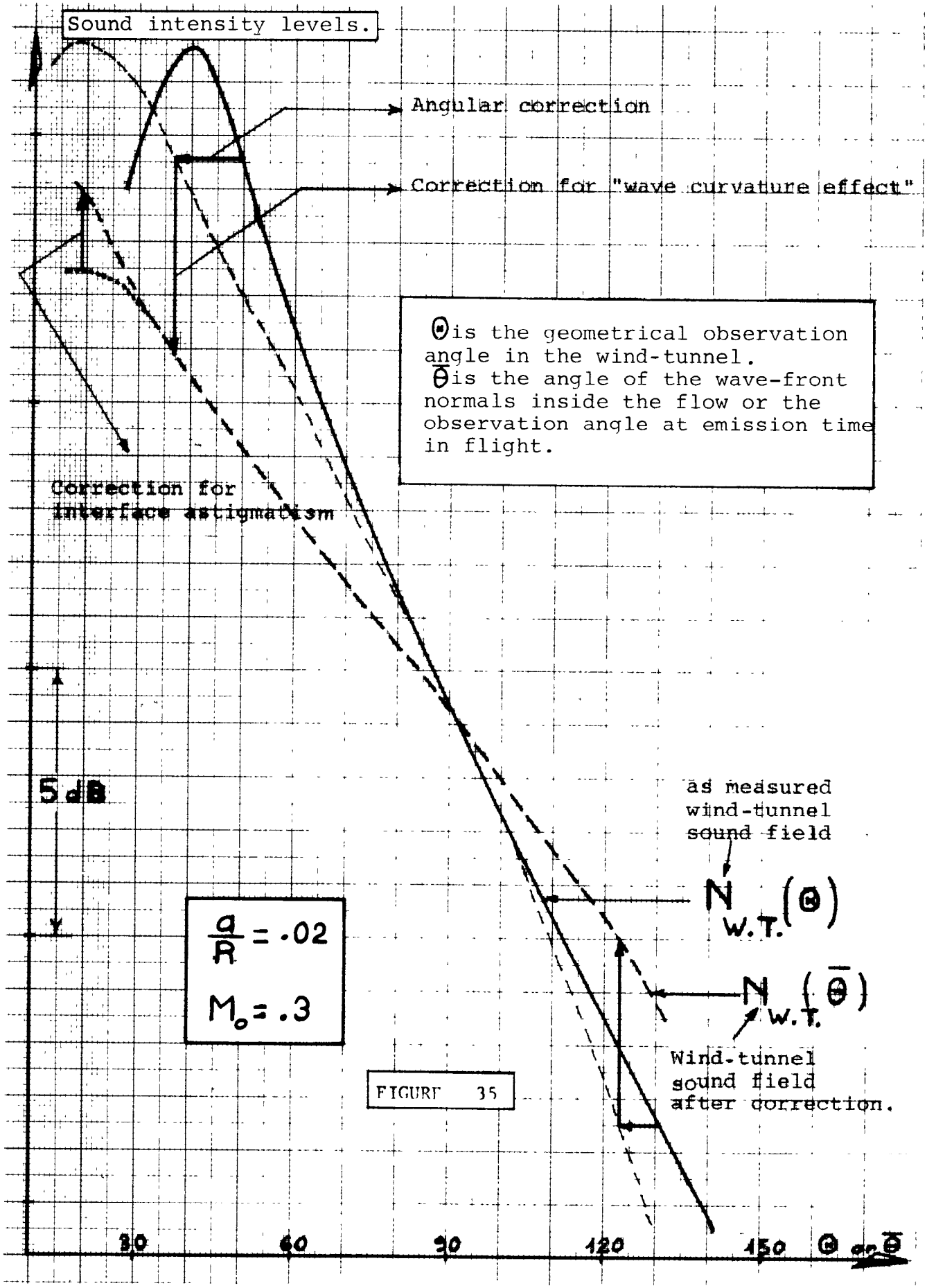

FIGURE 35

SCALED SCHEME DEPICTING THE MIXING ZONES OF A SUBSONIC JET

(upper scheme) AND A SUPERSONIC JET (lower scheme)

FOR A SECONDARY FLOW MACH NUMBER M_o = .3.

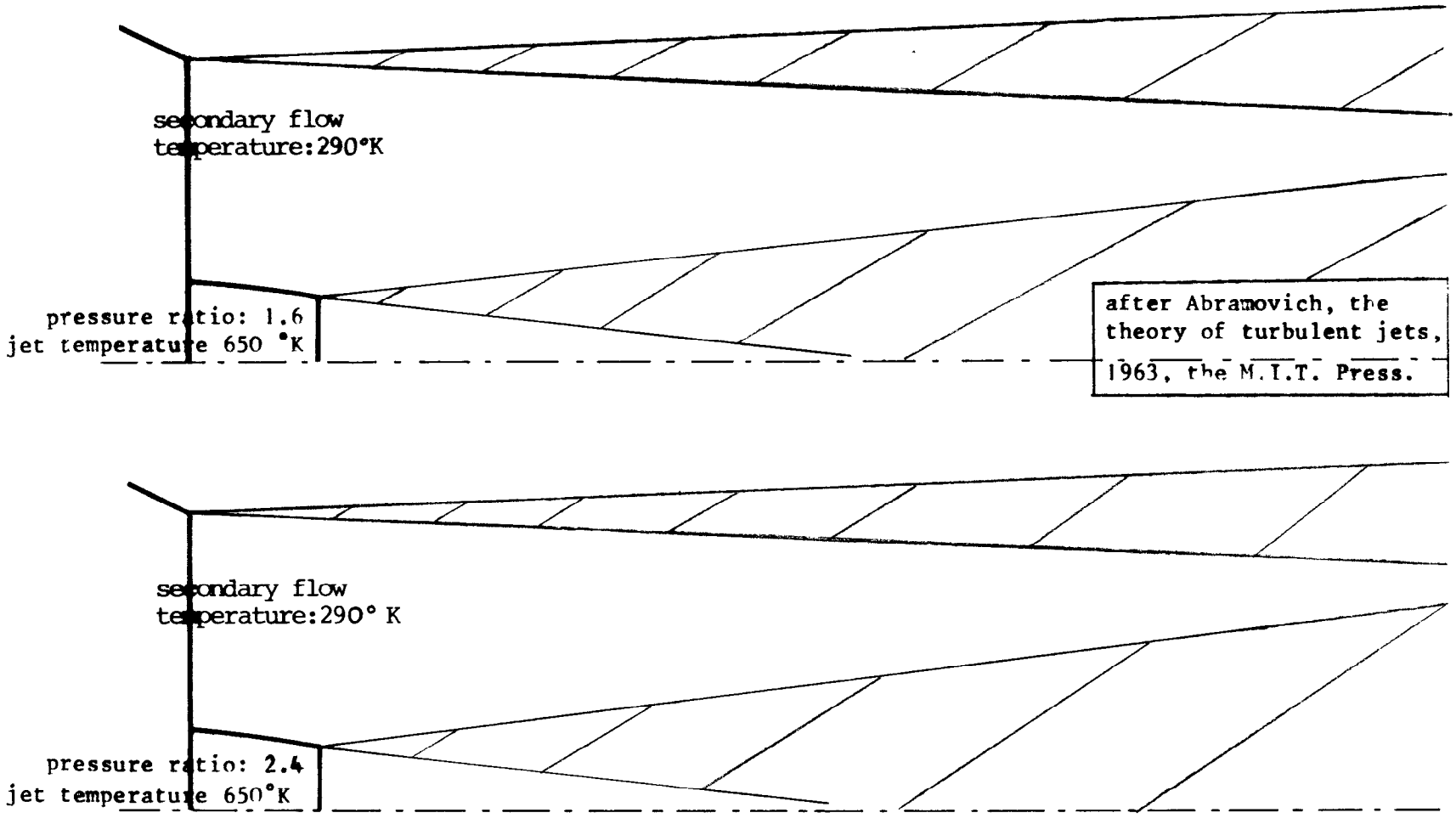

FIGURE 36

SOUND FIELD AND SPECTRUM AT 90° OF A SUBSONIC JET WITH AND WITHOUT EXTERNAL FLOW AS MEASURED IN THE C.E.Pr. FACILITY

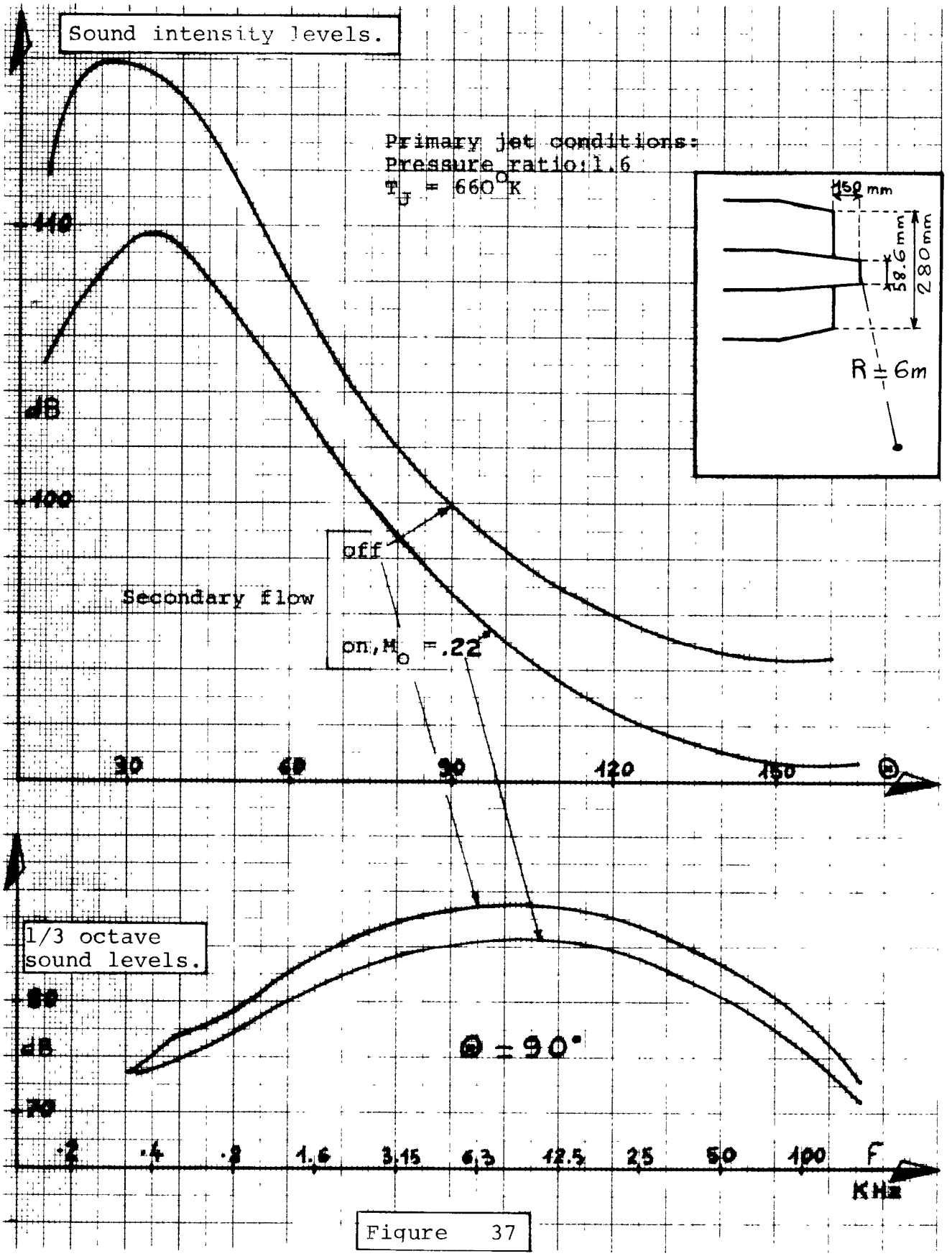

Figure 37

SOUND FIELD AND SPECTRUM AT 90° OF A SUPERSONIC JET WITH AND WITHOUT EXTERNAL FLOW AS MEASURED IN THE C.E.Pr. FACILITY

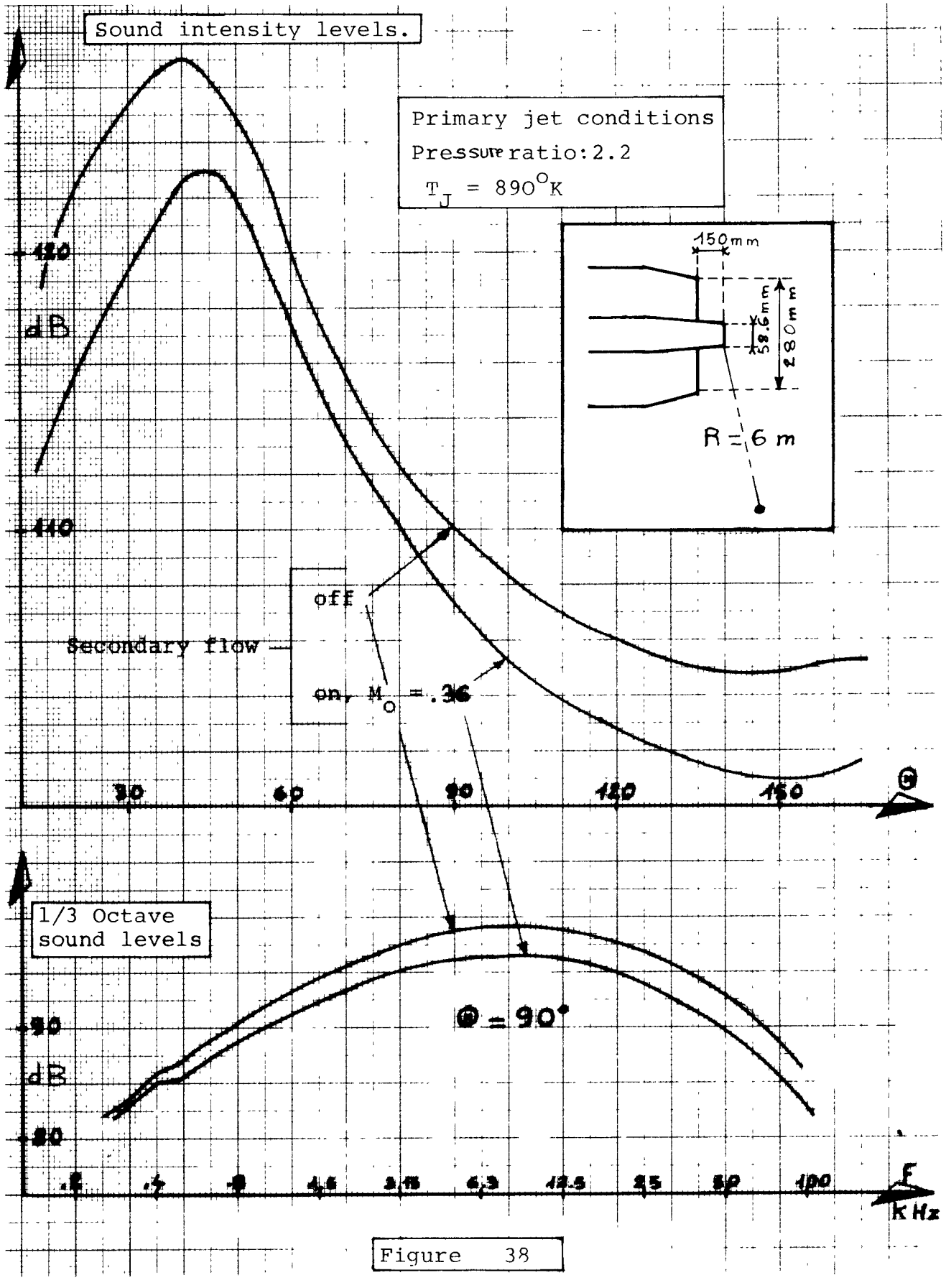

Figure 38

COMPARISON BETWEEN FLIGHT AND STATIC MEASUREMENTS FOR REAL FLIGHT AND FLIGHT SIMULATED IN A WIND-TUNNEL (C.E.Pr. FACILITY)

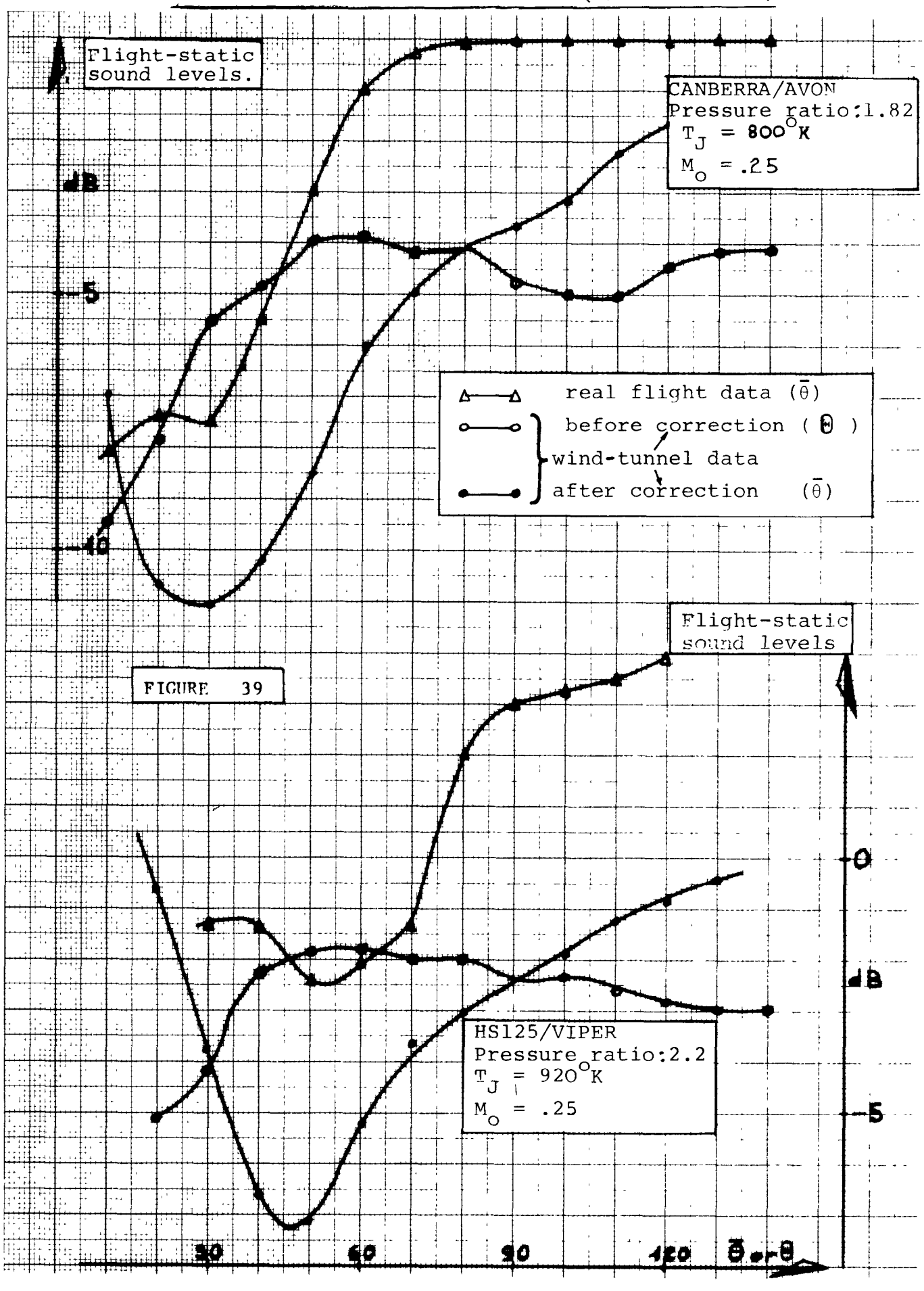

FIGURE 39

COMPARISON BETWEEN FLIGHT AND STATIC MEASUREMENTS FOR REAL FLIGHT AND FLIGHT SIMULATED IN A WIND-TUNNEL (C.E.Pr. FACILITY)

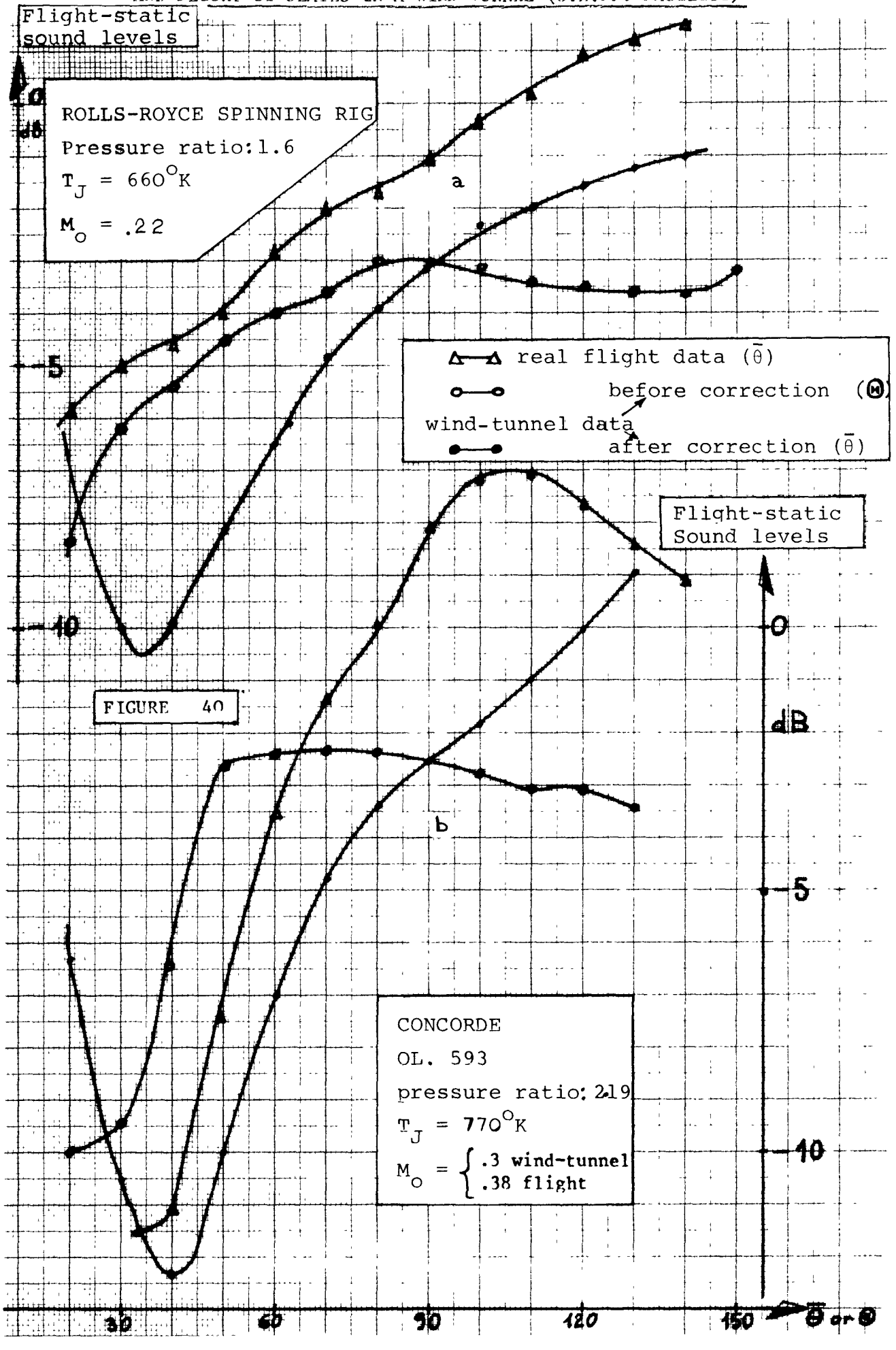

FIGURE 40

COMPARISON BETWEEN FLIGHT AND STATIC MEASUREMENTS FOR REAL FLIGHT AND FLIGHT SIMULATED IN A WIND-TUNNEL (C.E.Pr. FACILITY)

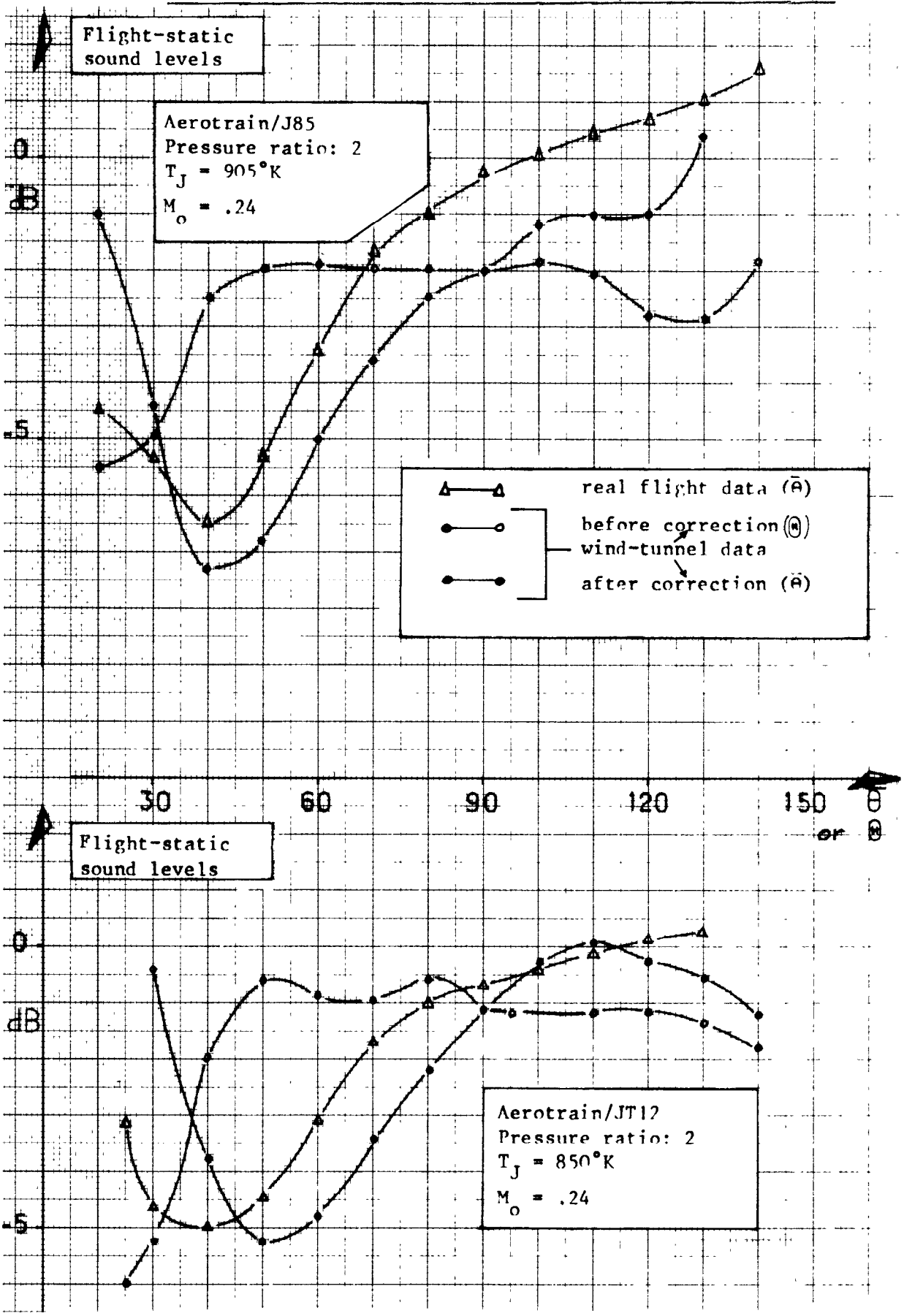

FIGURE 41

COMPARISON BETWEEN FLIGHT AND STATIC MEASUREMENTS FOR REAL FLIGHT AND FLIGHT SIMULATED IN A WIND-TUNNEL (C.E.Pr. FACILITY)

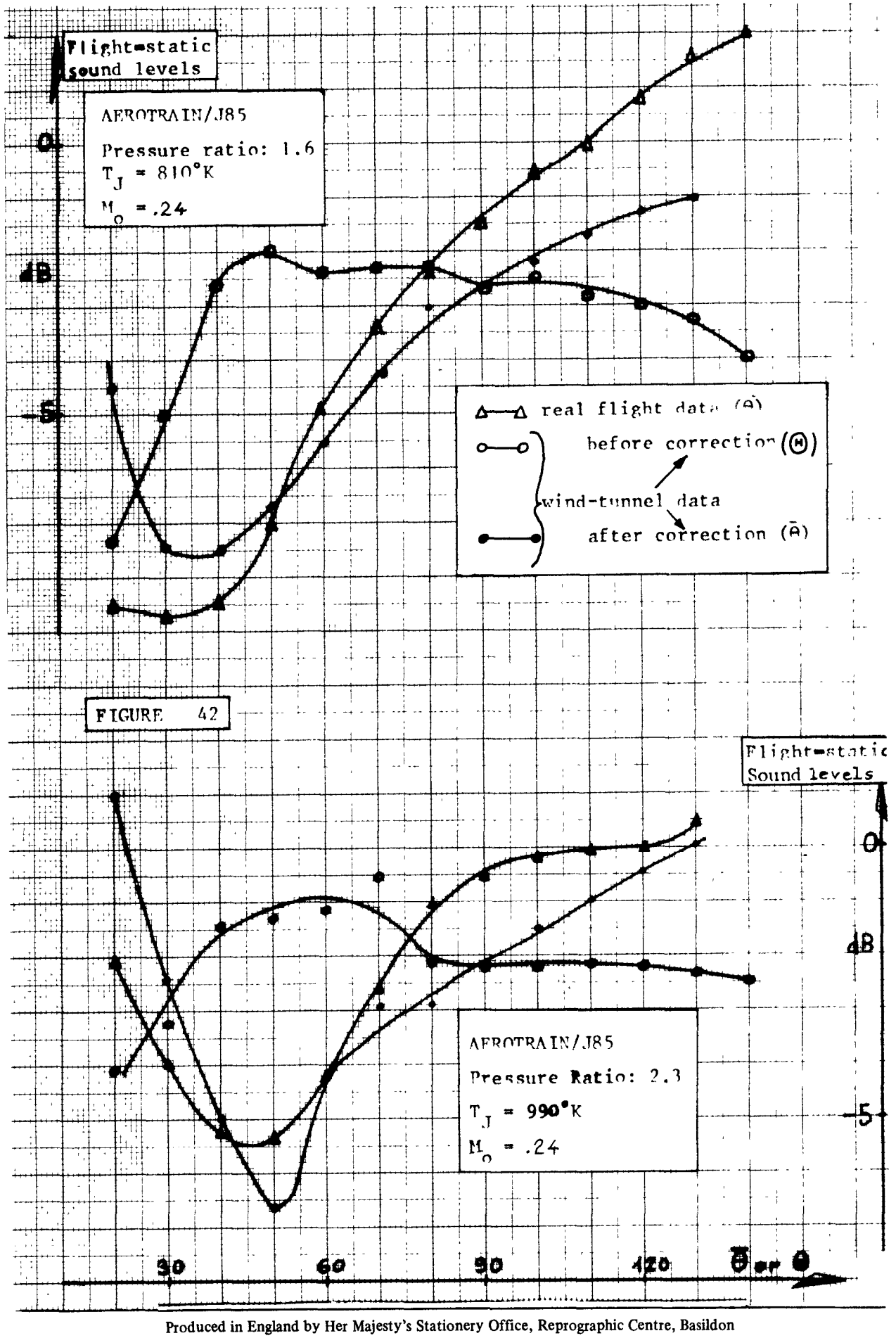

FIGURE 42

Produced in England by Her Majesty's Stationery Office, Reprographic Centre, Basildon

Bas 30268/290279 K4 11/76 PQ3

ARC CP No.1351
March 1976
Jacques, J.

WIND-TUNNEL SIMULATION OF THE EFFECTS OF FLIGHT ON RADIATED SOUND

The validity of wind-tunnel simulation of the noise radiated by a moving source is studied. Theoretical corrections are derived that allow acoustic measurements in a wind tunnel with microphones outside of the flow to be transposed to a real flight situation. Some corrected coaxial jet data are then compared with real flight data.

ARC CP No.1351
March 1976
Jacques, J.

WIND-TUNNEL SIMULATION OF THE EFFECTS OF FLIGHT ON RADIATED SOUND

The validity of wind-tunnel simulation of the noise radiated by a moving source is studied. Theoretical corrections are derived that allow acoustic measurements in a wind tunnel with microphones outside of the flow to be transposed to a real flight situation. Some corrected coaxial jet data are then compared with real flight data.

ARC CP No.1351
March 1976
Jacques, J.

WIND-TUNNEL SIMULATION OF THE EFFECTS OF FLIGHT ON RADIATED SOUND

The validity of wind-tunnel simulation of the noise radiated by a moving source is studied. Theoretical corrections are derived that allow acoustic measurements in a wind tunnel with microphones outside of the flow to be transposed to a real flight situation. Some corrected coaxial jet data are then compared with real flight data.

ARC CP No.1351
March 1976
Jacques, J.

WIND-TUNNEL SIMULATION OF THE EFFECTS OF FLIGHT ON RADIATED SOUND

The validity of wind-tunnel simulation of the noise radiated by a moving source is studied. Theoretical corrections are derived that allow acoustic measurements in a wind tunnel with microphones outside of the flow to be transposed to a real flight situation. Some corrected coaxial jet data are then compared with real flight data.

DETACHABLE ABSTRACT CARDS

HER MAJESTY'S STATIONERY OFFICE

Government Bookshops

49 High Holborn, London WC1V 6HB
13a Castle Street, Edinburgh EH2 3AR
41 The Hayes, Cardiff CF1 1JW
Brazennose Street, Manchester M60 8AS
Southey House, Wine Street, Bristol BS1 2BQ
258 Broad Street, Birmingham B1 2HE
80 Chichester Street, Belfast BT1 4JY

Government publications are also available through booksellers

ISBN 0 11 470987 4